Past and Future Sea-Level Changes in French Polynesia

by

Albéric Botella

A thesis submitted
to the Faculty of Graduate and Postdoctoral Studies
in partial fulfillment of the requirements
for the MSc in Earth Sciences
with specialization in Environmental Durability

Department of Earth and Environmental Sciences
Faculty of Sciences
University of Ottawa

Table of contents

List of Tables ..... **iv**

List of Figures ..... **v**

Abstract ..... **vii**

Declaration ..... **viii**

Aknowledgments ..... **ix**

CHAP 1: Introduction **1**

1.1 Motivation **1**

1.2 From observation to projections **3**

1.2.1 Absolute and relative sea levels 4
1.2.2 Processes driving sea-level changes 5

1.3 Research goals and outline of the thesis **14**

CHAP 2: Reconstructing past sea-level changes **15**

2.1 Introduction **15**

2.2 Data description **15**

2.2.1 Choosing suitable proxies 15
2.2.2 Opting for coral microatolls 16
2.2.3 Survey areas 17

2.3 Data acquisition **19**

2.3.1 Measurement of position and elevation 19
2.3.2 Radiometric dating 20

2.4 Processing elevation data **22**

2.4.1 First method: using an orthometric datum 22
2.4.2 Second method: comparing fossil and modern microatolls 28
2.4.3 Third method: measuring height with respect to the instant water level 30

2.5 Reconstructing sea-level curve **30**

2.5.1 Corrections for GIA 30
2.5.2 Corrections for thermal subsidence and volcanic loading 31

2.6 The reconstructed sea-level curves **32**

CHAP 3: Interpreting past sea-level changes **34**

3.1 Introduction **34**

3.2 Model description **34**

3.2.1 Ice models 34
3.2.2 Earth model 35
3.2.3 Sea-level calculation code 35

3.3 Model calibration 36
3.3.1 Defining a parameter space 36
3.3.2 Evaluating goodness of fit 36
3.3.3 Determining a best-fitting set of parameters 37
3.4 Model applications 42
3.4.1 Long-term GIA signal 42
3.4.2 Estimating millennial-scale ice volume changes 45
3.4.3 Submillennial-scale sea-level variability 47
3.5 Next steps for data collection and model improvement 50
3.5.1 Reducing vertical uncertainty 50
3.5.2 Filling temporal gaps 51
3.5.3 Extending survey area 52
3.6 Conclusions 53
CHAP 4: Projecting future sea-level changes 55
4.1 Introduction 55
4.2 Sea-level rise in the decision-making process 55
4.2.1 A challenge for insular communities 55
4.2.2 The need for updated and regionalized projections 58
4.3 Description of studied localities 61
4.3.1 Rangiroa 61
4.3.2 Ile de Sein 65
4.4 Methodology for sea-level projections 67
4.4.1 Steric contribution 67
4.4.2 Mass contribution 69
4.4.3 Isostatic contribution and vertical land motion 73
4.4.4 Combination of contributions and uncertainties 75
4.5 Projections of sea-level changes 77
4.5.1 Amplitude and rate of sea-level changes 77
4.5.2 Causes of spatial variability 79
4.5.3 Sensitivity of projections to uncertainties 81
4.6 Conclusion 82
CHAP 5: Conclusion 83
5.1 Summary of key results 83
5.2 Future work 84

List of Tables

Table 2-1. **Errors associated with sea level reconstruction**. 24

Table 2-2. **Adopted tide corrections**. 28

Table 2-3. **GIA corrections with respect to Bora-Bora sea-level curve.** 31

Table 4-1. **Climate models used for calculating the steric contribution and global mean steric sea-level change.** 68

Table 4-2. **Projections of GIC mass losses.** 69

Table 4-3. **Projections of GIS and AIS mass changes.** 72

Table 4-4. **Contributions to sea-level changes between 2010 and 2100 in Rangiroa and Ile de Sein.** 77

List of Figures

Figure 1-1. **Records from tide gauges of several coastal cities**. 4

Figure 1-2. **Description of glacio- and hydro-isostatic deformations associated with GIA.** 6

Figure 1-3. **Modeled RSL at 4 kyr BP with respect to the present sea level.** 8

Figure 1-4. **Athabasca Glacier, Alberta, Canada**. 9

Figure 1-5. **Description of the gravitational effects of land ice melting, illustrated with projections of the Greenland ice sheet.** 11

Figure 1-6. **Mean dynamic topography averaged over the past 12 years**. 13

Figure 2-1. **A fossil microatoll in Maupiti Island, French Polynesia**. 17

Figure 2-2. **Topographic and bathymetric map of French Polynesia indicating islands selected and surveyed for interpretation**. 18

Figure 2-3. **Measuring microatolls using GPS**. 20

Figure 2-4. **Radial slab of a microatoll**. 21

Figure 2-5. **Tide heights and microatolls**. 22

Figure 2-6. **Gravity field in French Polynesia** 23

Figure 2-7. **Sea surface height above WGS-84 in French Polynesia**. 24

Figure 2-8. **Maximal tide amplitude**. 27

Figure 2-9. **Sea surface height above WGS-84 in Bora Bora**. 30

Figure 2-10. **Reconstructed sea-level curve for French Polynesia**. 32

Figure 2-11. **Reconstructed sea-level curve for Christmas Island.** 33

Figure 3-1. **Misfit calculation for combined datasets, French Polynesia and Christmas Island.** 38

Figure 3-2a. **Misfit calculation for French Polynesia and Christmas Island datasets.** 40

Figure 3-2b. **Misfit calculation for combined datasets, French Polynesia and Christmas Island.** 40

Figure 3-3. **Comparison of observations and predictions of sea-level change for French Polynesia.** 41

Figure 3-4. **Comparison of observations and predictions of sea-level change for Christmas Island.** 41

Figure 3-5. **Spread of best-fitting models.** 42

Figure 3-6. **RSL and component signals for French Polynesia (Bora Bora Island) and Christmas Island.** 43

Figure 3-7. **Spatial variability of sea-level change in the South Pacific and decomposition of the GIA signal.** 44

Figure 3-8. **Comparison of observations and predictions of eustatic sea-level change.** 46

Figure 3-9. **Variability of ice and steric contributions.** 48

Figure 3-10. **Comparison of sea-surface temperature and sea level.** 49
Figure 3-11. **Comparison of total solar irradiance and sea level.** 50
Figure 4-1. **Location of French overseas territories.** 56
Figure 4-2. **Projected spatial variability of sea-level rise for French coasts.** 60
Figure 4-3. **The southern side of the atoll of Rangiroa**. 61
Figure 4-4. **A beach on Rangiroa, French Polynesia**..... 63
Figure 4-5. **Ile de Sein**. 66
Figure 4-6. **Fingerprints of GIC groups.** 71
Figure 4-7. **Data-model fit of relative sea-level change near Brest during the Holocene.** 74
Figure 4-8. **Present-time GIA rates in West Britanny.** 74
Figure 4-9. **Mean regional contributions to sea-level change between 2010 and 2100.** 76
Figure 4-10. **Projection of sea level in Rangiroa between 2010 and 2100.** 78
Figure 4-11. **Projections of steric sea level in Rangiroa and Ile de Sein between 2010 and 2100.** 79
Figure 4-12. **Contributions to sea-level changes at Rangiroa and Ile de Sein.** 80

List of abbreviations

AIS	Antarctica Ice Sheet
AOGCM	Atmosphere-Ocean General Circulation Model
ARAI	*Aléas, Risques naturels, Aménagement et Information*
BRGM	*Bureau de Recherches Géologiques et Minières*
CBA	Cost-Benefit Analysis
CMIP	Coupled Model Intercomparison Project
CNES	*Centre National d'Etudes Spatiales*
ENSO	El-Nino Southern Oscillation
ESL	Equivalent Sea Level
GHG	Greenhouse Gas
GIA	Glacial Isostatic Adjustment
GIC	Glaciers and Ice Caps
GIS	Greenland Ice Sheet
GMSL	Global Mean Sea Level
GPS	Global Positioning System
HAT	Highest Astronomical Tide
HLC	Height of Living Corals
IGN	*Institut Géographique National*
IPCC	Intergovernmental Panel on Climate Change
LAT	Lowest Astronomical Tide
LGM	Last Glacial Maximum
LIS	Laurentide Ice Sheet
LMV	Lower Mantle Viscosity
LT	Lithospheric Thickness
MC-ICP-MS	Multiple Collector Inductively Coupled Plasma Mass Spectrometry
MLWS	Mean Low Water Spring
MSL	Mean Sea Level
MSS	Mean Sea Surface
ONERC	*Observatoire National sur les Effets du Réchauffement Climatique*
PIMP	Paleoclimate Modelling Intercomparison Project
PPR	*Plan de Prévention des Risques*
RCP	Representative Concentration Pathway
RGI	Randolph Glacier Inventory
RGPF	*Réseau Géodésique de la Polynésie Française*
RSL	Relative Sea Level
RTK	Real Time Kinematic
SHOM	*Service Hydrographique et Océanographique de la Marine*
SIDS	Small Island Developing States
SMB	Surface Mass Balance
SPC	Secretariat of the Pacific Community
SRES	Special Report on Emissions Scenario
SST	Sea Surface Temperatures
TSI	Total Solar Irradiance
UMV	Upper Mantle Viscosity
WGS-84	World Geodetic System 1984

Abstract

Among the various adverse effects of climate change, sea-level rise is expected to increase the severity and frequency of flooding events impacting the vulnerable, low-lying islands of French Polynesia. It has long been understood that sea-level changes are not spatially uniform, yet this aspect is not taken into account in the decision-making. Notably, no projections of future sea level have been produced specifically for this region so far, partly because the processes driving sea-level changes remain poorly constrained. To approach the issue, we present a detailed reconstruction of sea-level changes for the mid-to-late Holocene, based on the observation of coral proxies. This dataset is then used to calibrate a sea-level model in order to estimate the contribution of glacial isostatic adjustment to regional sea-level changes and to infer past variations in global ice volume. Building upon this baseline and exploiting recent outputs of climate models, we project that in a "worst-case" scenario, sea level would rise 1.05 meters by 2100 in French Polynesia, exceeding the value adopted in the French adaptation strategy by 0.45 meters. We conclude that spatial variability of sea-level rise should be considered in future risk studies for this and other regions.

Declaration

The following is a declaration regarding the authorship of the second chapter of this thesis. The reconstruction of sea-level changes in French Polynesia, which is presented in Chapter 2, is the main outcome of a field research project initiated by G. Camoin at the European Centre for Research and Education in Environmental Geosciences (CEREGE) based in Aix-en-Provence, France; co-contributors to the project are N. Hallmann, G.A. Milne, C. Vella, A. Eisenhauer, E. Samankassou, V. Pothin and A. Botella. My personal contribution focused on the processing of elevation data (Section 2.4). Specifically, I designed the method to compute tide amplitude in localities where relevant information was not available (presented in Section 2.4.1.2), and I suggested practical solutions to solve the issues regarding the estimation of mean sea level (Section 2.4.1.1) and the geoidal gradient (described in Section 2.4.2). Having conducted all the numerical modeling related to the interpretation of this dataset, I also applied a calibrated GIA model to calculate the spatial corrections provided in Section 2.5.1. At the time of writing, the data collection is ongoing and the methodology to process elevation data is not yet fully determined. Beyond the presentation of the dataset, Chapter 2 also reflects the content of discussions with the above-mentioned colleagues and the methodological choices I have made at this stage of the project in order to proceed with the interpretation of the data.

Acknowledgments / Remerciements

First of all, I would like to express my gratitude to my supervisor, Glenn Milne. You were always available to answer my questions, providing guidance with patience and in a friendly manner; not only I learned so much from you about sea-level research and science in general, but you also provided me with the great opportunity to do field work. I wish you fair winds and following seas!

I would also like to thank my research group in Ottawa, notably Ryan Love for his help on climate models and sea-level fingerprints; and my colleagues in Aix, especially Nadine Hallmann and Gilbert Camoin, for having shared their data, their invaluable experience in field research and their inspiring enthusiasm.

Ma gratitude va aussi aux parents, amis et voisins qui, au Canada comme en France, m'ont soutenu de maintes façons dans ce voyage au long cours. Merci notamment à Beatrice et Susan, qui ont gardé le petit mousse quand j'étais de quart; merci aussi à JP, qui m'a aidé à armer le rafiot qui m'a fait traverser l'océan, à PA, qui a installé une chouette dans la vigie, à Frédéric, qui m'a fait partager les secrets des coraux, à Jean-Christophe, pour sa générosité et ses bons contacts, ainsi qu'à tous ceux qui, par delà l'Atlantique, m'ont soutenu par leurs messages d'encouragement et leurs délicates attentions.

Mes plus chaleureux remerciements vont enfin à ma compagne - tu faisais invariablement souffler une brise salvatrice quand il fallait sortir les rames - et à mon fils Arthur, dont la naissance a donné un véritable sens à cette quête scientifique.

"*Nous n'héritons pas de la terre de nos ancêtres, nous l'empruntons à nos enfants.*"

(proverbe amérindien)

CHAP 1: INTRODUCTION

1.1 Motivation

Since the termination of the last glacial period several thousand years ago, sea level has been relatively stable at the global scale, allowing human communities to migrate and safely settle in coastal areas. This trend has greatly accelerated with urbanization and the industrial revolution: coastal cities became able to import supplies and resources from afar while coastal engineering was developed in order to mitigate flood risks and even to reclaim land. Although more difficult to reach, low-lying islands of the South Pacific Ocean were by no means exempt from human migration. According to Nunn (2007), archipelagic colonization by the Polynesian peoples was facilitated by the relative stability of sea level for the last two millennia – and even by a sea-level fall at the regional scale, as discussed later.

Nowadays, such a growth does not appear sustainable in the face of the disruptive impacts of climate change that could affect coastal communities. In 2005, US$ 3,000 billion worth of assets and 40 million people living in port cities around the globe were exposed to a 1-in-100 year flood event; under the combined effects of sea-level rise, increased storminess, land subsidence, urbanization and population growth, exposure could reach US$ 35,000 billion and 150 million people by 2070 (Nicholls et al. 2008). While the vulnerability of individual cities can be reduced in the frame of a nation-wide effort, sea-level rise is a threat to the very existence of Small Island Developing States (SIDS). Vital functions are at stake, including food production, fresh water resources and tourism, because their exposure to storm surge and sea-level rise is generally higher compared to that of continental countries. Having no control over the world's greenhouse gases (GHG) emissions and negligible weight in the international negotiations on climate change, SIDS have also limited expertise and financial resources to develop adequate adaptation policies. Finally they lack the "strategic depth"[1] required to strengthen their resilience capacities, or ultimately to migrate and resettle landwards.

Although French Polynesia shares similar environmental, geographical and cultural features with the nearby SIDS of the South Pacific Ocean, this overseas territory can rely on its

[1] "Strategic depth" is a military term that commonly refers to the distance between the battlefront and the industrial production centres that support the defensive capacities.

political and economical ties to France in its efforts to tackle climate change. However, the efficiency of this support is questionable, as the French national adaptation strategy did not consider aspects of importance to overseas communities in its earlier developments. Indeed, the issue of sea-level rise in French Polynesia has not been specifically assessed or addressed until recently. In recognition of the fact that decision makers lack the relevant scientific inputs to build efficient adaptation policies at the local level, the latest national report on climate change (Jouzel et al. 2015) concludes that regional projections of sea-level rise should be produced, underlining that such an assessment should also include the overseas territories.

This recommendation implies not only that additional research is required, but also that sea-level changes are not uniform across the globe – a recurring point of discussion throughout this thesis. According to the Intergovernmental Panel on Climate Change (IPCC 2013), a global mean sea-level rise of 52 to 98 cm is expected by 2100 in the worst-case scenario, and "about 70% of the coastlines worldwide are projected to experience sea level change within 20% of the global mean". Providing estimates of global mean sea-level rise is not a trivial task, but predicting sea level at the regional scale is even more challenging. It requires an intimate understanding of numerous physical processes intertwined at various spatial scales, and characterized by various response times.

As a matter of fact, temporal aspects add another layer of complexity to the challenge. Future sea-level changes cannot be simply projected by extrapolating current trends, nor can they be considered as a combination of linear processes. In particular, several potential tipping points in the climate system have been identified (Lenton et al. 2008); some of them could be crossed by 2100 and would have a major impact on sea level over the following centuries. Two examples that are currently in the scope of sea-level research are the weakening of the Atlantic meridional overturning circulation, and the instability of marine sectors of the Antarctic ice sheet; while the former would have a significant influence on sea level and climate along the coasts of the North Atlantic Ocean, the latter would have dramatic implications globally.

The complexity of the temporal and spatial aspects of sea level changes calls for further development of process-based models, which are preferred over semi-empirical models (IPCC 2013). To identify the numerous physical processes at play, quantify their importance, and develop accurate models, observational inputs are critical. Modern instrumentation like

satellites provide invaluable databases, but setting a baseline or detecting an anthropogenic signal within the internal variability of the climate system remain a challenge in some cases, especially with sea level in the Tropical Pacific (Meyssignac et al. 2012). In this respect, paleo-archives complement well the records from modern instrumentation, allowing better understanding of past sea-level changes and leading to improved constraints on future sea-level rise. Although geological records can lack the temporal resolution needed for a reconstruction precise enough to reveal underlying climate signals (e.g., ice volumes, sea temperatures, or the sea level itself), they offer much longer time series in various environmental conditions – including interglacial periods when sea level was relatively stable. In this respect, two interesting periods to investigate are the Last Interglacial, which offers an example of a sea-level highstand in a slightly warmer climate, and the mid-to-late Holocene, during which the radiative forcing was similar to present time, but without the influence of anthropogenic GHGs (PALSEA 2010).

In this context, the present thesis constitutes an effort to provide a historical background for sea-level changes in French Polynesia, based on an unpublished sea-level reconstruction from the mid-to-late Holocene period. It is also a first attempt to produce regional projections of future sea level in French Polynesia using state-of-the-art models, ahead of the national scientific assessment to be issued in the coming years.

1.2 From observation to projections

In this section, we first introduce the concepts of absolute and relative sea levels and then present the three main processes that contribute to sea-level changes at global and regional scales. Changes in land ice and the associated exchanges of water between the cryosphere and the ocean have a major influence on past and future sea level, and are also a significant cause of spatial variability. The influence of past changes in land ice contributes to future sea levels through the on-going viscous deformation of the solid Earth. This process, known as glacial isostatic adjustment, is a key contributor to sea-level changes in the time frame spanned by the dataset presented in Chapter 2 and is introduced in Section 1.2.2.1. The influence of future changes in land ice and their sea level implications will be described in Section 1.2.2.2. The last important factor to be considered in the context of a fast transient response of the climate system is the steric component, which is caused by variations of density in the ocean, is the subject of Section 1.2.2.3.

1.2.1 Absolute and relative sea levels

Following the natural changes in insolation described in the orbital theory of the Ice Ages (Milanković 1941), the Earth's climate has warmed significantly over the last twenty thousand years, with an increase of 4 to 5°C in the global mean surface temperature, resulting in the melting of huge quantities of land ice around the world. During this period, global mean sea level rose by about 130 meters, stabilizing 6,000 years ago within a few meters of the present sea level. Examining records from modern instrumentation, a global mean sea-level rise of ~21 cm has been observed since 1880; for the 1993-2009 period, a rate of change of ~3.2 mm/yr has been measured with satellite altimetry (Church & White 2011).

By contrast, a sea level fall of about 250 meters over the past 8,000 years is inferred from geological evidence collected on the shorelines of Hudson Bay, Canada (Peltier 1998); beaches and cliffs that were submerged thousands years ago are now out of the water. Moreover, this trend is ongoing: a tide gauge record from Churchill, Canada (Figure 1-1) indicates a mean rate of change of about –10 mm/yr for the past 60 years.

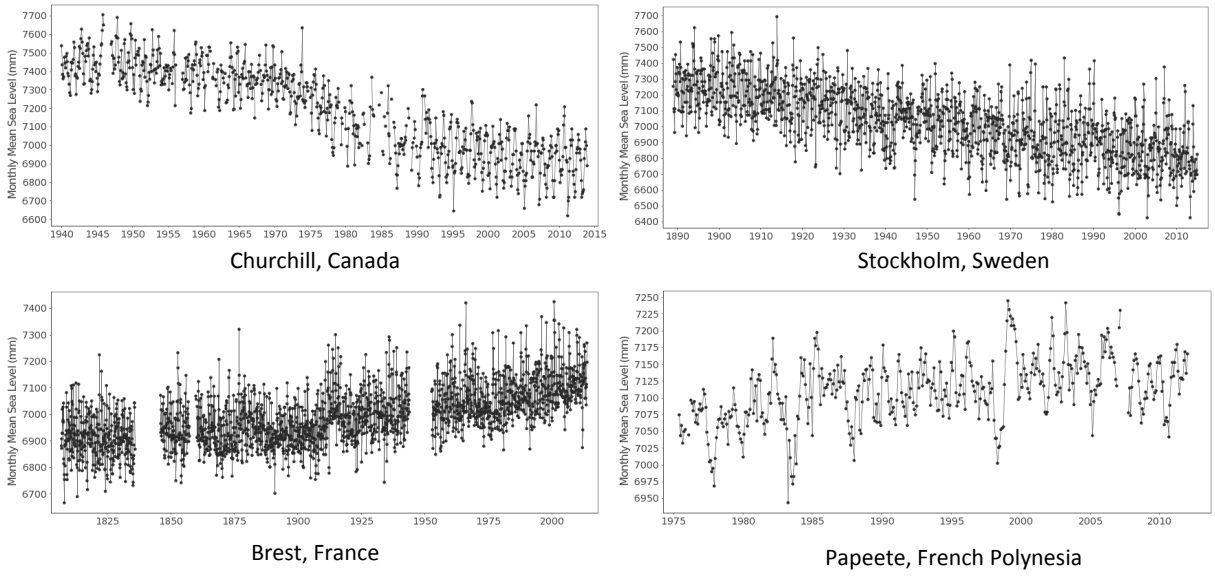

Figure 1-1. **Records from tide gauges of several coastal cities**. Monthly-averaged data retrieved 15 June 2015 from the database of the Permanent Service for Mean Sea Level (Holgate et al. 2012, PSMSL 2015)

To understand this apparent discrepancy – global mean sea-level rise versus local sea-level fall – it is necessary to define in the first place what is meant by "sea level" and to distinguish "absolute" sea level from "relative" sea level:

- absolute sea level (also called "geocentric" sea level) represents the sea surface height relative to the Earth's center, and its variations over time can be measured by satellite altimetry;
- relative sea level (RSL) represents the sea surface height relative to the Earth's surface, and it can be measured by tide gauges or recorded by sea-level proxies.

Thereby, RSL change reflects variations of local absolute sea level plus the vertical land motion (uplift or subsidence) of the Earth's surface. While global mean sea level (GMSL) represents a global average of absolute sea level and is a useful integrated measure of climate change, RSL is the meaningful parameter in order to assess local impacts of sea level changes.

1.2.2 Processes driving sea-level changes

1.2.2.1 Glacial Isostatic Adjustment

As seen previously, GMSL and RSL rates of change can differ significantly because of vertical land motion; in the case of Hudson Bay, such changes result from adjustments of the Earth in response to long-term, large-amplitude changes in Earth's climate. Approximately 21,000 years ago, at the Last Glacial Maximum (LGM), the Laurentide ice sheet (LIS) covered most of Canada and a part of the United States; ice thickness exceeded 3,000 meters in some places. During a glacial episode like the one that preceded the LGM, ice accumulates over the Earth's surface leading to subsidence and deformation of the underlying rocks. This ice loading compresses the mantle material beneath the ice sheet, leading to a subtle and long-wavelength uplift of the Earth's surface in the surroundings of the ice sheet – the so-called "peripheral bulge". When the ice sheet starts to melt, the process is reversed, causing the land surface beneath the ice or in its immediate vicinity to uplift, and the bulge to subside (Figure 1-2, left side of the figure). Moreover, the deformation and the relaxation of the Earth's surface are viscoelastic processes. Consequently, a melting event results in an instantaneous but limited uplift of the crust, driven by the elastic behavior of the solid Earth; the main part of the response is delayed because the mantle material below the lithosphere is highly viscous and flows very slowly. As a consequence, it would take tens of thousands of years for the Earth to return to an equilibrium state after the ice has ceased to melt.

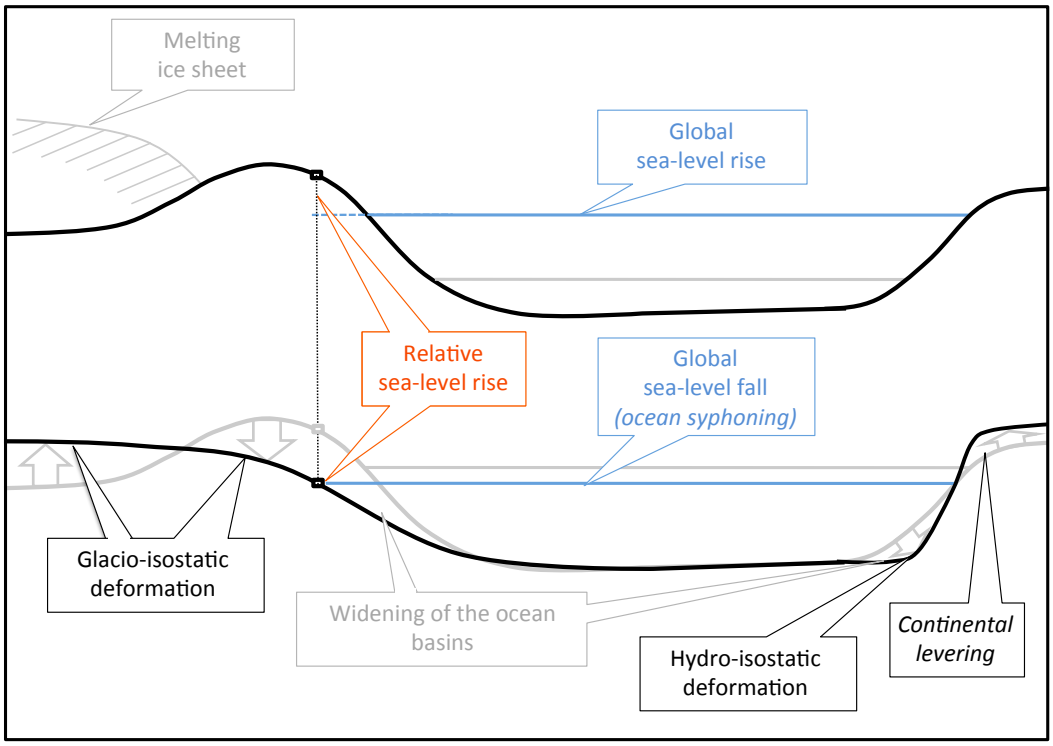

Figure 1-2. **Description of glacio- and hydro-isostatic deformations associated with GIA.** Top: following the melting of the ice sheet, the solid Earth responds slowly due to high viscosities within the mantle and so remains deformed even after the ice melting and global sea level rise is complete (gravitational effects on the sea surface are excluded in this figure for clarity). Bottom: glacio-isostatic deformation causes a progressive relaxation of the crust near the former ice sheet, while hydro-isostatic deformation causes a progressive widening of the ocean basins.

This delayed geodynamic response to long-term climate change, called glacial-isostatic adjustment (GIA) or post-glacial rebound, is a dominant process driving RSL in the vicinity of present or former ice sheets; in this "near-field" zone, the vertical land motion associated with GIA is still ongoing and can dominate other contributions to sea-level changes. In some regions of Northern Canada like Hudson Bay, the crust is currently uplifting at a faster rate than the absolute sea level rise, resulting in a RSL fall. On the contrary, a city like New York, which is located on the receding peripheral bulge of the LIS, is presently subsiding at a rate of about 1.5 mm/yr (Love 2014, Slangen 2012), thus enhancing the detrimental impacts of oceanic warming and ice melting. Similar observations have been made in Northern Europe, which was partly covered by the British-Irish and Fennoscandian ice sheets at the LGM. Stockholm, which used to be buried under the ice, is currently uplifting (Figure 1-1, top right), while Brest, which is located on the peripheral bulges of these ice sheets, is slowly subsiding (see Section 4.4.3.2).

Another consequence of the large sea level rise during the termination of the last glacial period is hydro-isostatic deformation. Under the additional pressure caused by the massive influx of melt water, the seafloor has been subsiding in many areas of the oceans. This effect is most perceptible along the ocean-continent margins, where there is a differential load that results in a flexure of the lithosphere and in a flow of mantle material from oceanic to continental mantle; this causes not only a subsidence of the seafloor surrounding the continents but also an uplift of the continents themselves (Figure 1-2, right side of the figure). This process, referred to as "continental levering" (Clark et al. 1978), can result in a RSL fall along some continental coasts during the late Holocene (e.g., Stattegger et al. 2013).

Besides local changes in RSL, the two processes described above (i.e., the collapse of submerged peripheral bulges and the subsidence of the seafloor along continental margins) have also a global influence on sea level by increasing the global volume of the ocean basins. Since the mass of the oceans has been relatively stable over the last few millennia, the net contribution of these processes affecting the global mean (or "eustatic") sea level is negative and so RSL has been falling over this period in "far-field" regions that are remote from near-field regions. The existence of this phenomena, known as "ocean syphoning", is supported by observational evidence (e.g., Goodwin & Harvey 2008, Pirazzoli & Montaggioni 1986) and is predicted by theoretical calculations (Mitrovica & Milne 2002, Mitrovica & Peltier 1991). In particular, GIA models show that sea level was higher 4,000 years ago than at the present time in a large part of the South Tropical Pacific, our region of interest (Figure 1-3). This is due to a combination of GIA effects including syphoning, rotational changes associated with GIA and hydro-isostasy (see Section 3.4.1).

GIA and all related processes that contribute to RSL change (e.g. glacio- and hydro-isostatic deformation) will be referred to as the "isostatic contribution" in the following chapters.

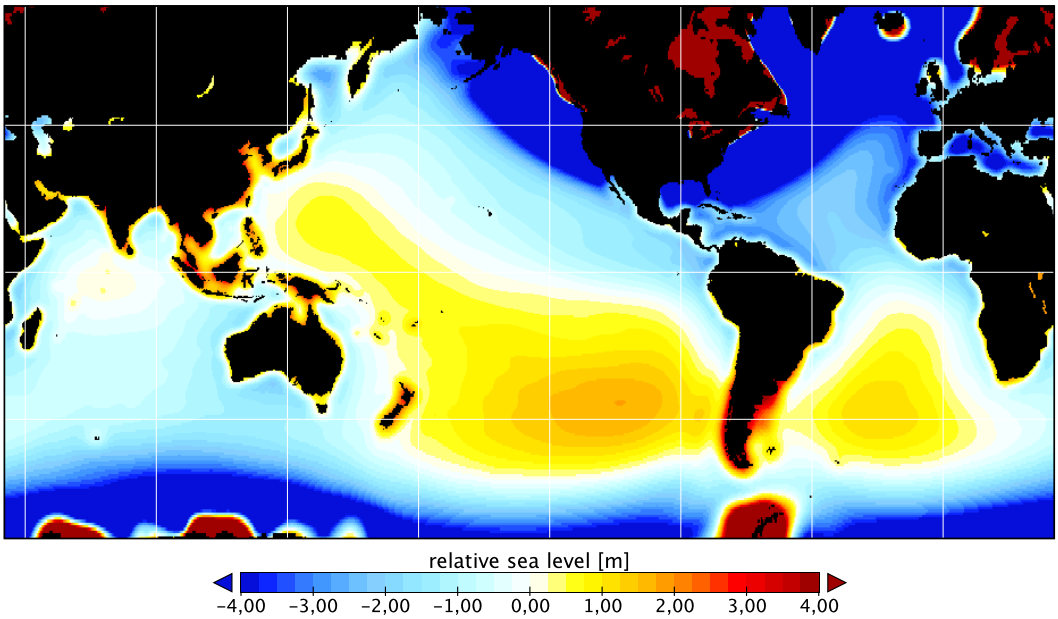

Figure 1-3. **Modeled RSL at 4 kyr BP with respect to the present sea level.** This map was generated using the EUST3 ice model and the following parameters for the Earth model: lithospheric thickness 71 km; upper mantle viscosity 0.3×10^{21} Pa.s; lower mantle viscosity 30×10^{21} Pa.s. See Chapter 3 for information on GIA model parameters.

1.2.2.2 Changes in land ice and groundwater

Current land ice, i.e., glaciers, ice caps and the ice sheets of Greenland and Antarctica, represent a considerable amount of water; if this ice were to melt entirely, global mean sea level would rise by about 70 meters. Although glaciers and ice caps (GIC) represent a very small proportion of the land ice - less than one percent of its total mass - their melting has caused nearly a third of the sea level rise observed since 1971 (Church et al. 2013). Generally located in warmer regions than the ice sheets, glaciers are indeed more sensitive to climate change and are presently receding everywhere in the world (an example is shown in Figure 1-4), while the Greenland and Antarctic ice sheets (GIS and AIS) are expected to lose mass at an accelerating rate in the next decades or centuries.

For both GIC and ice sheets, two main factors contributing to mass changes are snowfall and surface melting; these two competing processes affect positively or negatively the “surface mass balance” (SMB). In addition, gravity-driven ice flow, or “ice dynamics”, result in a loss of mass at the periphery of the ice sheets by iceberg calving. The contribution of SMB to the sea-level budget is fairly well estimated, either by the application of regional surface-mass balance models forced with precipitation and temperature projections from global climate models, or by the use of statistical and upscaling relationships in the case of the numerous

glaciers. By contrast, ice dynamics are more difficult to understand and to model given the lack of observational data, the complexity of the processes at play, and the sensitivity to local parameters, for example the topography of the bedrock or the local ocean currents.

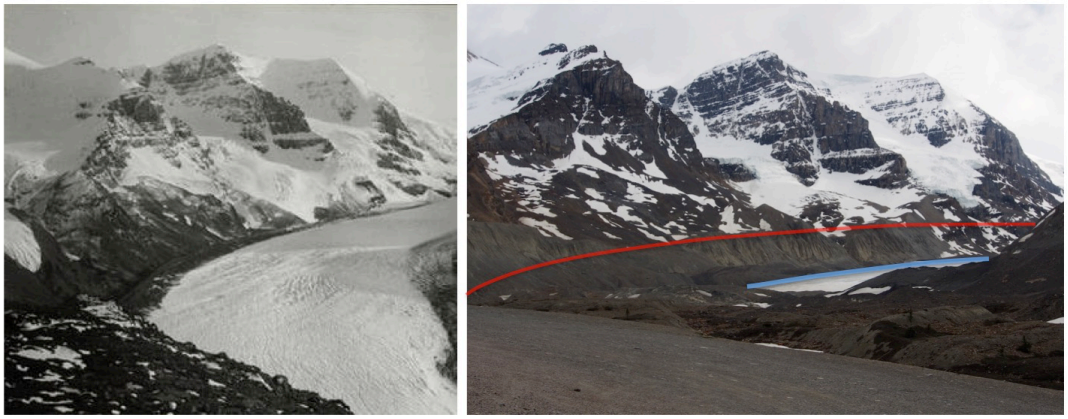

Figure 1-4. **Athabasca Glacier, Alberta, Canada**. This valley glacier is one of the five glaciers flowing out of the Columbia ice field, a remnant of the Laurentide ice sheet. Picture on the left: the glacier photographed by the artist and explorer Mary Schäffer at the beginning of the 20th century (Schäffer, 1908). Picture on the right: the glacier in June 2015. Outlined in red, the approximate trimline of the glacier on the southeast wall of its valley, as of 1908; the current surface of the glacier is outlined in blue.

Water is also stored on land in other forms, for example in snow cover, permafrost, interior seas and lakes, groundwater, fossil aquifers and man-made dammed reservoirs. Climate change and human activities are expected to alter the hydrological cycle and these terrestrial stocks, which would, in turn, affect the sea level.

Either in the form of ice or liquid water, all the mass exchanges between the land and the ocean, hereafter referred to as the "mass contribution", do not impact sea level uniformly, because they are also affected by the same geophysical processes associated with GIA: visco-elastic solid Earth deformation associated with the surface loading changes and associated changes in the gravity field; the surface mass redistribution and Earth deformation also affect the Earth's inertia tensor leading to changes in Earth rotation which, in turn, also produces deformation and gravity changes. These processes are outlined below.

First, the ocean surface – or geoid – is shaped by the irregular Earth's gravitational field and is therefore not ellipsoidal. In particular, oceanic water is attracted by land ice; when a body of ice starts to melt, the gravitational force it exerts on the surrounding water decreases according to Newton's law, and this mass of water is not uniformly redistributed across the

globe (Woodward 1888, Farrell & Clark 1976). Sea level falls in the near field, while a sea-level rise exceeding the global average is observed thousands of kilometers away in the far field (Figure 1-5). Each body of ice, either the portion of an ice sheet or GIC, generates its own gravitational field, and any rapid change in its mass therefore causes a redistribution of water across the ocean that follows a specific and unique spatial pattern called a "sea-level fingerprint" (Mitrovica et al. 2001, Tamisiea et al. 2003). In practice, fingerprints are provided as normalized fields of RSL change; to obtain the RSL change caused by the melting of a given quantity of ice, the fingerprint associated to the body of ice that is melting has to be multiplied by the quantity of melted ice, expressed in meters equivalent to a global sea level rise; here we introduce the notion of "equivalent sea level" (ESL) to refer to such a volume of ice. Figure 1-5 (bottom) shows the fingerprint of the GIS multiplied by its projected loss of mass by the end of the century in a worst-case scenario (IPCC 2013). These projections indicate that the GIS could lose an ice volume equivalent to a global sea level rise of 15 cm; in the absence of other contributions, it would cause a sea-level fall of 32 cm on the northern coast of Iceland and a rise of 18 cm in French Polynesia.

Second, the mass redistribution at the Earth's surface and the consequent deformation of the solid Earth affect its rotation vector (speed and direction), which in turn induces a deformation of both the geoid and the Earth's surface (Milne & Mitrovica 1998). These rotational effects can significantly alter the signal of RSL change and are included in sea-level models.

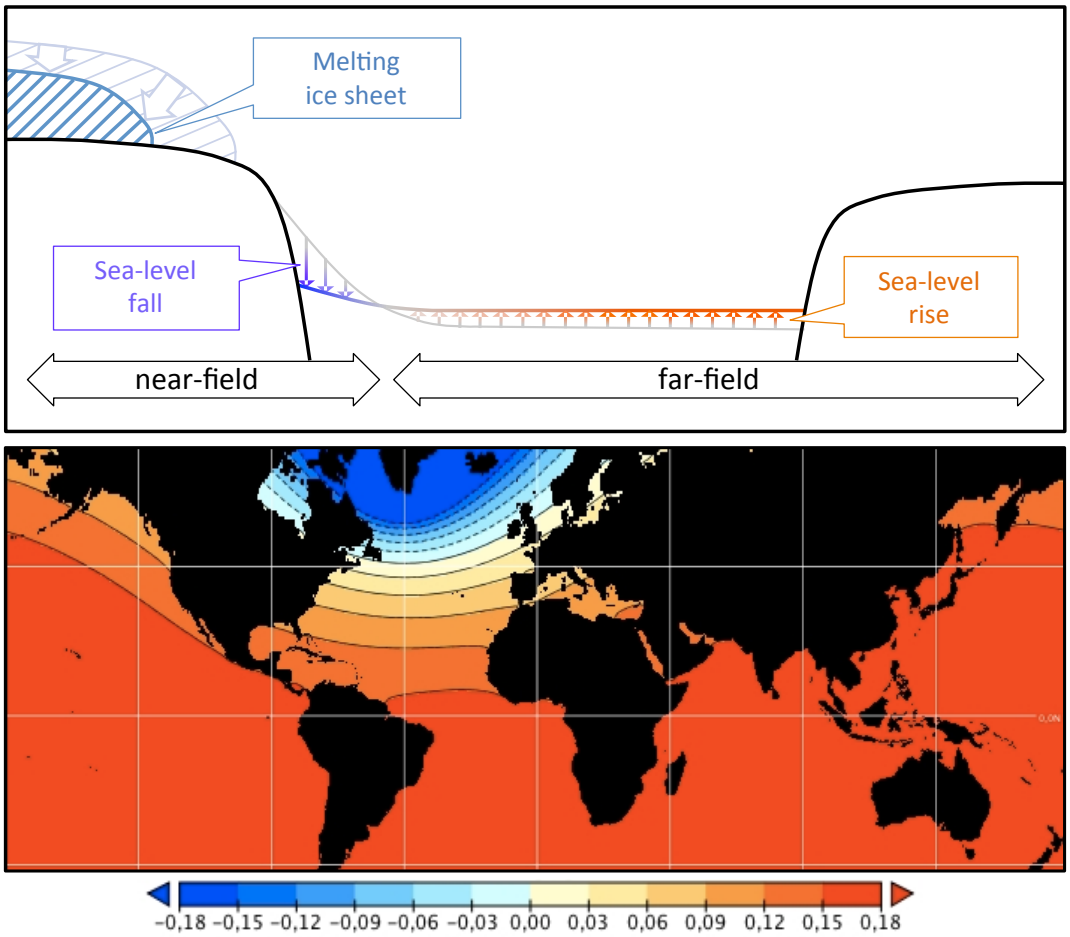

Figure 1-5. **Description of the gravitational effects of land ice melting, illustrated with projections of the Greenland ice sheet.** Top: in near-field, RSL falls (blue arrows) because the attraction force of the shrinking ice sheet weakens; water is redistributed across the globe, causing the sea level to rise in the far-field (orange/red arrows). Note that deflections of the Earth's solid surface are not shown. These are significant, particularly in near-field areas. Bottom: contribution of the GIS (SMB and ice dynamics) to RSL change (in m) between 1986-2005 and 2100 for the worst-case scenario considered by the IPCC; RSL is expected to fall in blue areas, and to rise in yellow/orange areas. This map has been generated using gridded data made available by the IPCC (Church et al. 2013).

1.2.2.3 Steric and dynamic sea-level changes

With a heat capacity a thousand times larger than that of the atmosphere and a lower albedo, the global ocean has stored more than 90 % of the solar energy accumulated in excess by the climate system during the past 40 years (IPCC 2013). Seawater expands as it warms, causing a global sea-level rise – even without water being added to the ocean. Thermal expansion is presently the dominant cause of sea-level changes at the global scale, but is not the only one at the regional scale; actually, any process that would alter the thermodynamic state or the chemical composition of a portion of the ocean would also affect the local sea level.

If the specific volume of seawater were constant, the mean (tide-free) sea surface would match the geoid. However, the ocean is a complex body of seawater characterized by non-homogenous physical and chemical properties. In particular, seawater density is a function of three parameters, namely pressure, temperature and salinity; density increases with depth and salinity, while it decreases with temperature. As a consequence, sea level in a given location depends on the profile of these three parameters along the water column. In the following chapters, sea-level changes associated with density variations are named the "steric contribution"; sea-level variations associated with temperature changes (e.g., an increase in surface heat flux) are called "thermosteric" changes, while those associated with salinity (e.g., an influx of freshwater from melting ice sheets) changes are called "halosteric" changes. Finally, when they are driven by variations in a pressure gradient, sea-level changes are referred to as "dynamic" changes.

The horizontal variability of steric sea level is illustrated in Figure 1-6. This figure shows the dynamic topography of the ocean, which is the difference between the sea surface height (measured by satellite altimetry) and the geoid height (measured by satellite gravimetry). Steric- and dynamic-driven patterns are clearly visible, for example higher sea levels in the Western Tropical Pacific, caused by geostrophic currents and higher surface temperatures, and lower sea levels in the North Atlantic (Levermann et al. 2005), where saltier water carried in by the thermohaline circulation cools down and sinks.

Regarding temporal aspects, density changes occur even without any change in external forcing. For instance, the signal observed on the tide gauge record from Papeete (Figure 1-1, bottom right) is a combination of internal oscillations of the climate system at various time scales, including seasonal variations and a multi-year oscillation. But the current imbalance of the climate system and the ongoing changes in radiative forcing are very likely to alter the spatial distribution of ocean water density on the longer term. While the thermosteric contribution, once integrated over the world's oceans, results in a significant thermal expansion component to GMSL, the halosteric contribution is almost negligible at the global scale; nonetheless, it can be dominant in regions where the influx of fresh water is significant. Variations in atmospheric pressure, atmosphere-ocean heat fluxes and wind patterns also contribute to regional sea-level changes on the long term. For instance, Lowe and Gregory (2006) showed that changes in freshwater fluxes are expected to be the dominant causes of

sea level change in the North Atlantic and the Austral Ocean, while changes in wind stress will have a more pronounced influence in the Tropical Pacific. Beside the complexity of the spatial and temporal aspects of steric and dynamic sea level, it also illustrates the fact that the ocean and the atmosphere are two highly coupled components of the climate system.

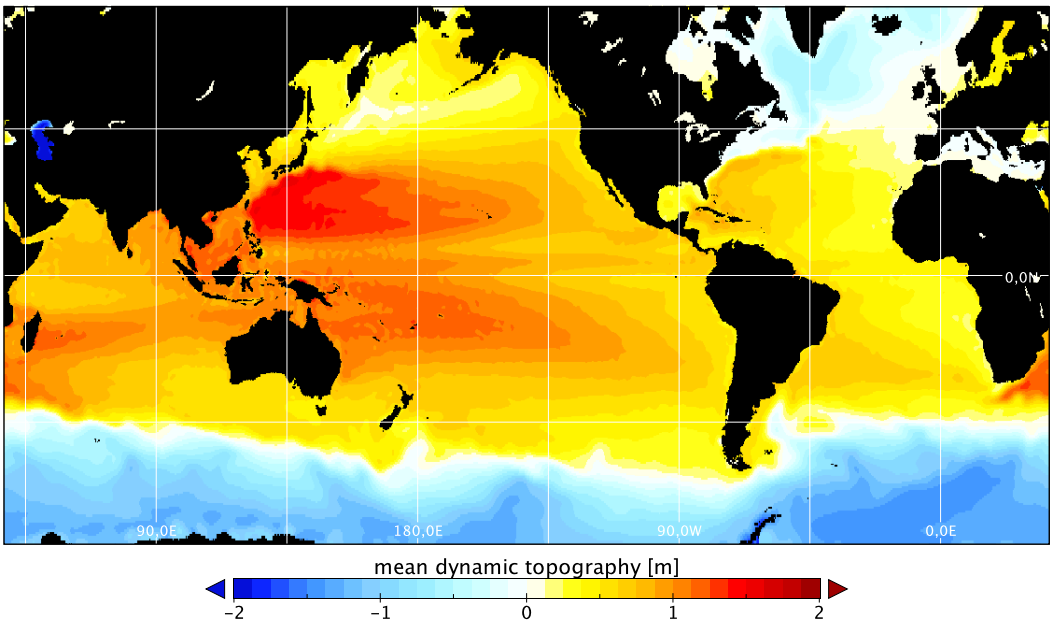

Figure 1-6. **Mean dynamic topography averaged over the past 12 years**. This map has been generated using the DTU10 mean dynamic topography gridded data (Andersen et al. 2010).

Although the terminology presented previously seems to imply that each of the processes that affect seawater density is driven by a single physical parameter, they are actually not independent from one another and cannot be analyzed or modeled separately. As a matter of fact, the equation of state that defines seawater density is non-linear and can't be solved analytically, given the complex geometry of the ocean basins and the highly dynamic boundary conditions. In practice, numerical models of various levels of complexity are applied to estimate steric sea-level changes. Among these models, the atmosphere-ocean general circulation models (AOGCMs) are of particular interest for sea-level research; some of these global climate models are commonly used to predict the evolution of ocean-related physical parameters under various forcing scenarios called "representative concentration pathways" (RCP). With some precautions, AOGCM can also be used in a downscaling approach, for example to define boundary conditions (temperature and precipitations) for ice sheet models, or even to predict sea level in a particular region. For modeling purposes, the IPCC has defined four standard RCP scenarios, corresponding to different GHG concentration trajectories throughout the 21st century (van Vuuren et al. 2011). RCP8.5, also known as the

"business-as-usual" scenario, is the worst-case scenario that is considered in Chapter 4. It is characterized by a worldwide, sustained economic growth without any mitigation measure.

1.3 Research goals and outline of the thesis

The primary goal of this thesis is to better understand past RSL changes in French Polynesia as a means to improve future projections for this region. The approach to achieve this aim is conducted in two steps. In Chapter 2, we present a reconstruction of past sea level changes based on paleo-records of the mid-to-late Holocene period. In order to develop a meaningful comparison with observations from modern instrumentation and with projections for the coming century, it is necessary to infer rates of sea-level changes at the century scale. To this end, data accuracy is critical, thus we take a deeper look into several geophysical processes that have to be thoroughly understood and quantified in order to reconstruct past sea-level changes with the desired accuracy. In Chapter 3, the reconstructed sea-level curve is interpreted with a focus on GIA and its contribution to the spatial and temporal variability of sea level in the region. Calibrating a sea-level model with the aforementioned dataset, we determine the long-term, isostatic contribution to RSL changes; removing this signal from the reconstructed sea-level curve, we then seek to estimate global changes in ice volume over the last 6,000 years, as well as regional ice and steric contributions. Finally, we suggest future avenues to fill the gaps in the existing dataset and to improve our model constraints.

As a secondary goal, we assess the ability of the French adaptation strategy to address future risks associated with sea-level rise in French Polynesia. This analysis is developed in Chapter 4. First, we conduct a literature review to identify what are the scientific inputs regarding sea-level rise that are adopted in national regulations and local risk studies. Second, we produce up-to-date, worst-case (RCP8.5) projections of sea-level rise by 2100 by estimating each of the contributions to sea-level change: the steric contribution by using recent outputs of global climate models; the mass contribution by combining fingerprints and published estimates of volume changes in ice sheets, glaciers and groundwater storage; and the isostatic contribution by using the GIA model calibrated in Chapter 3. We chose to focus on Rangiroa, an atoll of French Polynesia, and to provide projections of future sea level changes in the specific socio-economical context of this single island. However we emphasize that this case study is representative of the most part of the inhabited islands of French Polynesia, both in terms of projections and potential impacts.

CHAP 2: RECONSTRUCTING PAST SEA-LEVEL CHANGES

2.1 Introduction

In this chapter, we present two datasets that were used to reconstruct sea-level changes in the Tropical Pacific during the mid-to-late Holocene. The first one is based on field samples collected in French Polynesia (Hallmann et al. 2014) and the second one is a published sea-level curve for Christmas Island (Woodroffe et al. 2012). After presenting the proxies that were selected for their ability to accurately record sea level during a period characterized by a relative stability, we succinctly describe where these proxies were surveyed, what information was collected and how the data were processed in order to produce a series of sea-level index points. Regarding data processing, we focus on several geophysical processes and features (tides, geoidal gradient, isostatic adjustment, volcano loading) that need to be quantified in order to combine data from various sites into a single sea level curve. To conclude this chapter, we present the reconstructed sea-level curve for French Polynesia, which is interpreted in the following chapter in combination with the sea-level curve for Christmas Island.

2.2 Data description

2.2.1 Choosing suitable proxies

According to model predictions and observational evidence obtained in far-field locations, rates of sea-level changes during the mid-to-late Holocene period are relatively low, typically less than 1 mm/yr at the millennial scale. To resolve these relatively small variations in sea level, good height precision and accuracy in the sea-level reconstruction is critical. In particular, a centimeter- to decimeter-scale vertical accuracy/precision is sought.

To achieve this level of accuracy/precision, the proxies have to be (1) uncontaminated by undocumented or unpredictable causes of vertical land motion associated with, for example, tectonic activity or surface loading, (2) accessible for measurement with precise instrumentation, and (3) insensitive to weathering, wave action or other processes altering the vertical position of the proxy. In addition, (4) well-defined upper and lower hard constraints are required for an accurate reconstruction.

2.2.2 Opting for coral microatolls

A coral is usually composed of an animal called a polyp and a seawater alga named zooxanthellae. The polyp provides the algae with metabolic waste products like carbon dioxide; in return the alga photosynthesizes carbohydrates that are used by the polyp in a calcification process. The resulting calcium carbonate is then added to the skeletal structure of the reef. Because of the very nature of this symbiotic relationship, the depth range in which corals can live is restricted: on the one hand, they are limited to depths where photosynthesis can occur, and on the other hand, they can't grow above the sea surface. Therefore, corals in tropical waters are typically found in the range 0 to 30 meters (Woodroffe 2013), with certain species being found within a more restricted depth range that is dependent on environmental parameters such as temperature.

When a coral dies, its skeleton remains as a carbonate fossil. It can either remain *in situ* or be displaced by waves, currents or winds. In the first case, fossil corals can be recovered and used as proxies for past sea level. Because the depth range of living corals can be quite large and provides a hard-constrained lower limit on sea level (as they cannot live above the sea surface), corals are considered as low-level indicators, i.e., indicating the lowest possible sea level at the time they formed. Additional upper and lower soft constraints on sea level can also be inferred depending on species and growing conditions, but the resulting range would remain too large for an accurate reconstruction.

Massive microatolls are good candidates to reach the required precision and accuracy in sea-level reconstruction. The term "micro-atoll" was first used by Armand Krempf in 1927, but early attempts to explain the morphogenesis of this kind of reef were made by Charles Darwin and James Dana during the 19th century (Stoddart & Scoffin 1979). A microatoll is an individual coral colony, usually a stony coral of the genus *Porites* that has caught up with sea level and cannot grow upwards anymore. Instead it grows laterally, forming a disc-shaped, top-flat reef (Figure 2-1). Therefore, the elevation of the upper surface of a fossil microatoll allows the inference of both upper and lower limits on past sea level with a good precision, depending on growing conditions (Meltzner & Woodroffe 2015). In addition, its massive, bulky morphology makes it more resistant to weathering, which could alter the apparent height of the upper surface.

Figure 2-1. **A fossil microatoll in Maupiti Island, French Polynesia**. The ruler (white and yellow) is one meter long. Photo credit: G. Camoin.

2.2.3 Survey areas

2.2.3.1 French Polynesia

Regarding the criteria defined in Section 2.2.1, French Polynesia is a suitable place to look for sea level proxies.

First, this far-field region is not significantly affected by GIA and gravitational changes (see Sections 1.2.2.1 and 1.2.2.2) occurring in the vicinity of large ice masses, thereby the uncertainties associated with the meltwater source have little influence on RSL.

Secondly, the seafloor in this region formed 85 to 25 million years ago, thus thermal subsidence caused by lithospheric cooling is relatively small. Far from active margins, French Polynesia is also not significantly affected by tectonic-related lithospheric deformation. This area is, however, subject to intraplate volcanism, with most of its islands belonging to hotspot volcanic chains. In the highest and most recent islands like Tahiti, volcanic loading causes either subsidence in the immediate vicinity of the island, or uplift in the surrounding areas. In this case, past RSL reconstructions have to be corrected for the local vertical land movement, provided that the flexural moat can be modeled or derived from observational data.

Finally, French Polynesia has experienced a sea-level highstand during the past 6,000 years, meaning that the relevant sea-level proxies for this period are above the present sea level. It makes them far more accessible to sampling and elevation measurements, as opposed to late Pleistocene and early Holocene samples, which have to be recovered using core drilling techniques (e.g. Bard et al. 1996), usually offshore.

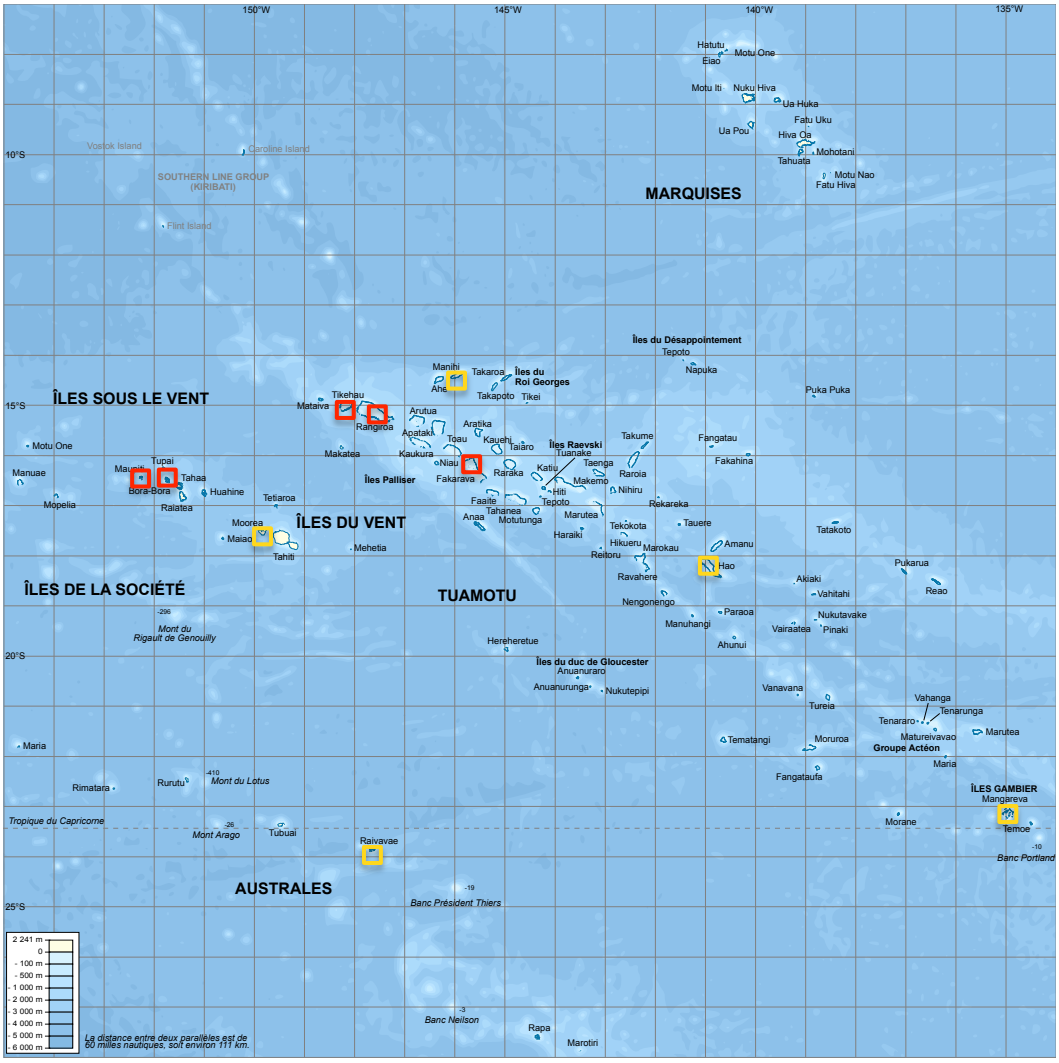

Figure 2-2. **Topographic and bathymetric map of French Polynesia indicating islands selected and surveyed for interpretation**. Red: islands selected for interpretation. Yellow: islands excluded. Map background: "French Polynesia relief map" by L. Claudel (https://commons.wikimedia.org/wiki/File:French_Polynesia_relief_map.svg), licensed under CC BY-SA 3.0 (http://creativecommons.org/licenses/by-sa/3.0/).

The main dataset presented in this chapter has been collected during three field trips in 2012, 2013 and 2014 (Hallmann et al. 2014), in five atoll islands from the Tuamotu Archipelago (Fakarava, Manihi, Rangiroa, Tikehau, Hao), and five high islands (Moorea, Bora Bora, Maupiti, Raivavae, Mangareva) from the Society, Gambier and Austral Archipelagos. At this

stage of the project, data from five islands only have been selected for further interpretation (Bora Bora, Maupiti, Rangiroa, Fakarava and Tikehau), for a total of 54 sea-level index points; islands in which only low-level indicators or isolated microatolls have been surveyed were excluded. The dataset is going to be consolidated and completed during future field trips.

2.2.3.2 Christmas Island

Christmas Island (Republic of Kiribati) is an atoll also lying on the Pacific plate, far from tectonic margins, 2300 km north of Tahiti. A large sea-level dataset has been collected in this area, allowing Woodroffe et al. (2012) to reconstruct RSL for the past 6,000 years with an exceptional continuity. No modern microatolls – which provide a reference height that the height of fossil corals can be compared to – are available near the fossil microatolls located at the center of the island, in the former lagoon, where the tidal amplitude may have been considerably attenuated. Therefore, only the fossil microatolls that were surveyed in the outer sites (Northeast Point, Southeast Point, Cecile Peninsula and Benson Point) are considered in our study, for a total of 33 sea-level index points. In Chapter 3, we use this data subset in combination with the data collected in French Polynesia in order to improve the parameter determination of our RSL model.

2.3 Data acquisition

2.3.1 Measurement of position and elevation

The position of microatolls and the mean elevation of their upper surface were measured using Global Positioning System (GPS) in carrier phase tracking mode, also known as Real-Time Kinematic (RTK). The system is made up of a base station that is set ashore at a known point, and of a mobile unit used to measure the height of the sample relative to this point (Figure 2-3). In RTK mode, GPS precision is greatly improved in comparison with the standard positioning service; the height of the sample with respect to the WGS-84 ellipsoidal datum can be measured with a precision of ± 2 cm in our case (Table 2-1).

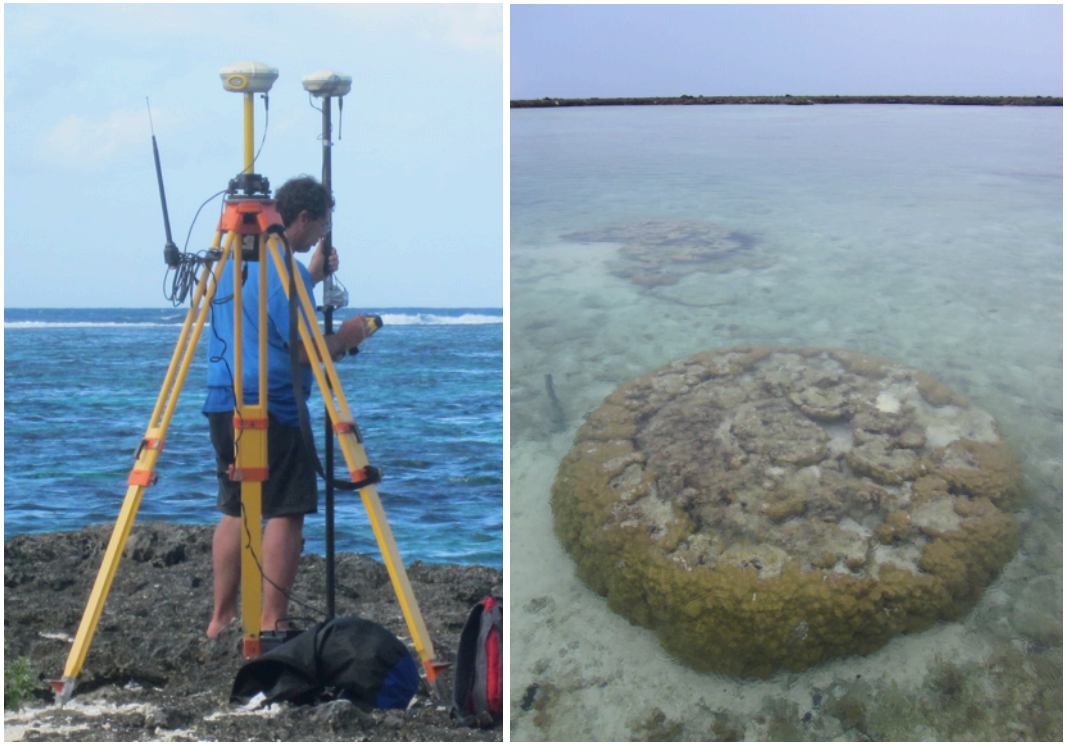

Figure 2-3. **Measuring microatolls using GPS**. Left picture: the GPS base station (yellow tripod) and the mobile unit (black pole) used to measure elevations of microatolls. Right picture: a living microatoll at sea level. Photo credits: G.A. Milne.

2.3.2 Radiometric dating

The lifetime of a microatoll typically ranges from several years to a few hundred years, with the oldest ones reaching several meters in diameter. To sample a microatoll, one solution is to use a hammer and a chisel to take a sample from the outer rim, resulting in a single sea-level index point; multiple reefs have to be sampled this way in order to collect enough data to reconstruct a curve. This first method is efficient to explore a large time frame and is suitable to quantify spatial variability of sea-level, but is not reliable to estimate rates at century scales and below, as will be discussed in Chapter 3. Alternatively, a radial slab can be removed with a saw, producing a RSL reconstruction over a shorter time frame that corresponds to the microatoll's lifetime (Figure 2-4). An individual microatoll is indeed able to keep track of yearly sea-level variations as long as environmental parameters remain stable and rates of changes in sea level do not exceed growing rates (e.g., Goodwin & Harvey 2008, Smithers & Woodroffe 2001). Such high-resolution sampling can be used to estimate sea-level changes at the century or decennial scale and complements well the first method described.

Figure 2-4. **Radial slab of a microatoll**. The ruler (yellow) is 60 centimeter long. Photo credit: A. Eisenhauer.

Uranium-thorium dating was used to date the samples of the French Polynesia dataset. To use this technique, it is assumed that the sampled corals are closed systems that exchange no isotopes with the environment after their formation (Dutton 2015), which is usually the case for the relatively unaltered fossils of the Holocene period. Nevertheless, screening procedures were followed to ensure the level of diagenesis was small. If the samples passed these criteria, the interesting isotopes are separated by chemical means and ^{238}U, ^{234}U, and ^{230}Th activities are then measured using multi-collector inductively coupled plasma mass spectrometry (MC-ICP-MS) (Fietzke et al. 2005). The age of the sample is eventually calculated based on activity ratios. In the case of samples from the Holocene period, the main benefit of this technique is the precision of measurement, with an uncertainty (2σ) of usually less than a few tens of years, a century at most.

In Christmas Island, most of the microatolls were dated using radiocarbon accelerator mass spectrometry or U-series laser ablation ICP-MS (Woodroffe et al. 2012). These techniques tend to produce greater time uncertainties, with a 2σ typically exceeding one century. Dealing with relatively large time uncertainties made it necessary to consider both time and height uncertainties when calculating data-model misfits (see Section 3.3).

2.4 Processing elevation data

As microatolls are not mean sea level (MSL) indicators, GPS-determined elevations have to be processed in order to calculate the difference between past mean sea level and present mean sea level, and to compare the results between the various survey sites. To this end, two methods are presented in the following sections. The first method consists of converting the GPS-determined elevations of the fossil microatolls to an orthometric datum; a derived method has been applied to the data that were collected during the previous field trips in French Polynesia. The second method, presented in Woodroffe et al. (2012), was applied to the Christmas Island dataset; it relies on the comparison of the fossil microatolls with their modern counterparts. It appears more accurate and robust than the first method when compiling data from large islands and distant sites. However, at the present time, observational data on modern microatolls are not available to extensively apply this method to the French Polynesia dataset.

2.4.1 First method: using an orthometric datum

The GPS elevation of the upper surface of a fossil microatoll is provided with respect to an ellipsoidal datum (WGS-84) and is an indicator of the local Mean Low Water Springs (MLWS) during its lifetime (Figure 2-5) (Woodroffe et al. 2012). To compare past and present MSL based on this single piece of information, two tasks have to be performed:

- The GPS-determined elevations of the microatolls have to be converted to elevations above the present sea surface (Section 2.4.1.1);
- The elevation of MLWS with respect to MSL has to be determined (Section 2.4.1.2).

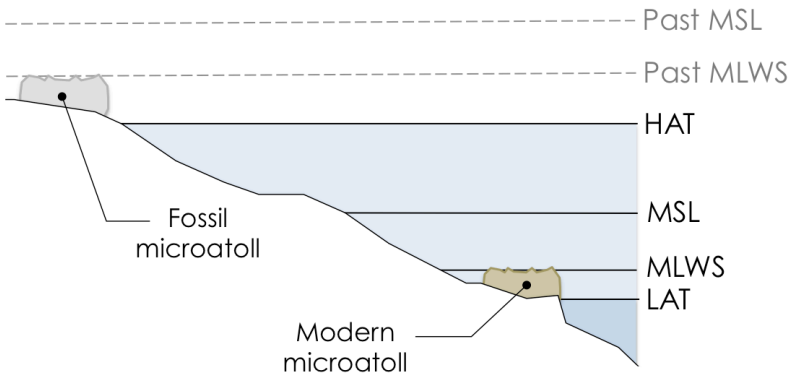

Figure 2-5. **Tide heights and microatolls**. LAT: Lowest Astronomical Tide; MLWS: Mean Low Water Springs; MSL: Mean Sea Level; HAT: Highest Astronomical Tide.

2.4.1.1 Conversion from an ellipsoidal datum to a mean sea surface

Estimating the local MSL by using GPS elevations is not a straightforward process, as the WGS-84 ellipsoidal datum is not representative of the irregular mean sea surface. In other words, the height of MSL, as it would be measured by a GPS system, is not identical everywhere. This can complicate the task of compiling data from different sites, both at the scale of a single island and of a large region, to produce a single RSL curve.

Lateral variations of the gravity field (Figure 2-6) can indeed generate significant fluctuations of MSL in the vicinity of mid-ocean, volcanic islands of French Polynesia (Cazenave et al. 1980). For instance, spatial variations of up to 1 meter of the geoid height above ellipsoidal datum have been previously observed in Christmas Island (Woodroffe et al. 2012). In addition, ocean dynamic topography is an important cause of MSL spatial variability at the regional scale, particularly across the Tropical Pacific. Dynamic topography is defined here as the height of the sea surface above the geoid and is shaped by currents and lateral variations of the atmospheric pressure. Consequently, sea surface above the ellipsoidal datum is the sum of the geoid height and the dynamic topography (Andersen et al. 2010); both short- and long-wavelength gradients associated with geoid and dynamic topography are captured by satellite altimetry (Figure 2-7).

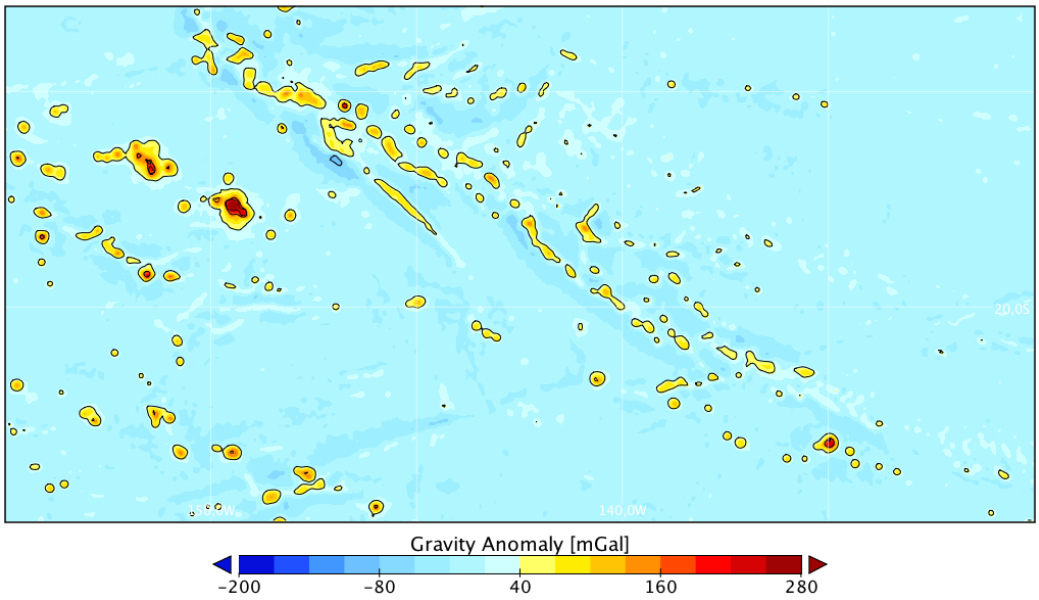

Figure 2-6. **Gravity field in French Polynesia**. This map has been generated using DTU10 gravity field model (Andersen et al. 2010).

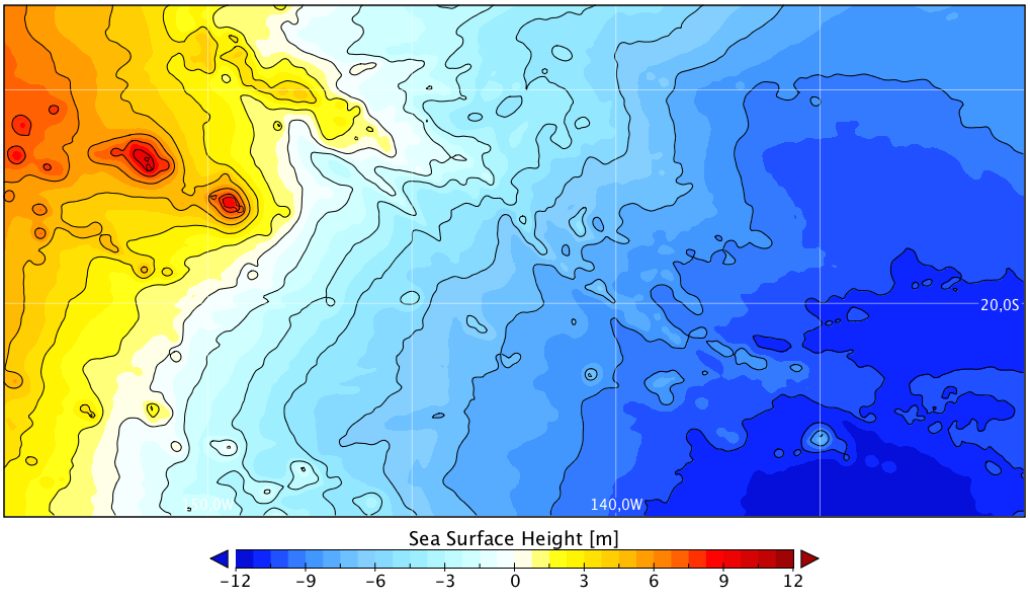

Figure 2-7. **Sea surface height above WGS-84 in French Polynesia**. This sea surface map has been generated using MSS_CNES_CLS10 mean sea surface, and converted from TOPEX/Poseidon ellipsoidal datum to WGS-84 ellipsoidal datum. MSS_CNES_CLS10 was produced by the CLS Space Oceanography Division and is distributed by Aviso, with support from CNES. Same geographic window as shown in Figure 2-6.

To address the problem, it was decided to convert the GPS-determined microatoll elevations with respect to the WGS84 ellipsoidal datum in a suitable orthometric/geodetic datum called RGPF (for *Réseau Géodésique de la Polynésie Française,* French Polynesian Geodetic Network). In each major island, this geodetic network defines altitude benchmarks that are related to the MSL using tidal measurements. These benchmarks are positioned with respect to the GRS80 ellipsoid, which differs from the WGS84 ellipsoid by up to 10 cm (ellipsoid error is reported in Table 2-1). Around benchmark sites, a local mean sea surface (MSS) is extended to the whole island using two published models of geoids, EGM96 and EGM08 (Lemoine et al. 1997, Pavlis et al. 2012); in practice the elevations above the geoid and their associated uncertainties were calculated using an application called *Circé* (IGN 2013).

Table 2-1. **Errors associated with sea level reconstruction**. Data courtesy of V. Pothin.

Site	**GPS error** (m)	**Ellipsoid error** (m)	**Elevation error** (m)	**Combined error** (m)
Bora Bora	± 0.02	± 0.1	± 0.1	± 0.14
Tikehau			± 0.1	± 0.14
Rangiroa			± 0.2	± 0.22
Fakarava			± 0.2	± 0.22
Maupiti			± 0.1	± 0.14

For the sites where no benchmark is available, or where the accuracy of the difference between the altitude datum and MSL is suspect, an alternative solution is to directly measure MSL. During the last field trip, water level loggers were deployed in several islands, including Bora Bora. They can help positioning MSL with respect to WGS-84. However, the records are short, meaning that the accuracy of the measurement can be altered by seasonal or multi-year steric sea-level variations, like those caused by El Niño Southern Oscillation (ENSO).

To determine the local MSL with respect to WGS84 and directly compare it to the GPS-determined elevations of the microatolls, an alternative method could be the use of a global mean sea surface model like CLS10 or DTU10. This method has been tested but it gave inconsistent results, especially for Fakarava where sea-level index points were far below the reconstructed sea-level curve. As these MSS models combine gravitational measurements and satellite altimetry near coastlines, their ability to precisely reproduce the sea surface around small islands is questioned.

2.4.1.2 Height of MLWS with respect to MSL

The heights of LAT and MLWS with respect to MSL are usually calculated by analyzing tide gauges records, which should, ideally, exceed 19 years in length in order to capture a full metonic cycle. Unfortunately, none of the surveyed islands are equipped with a tide gauge, except Rangiroa where permanent sea level monitoring started in 2009. Similarly, the records from water level loggers deployed during the last field trip are far too short (<2 weeks) to be used to determine LAT, or even MLWS. One alternative is to use tide prediction software, provided that the harmonic constituents for the site of interest are available (Woodroffe & Barlow 2015). Until recently, these constituents were calculated based on tide gauge records, which significantly limited the areas where predictions were valid. Nowadays satellite altimetry allows the calibration of global tide models and thus the ability to calculate constituents anywhere on the globe (Griffiths & Hill 2015).

In theory, the predicted tide height above the datum h, at time t and in location x, is given by the following equation:

$$h(t,x) = h_0 + \sum_{i \epsilon H} A_i\,(x) \cdot \cos(\omega_i \cdot t + \varphi_i(x)) \tag{2-1}$$

where h_0 is the mean sea level (MSL) above the datum, and ω_i, A_i and φ_i are respectively the angular frequency, the amplitude and the phase associated with the *i*-th constituent of the Laplace set of harmonic constituents *H*. Up to 37 constituents may be used to predict tide height in complex coastal configurations and shallow waters.

The UK National Oceanography Center defines the height of the MLWS as the average throughout the year of two successive low waters during those periods of 24 hours when the range of the tide is at its lowest (which occurs every half-lunation). Instead of analyzing predicted time series, we used a simplified approach to determine MLWS. The *h* function defined previously is minimized (or maximized) when all the summed cosines are simultaneously equal or almost equal to -1 (or 1). According to the theory of tides, this configuration is expected to occur once in every 19 years at a given location. In this particular configuration, the minimal value h_{min} of the h function, corresponding to the LAT, is equal to:

$$h_{min}(x) = h_0 - \sum_{i \epsilon H} A_i\,(x) \tag{2-2}$$

Using alternative notations and truncating summation to the eight primary harmonic constituents, the quantity (MSL – LAT), also referred to as the maximal tide amplitude, can be approximated as follows:

$$MSL - LAT \approx \sum_{i \epsilon H'} A_i \tag{2-3}$$

where A_i is the amplitude associated with the *i*-th constituent of subset *H'*, which includes the m2, s2, n2, k2, k1, o1, p1 and q1 constituents. Here it is assumed that only these eight primary constituents significantly contribute to tidal variations in mid-ocean islands. The amplitude of these constituents were extracted from the TPXO 7.2 tide model (Egbert & Erofeeva 2002). This global tide model was calibrated with TOPEX/Poseidon satellite altimetry and tide gauges, with a spatial resolution of 0.25° x 0.25°. A map representing maximal tide amplitude in French Polynesia is presented in Figure 2-8; it shows that the prevalent tide regime in the region is micro-tidal, with an amphidromic point located near Bora Bora; the maximal tide amplitude does not exceed 40 cm in the localities considered in this study.

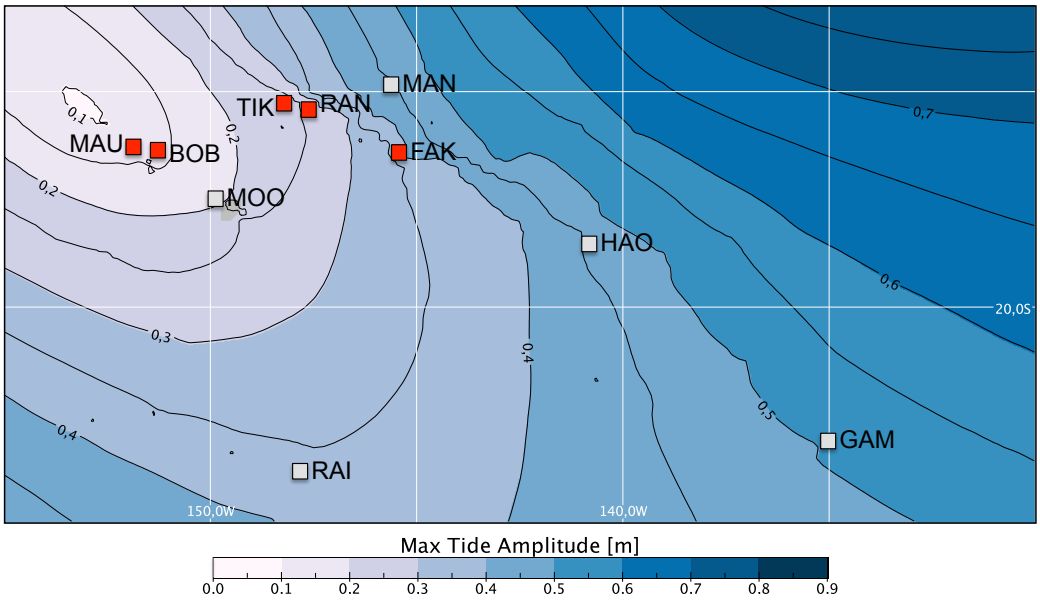

Figure 2-8. **Maximal tide amplitude**. The eight primary harmonic constituents were extracted from TPXO7.2 tide model to generate this map. Red squares: the islands considered in this study (MAU: Maupiti; BOB: Bora Bora; TIK: Tikehau; RAN: Rangiroa; FAK: Fakarava). Grey square: other surveyed islands (MOO: Moorea; MAN: Manihi; HAO: Hao; RAI: Raivavae; GAM: Gambier).

We verified the validity of this approximation for several sites, using official tidal reference levels published for French overseas localities (SHOM 2014). The French hydrographic service compiled measurements of LAT and MSL in or nearby all the islands indicated in Figure 2-8; measured and predicted values of maximal tide amplitude differ by less than 10 cm in all islands (except for Hao, which is not taken into account for further interpretation). Moreover, based on the observations of tide heights in 28 localities in French Polynesia, we developed an empirical relationship between MSL, LAT and MLWS:

$$MSL - MLWS \approx 0.7 \cdot (MSL - LAT) \tag{2-4}$$

It has to be noted that this relationship is only valid for French Polynesia and is almost exclusively based on short sea-level records; the other regions presented in the official documentation have not been examined. Nevertheless it appears consistent with what is observed in localities experiencing semi-diurnal tides; for example, the ratio is equal to 0.8 in Brest, where tide heights have been observed for decades. Combining equations (2-3) and (2-4), we can write:

$$MSL - MLWS \approx 0.7 \cdot \sum_{i \epsilon H'} A_i\,(x) \tag{2-5}$$

For each island, the correction to be applied to MLWS or the elevation of a microatoll in order to calculate the corresponding MSL is provided in Table 2-2.

Table 2-2. **Adopted tide corrections**.

Site	MSL - LAT (m)	Tide correction (m)
Bora Bora	0.12	0.08
Tikehau	0.23	0.15
Rangiroa	0.28	0.18
Fakarava	0.36	0.24
Maupiti	0.12	0.08

Finally, it has to be underlined that our method is based on the assumption that tidal amplitudes would not vary over the mid-to-late Holocene because Polynesian islands are mid-ocean islands remote from shallow waters, and because eustatic changes have been relatively small during the considered period. On the one hand, Griffiths and Hill (2015) underline that several studies make similar assumptions without justification, and on the other hand, they note that only small changes may have occurred at the basin scale for the past 7 kyr, citing regional modeling studies focusing on the North Atlantic (Hill et al. 2011, Uehara et al. 2006). Unfortunately, the evolution of the tidal regime in the mid-Pacific since the Last Glacial Maximum is undocumented so far.

2.4.2 Second method: comparing fossil and modern microatolls

The method described in the previous section combines errors and uncertainties from several sources, and the resulting error can be significant in comparison with the amplitude of the studied signal. An alternative approach consists of directly comparing past and present MLWS sea levels using the same proxy, i.e., comparing the elevation of fossil corals with their nearby living counterparts (Woodroffe & Barlow 2015). This methodology has been previously used to reconstruct sea level in Cook Islands over the last 2 kyr (Goodwin & Harvey 2008) and in Christmas Island over the last 6 kyr (Woodroffe et al. 2012). In both cases, it provided data precise enough to resolve RSL rates of a few tenth of mm/yr.

In this method, the fossil microatolls at a given site are surveyed along the nearby modern microatolls. The heights of the upper surfaces of the latter are averaged to define a so-called height of living corals (HLC). Assuming that tide amplitudes have not significantly varied over the last few millennia (as discussed previously), the difference between past and present

sea levels is obtained by comparing the height of a dated fossil microatoll and the HLC. The height uncertainty is relatively small; it combines the measurement errors of the elevation of modern and fossil microatolls (typically 2 cm for GPS/RTK, and less than a centimeter for direct leveling), and the standard deviation associated with the mean HLC (about a few centimeters).

Unfortunately, such modern microatolls were not available or not systematically sampled in French Polynesia. Based on the existing dataset, this method can be applied to three islands (Bora Bora, Maupiti and Fakarava), with a limited number of modern microatolls defining the HLC at each site.

In theory, it would be possible to define an average HLC for a whole island, as the spatial variability induced by steric effects is negligible at this scale; tide amplitude is likewise homogenous at the island scale (Figure 2-8). However, with respect to the geoidal fluctuations mentioned in Section 2.4.1.1, the domain where a given modern microatoll can be compared to the nearby fossil microatolls should be restricted depending on the local gradient of the gravity field. For example, horizontal gradients of 5 cm/km are commonly observed on Bora Bora (Figure 2-9); a difference of 40 cm in MSL above WGS-84 exists between the North West survey site (the white square in the upper-left corner), where most of the samples were collected and one modern microatoll is available, and the South East site (the white square in the lower-right corner), where no modern microatoll has been surveyed. Therefore it is suggested either to set a range of ~1 km around a given modern microatoll (but this would vary depending on the local geoid gradient), or, if no modern microatoll is available on site, to convert the HLC determined on a nearby site by using a geoid model.

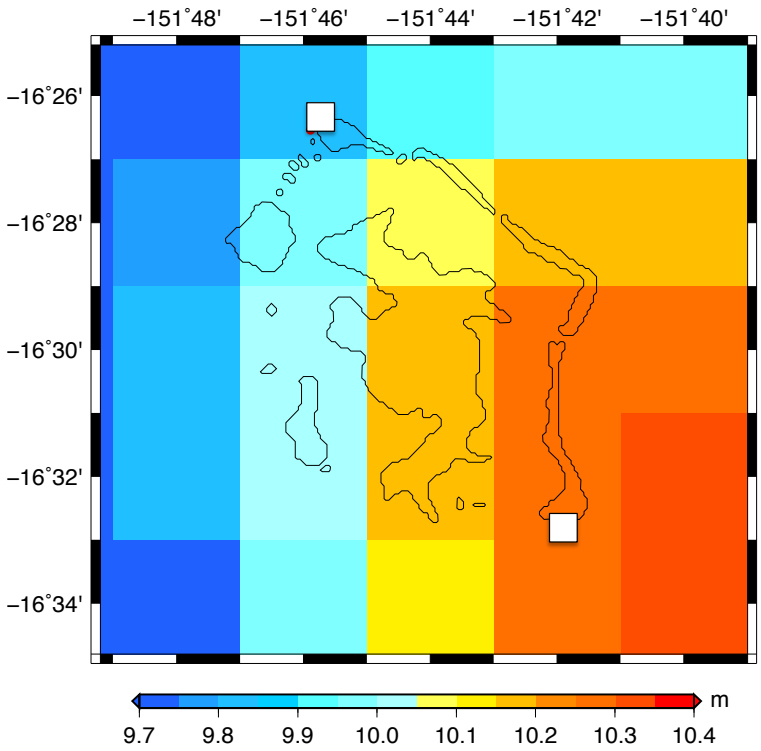

Figure 2-9. **Sea surface height above WGS-84 in Bora Bora**. This sea surface map was generated using MSS_CNES_CLS10 mean sea surface. The white squares indicate sites where microatolls were surveyed; the distance between the two sites is of 13 km.

2.4.3 Third method: measuring height with respect to the instant water level

Occasionally, heights were measured with respect to the instant water level, notably when the GPS receiver was not operational. As the date and time at which the height was estimated were not systematically reported, the water level could not be determined using tide charts. However, if these microatolls were located on one of the five islands that are selected for interpretation (see Section 2.2.3.1), they were eventually included in the dataset to fill temporal gaps. In this case, the raw estimated height above instant water level was considered, and an uncertainty equal to the maximal tide amplitude was adopted.

2.5 Reconstructing sea-level curve

2.5.1 Corrections for GIA

The elevation of samples of similar age but from remote localities can differ significantly, and this difference tends to increase with the age of the samples. One of the identified causes of such variability is GIA. To account for the GIA spatial gradient when plotting elevations from various sites on a single curve, the elevations observed in various localities across French

Polynesia have to be converted to a common datum. The sea level curve in Bora Bora was chosen for reference. GIA corrections were calculated using the models outlined in Section 3.2, applying the best-fitting model parameters estimated in Section 3.3.3.

RSL differences between Bora Bora on the one hand, and Rangiroa, Tikehau, Fakarava and Maupiti on the other hand, are not significant. Correction values are shown in Table 2-3 and barely exceed a few centimeters for the last 6,000 years. By contrast, and according to our best-fitting GIA model, the RSL in remote locations like Gambier Island or Raivavae would have been higher than in Bora Bora by more than 30 cm at 6 kyr BP.

Table 2-3. **GIA corrections with respect to Bora-Bora sea-level curve.** Corrections have been calculated using the following GIA model parameters: EUST3; LT = 71 km; UMV = 0.3×10^{21} Pa.s; LMV = 30×10^{21}.

Time (kyr)	**Correction value** (m)			
	RAN	TIK	FAK	MAU
1	0.01	0.01	0	0
2	0.01	0.01	0.01	0
3	0.02	0.02	0.02	0
4	0.03	0.03	0.02	0
5	0.04	0.04	0.03	0
6	0.05	0.05	0.04	0

2.5.2 Corrections for thermal subsidence and volcanic loading

In addition to the GIA process, vertical land motion caused by thermal subsidence and volcanic loading has to be taken into account in RSL reconstructions. Rates of uplift or subsidence as low as 0.05 m/kyr can generate decimeter-scale errors once integrated over the late Holocene period.

The only island surveyed during the field trips for which a significant subsidence rate is documented is Moorea (Pirazzoli & Montaggioni 1985), but no microatoll was available there. Regarding the islands selected for further interpretation, Bora Bora and Maupiti are high islands with ages 3.2-4.0 Myr and 4.5-4.6 Myr, respectively (Uto et al. 2007), while the atolls of Tikehau, Rangiroa and Fakarava are older; and the age of the lithosphere beneath the Tuamotus and Society Islands exceeds 50 Myr. Therefore the contribution of thermal subsidence and volcanic loading is considered to be negligible over the late Holocene and so no correction has been applied.

2.6 *The reconstructed sea-level curves*

The reconstructed curve for French Polynesia is shown in Figure 2-10. It displays a sea-level highstand during the period of interest, with a peak value of 0.9 m above present sea level and an average value around 0.6 m between 4.2 and 1.6 kyr BP. The observed trend at the millennial scale is consistent with previous observations in the Tropical Pacific, and will be further discussed in Sections 3.4.1 and 3.4.2. In addition, it should be noted that the vertical scatter in this time frame is quite large, with sea level values ranging from 0.2 to 0.9 m above present sea level. This scatter partly reflects the errors and uncertainties associated with data processing, but also suggests the existence of sea-level oscillations at the sub-millennial scale; this hypothesis is developed in Section 3.4.3.

By contrast, sea level in Christmas Island has been relatively stable over the past 6,000 years (Figure 2-11), with oscillations not exceeding 20 cm above or below present sea level. The absence of a sea-level highstand in this island, also located in the Tropical Pacific, is not inconsistent with observations from French Polynesia. This difference is studied in the next chapter using a GIA model.

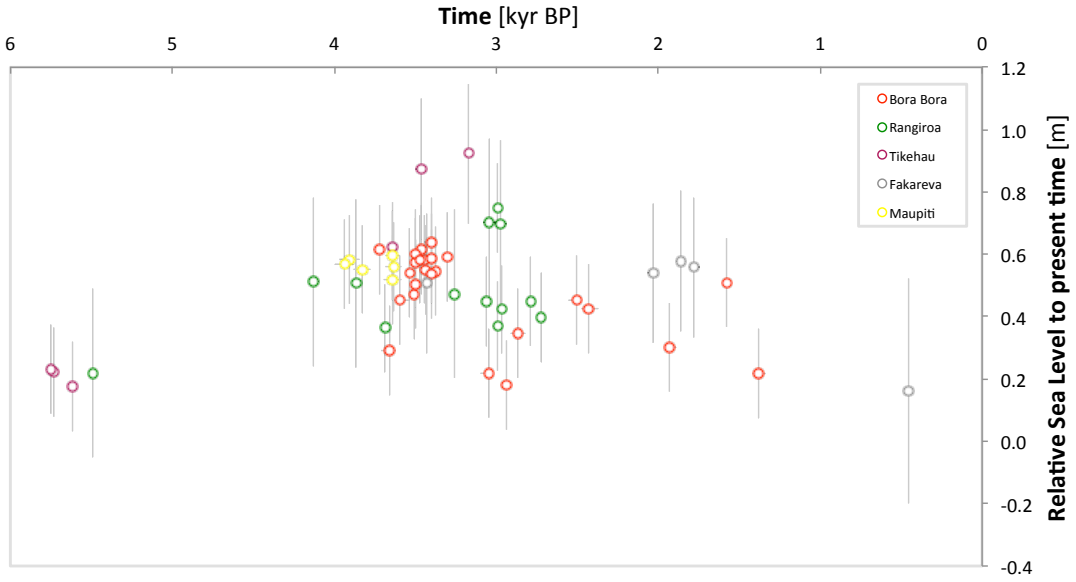

Figure 2-10. **Reconstructed sea-level curve for French Polynesia**. Elevations of microatolls from five Polynesian islands (colored plots and grey error bars). Data from Rangiroa, Tikehau, Fakarava and Maupiti are corrected to the location of Bora Bora using the following GIA model parameters: EUST3; LT = 71 km; UMV = 0.3 × 10^{21} Pa.s; LMV = 30 × 10^{21}.

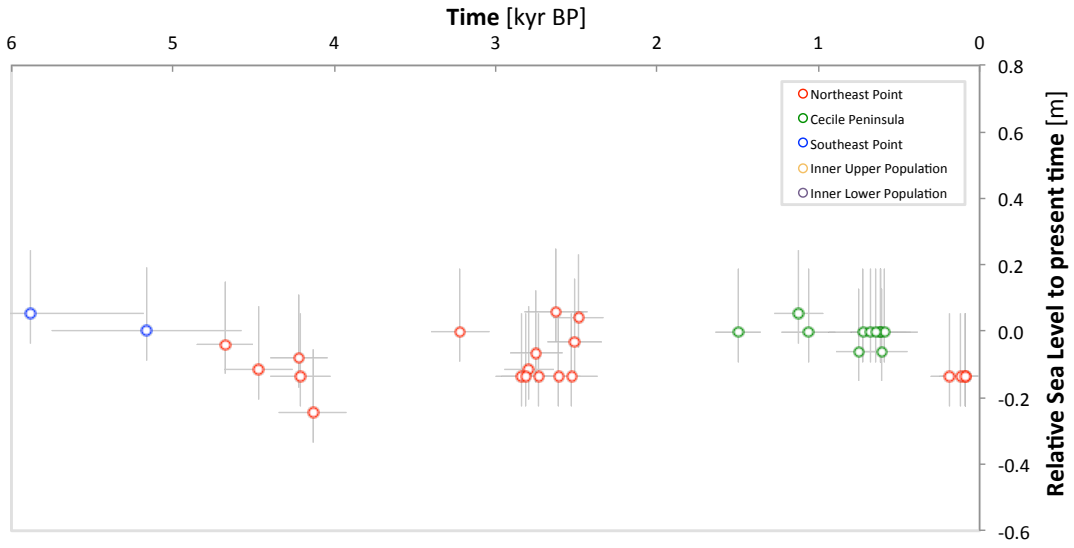

Figure 2-11. **Reconstructed sea-level curve for Christmas Island.** Elevations of microatolls from three outer sites (colored plots and grey error bars), corrected for the local geoidal gradient affecting the island (see Supplementary Material in Woodroffe et al. 2012)

CHAP 3: INTERPRETING PAST SEA-LEVEL CHANGES

3.1 Introduction

In this chapter, we interpret the reconstructed sea-level curve presented in the previous chapter with the aims of (1) quantifying and understanding the contribution of GIA to the spatial and temporal variability of past sea-level changes in the region, (2) estimating changes in global ice volume during the mid-to-late Holocene, (3) setting a baseline against which present sea-level rise in French Polynesia can be compared and (4) predicting the contribution of GIA-induced processes to future changes in relative sea-level.

To this end, we first seek to estimate long-term glacio-hydro-isostatic signal over the mid-to-late Holocene. After describing our GIA model, we perform a calibration to identify a set of model parameters that produce optimal fits to the dataset described in the previous chapter. A "best-fitting model" is then used to describe temporal and spatial variability of sea-level changes across French Polynesia. In Section 3.4.2, observational data are corrected for GIA and then compared to recent estimates of eustatic sea-level changes. In conclusion we examine these results in the context of present climate change, and based on model predictions, we also suggest next steps to be taken in terms of data collection.

3.2 Model description

The main component of our RSL model is a sea-level calculation code that computes RSL changes induced by deformation of the Earth's surface and redistribution of ice-ocean masses. The two main inputs to this code are an ice model describing the evolution of ice sheets over time, and an Earth model to predict the Earth's isostatic response to a loading history.

3.2.1 Ice models

Ice models provide topographical information on large-scale ice extent and thickness over time. This information is necessary to calculate redistribution of water masses over the globe and the consequent changes in absolute sea-surface height, but also as a component of the surface load to force deformation of the Earth model. As ice sheets grow or decay, the stress applied locally by the ice or ocean column varies, which drives in turn the deformation of

solid Earth. Two ice models are considered in this study: ICE-5G (Peltier 2004) and EUST3 (Bradley et al. 2011). ICE-5G was developed using a variety of observational constraints from both far-field and near-field locations (Peltier 2004). EUST3 is a revised version of the ICE-3G model (Tushingham & Peltier 1991) calibrated to far-field sea-level records over the last glacial and Holocene periods (Bassett et al. 2005, Bradley et al. 2011).

Both models are provided with an approximate spatial resolution of 1°x1° and time resolution of typically 0.5 or 1 kyr. This coarse temporal resolution is adapted to capture millennial-scale and longer changes over the most recent glacial cycle (~120 kyr ago to present), but does not capture lower-amplitude, higher-frequency changes in ice volume (see Section 3.4.3). In addition, sea-level rise observed since the industrial revolution (Church et al. 2013, Meehl et al. 2007) is not modeled in EUST3 or ICE-5G. Thereby, it was decided to include a linear eustatic sea-level rise of 20 cm for the past 100 years in RSL model results. This has the effect of lowering the modelled RSL curves prior to the 20th century by 20 cm and so improves the accuracy of the model calibration, as elevations of fossil microatolls are provided with respect to current sea level. A similar approach was adopted in a recent data-model comparison based on coral records from the Tropical Pacific (Woodroffe et al. 2012).

3.2.2 Earth model

Earth models are used to predict the deformation of solid Earth in response to surface loading and unloading events. In this study, the model Earth is a spherically-symmetric, compressible, Maxwell body whose response to surface loading is governed by a set of viscoelastic Love numbers (Peltier 1974). Its density and elastic properties are defined by the Preliminary Reference Earth Model (Dziewonski & Anderson 1981) and its viscous properties are varied in order to improve the data–model fit. Given the large uncertainty in Earth viscosity structure, depth paramerisation is often relatively crude and specified by the following free parameters: lithospheric thickness (LT), upper mantle viscosity (UMV) and lower mantle viscosity (LMV).

3.2.3 Sea-level calculation code

Based on the original sea-level equation by Farrell and Clark (1976), the algorithm of the sea-level code used here is the more recent version described by Kendall et al. (2005). It includes the influence of GIA-induced changes on Earth rotation (Milne & Mitrovica 1998, Mitrovica et al. 2005) and an improved treatment of time-dependent shoreline migration and marine-

based ice growth or ablation (Mitrovica & Milne 2003). Part of the complexity of the problem is that being a load component, RSL both drives and depends on GIA processes. An iterative approach is therefore required to numerically solve the sea-level equation.

3.3 Model calibration

3.3.1 Defining a parameter space

The purpose of this calibration is to determine a set of parameters that best matches the observational data described in the previous chapter. Regarding Earth model viscosity structure, the following parameter space has been explored: LT from 71 to 120 km; UMV from 0.05 to 5 × 10^{21} Pa.s; LMV from 1 to 50 × 10^{21} Pa.s. Each possible parameter set was combined with each of the two considered ice models (ICE-5G and EUST3) for a total of 486 model runs. In addition, ICE-5G was tested with its preferred Earth model characterized by a LT of 90 km and the depth-dependent viscosity profile VM2 (Peltier 2004).

It has to be noted that various combinations of ice and Earth models can give a good fit to observations. Apart from the intrinsic lack of accuracy and resolution of our dataset, this non-uniqueness issue prevents us from defining a definitive best-fitting model.

3.3.2 Evaluating goodness of fit

For each run, model results were compared to the observational data from French Polynesia. To improve model parameter determination, we took into account a recently published dataset from the nearby Christmas Island (Woodroffe et al. 2012), presented in Chapter 2. Since most of these fossil microatolls were dated using the radiocarbon method, age errors tend to be quite large compared to the Uranium-Thorium-dated corals from French Polynesia. Thus misfit calculations have been performed using a methodology (Mitrovica et al. 2000) that incorporates both age and height uncertainty in the sea-level index points. In this method, the 'distance' $DM_{m,i}$ of the ith plot of the dataset to the model curve m is computed numerically by varying time t until the following function $D_{m,i}(t)$ is minimized:

$$D_{m,i}(t) = \left(\frac{Hmdl_m(t) - Hobs_i}{\sigma H_i}\right)^2 + \left(\frac{t - Tobs_i}{\sigma T_i}\right)^2 \quad (3\text{-}1)$$

where i is the index of the observed point, $Hobs_i$ and $Tobs_i$ are the observed elevation and age of the ith point, $Hmdl_{m,i}$ is the predicted elevation at time t, σH_i and σT_i are the elevation and

age errors associated with the i[th] point. Therefore the data-model misfit χ^2 for a given model *m* is given by:

$$\chi^2 = \frac{1}{N}\sum_{i=1}^{N} DM_{m,i} \tag{3-2}$$

where *i* is the index of the observed point, $DM_{m,i}$ is the minimum of the function $D_{m,i}(t)$ as previously defined, and *N* is the total number of observed points.

In addition, a χ^2 value is defined for each dataset using an F-test in order to determine which models provide equivalent fits at the 95% confidence level. This cut-off value is equal to 1.79 for French Polynesia, 0.78 for Christmas Island, and 1.52 for the combination of the two datasets.

3.3.3 Determining a best-fitting set of parameters

Goodness of fit was examined in the first place for each dataset (French Polynesia, Christmas Island) separately. For both localities, the EUST3 ice model tended to produce the best fits (Figure 3-2a). Moreover, goodness of fit appears to be only mildly sensitive to lithosphere thickness; using the best-fitting UMV and LMV values, a local optimum was identified around LT = 71 km (see Figure 3-1).

For French Polynesia, results indicate a clear preference for average viscosity values in the upper mantle and either low or high viscosity values in the lower mantle (Figure 3-2a, top left graph). For this reason, two parameter subspaces have been defined ("low" LMV < 10×10^{21} Pa.s and "high" LMV > 10×10^{21} Pa.s) and one best-fitting parameter set was identified in each subspace. The lowest χ^2 values are achieved with the EUST3 ice model and the following Earth model parameters: LT = 71 km; UMV = 0.2×10^{21} Pa.s; LMV = 5×10^{21} Pa.s (Figure 3-3, green curve, $\chi^2 = 1.32$); and LT = 71 km; UMV = 0.3×10^{21} Pa.s; LMV = 30×10^{21} Pa.s (Figure 3-3, black curve, $\chi^2 = 1.14$); these two models provide equivalent fits at the 95% confidence level. The existence of two sets of solutions depending on LMV is consistent with the results of the inversion recently performed by Lambeck et al. (2014), although their best-fitting LMV values are slightly different (2×10^{21} Pa.s for "low" LMV and 70×10^{21} Pa.s for "high" LMV). For ICE-5G, the best fit is produced using the VM2 viscosity profile (Figure 3-3, blue curve, $\chi^2 = 2.8$), but the resulting χ^2 value is above the cut-off value.

For Christmas Island, results also show a preference for relatively low viscosity values in the lower mantle; some high viscosity values in the lower mantle also provide a relatively good fit but, unlike the Polynesian dataset, not as good as for low viscosity values (Figure 3-2a, bottom left graph). For the two subspaces previously described, the lowest χ^2 values were obtained with the EUST3 ice model and the following parameters: LT = 71 km; UMV = 0.5 × 10^{21} Pa.s; LMV = 2 × 10^{21} Pa.s (Figure 3-4, green curve, χ^2 = 0.5); and LT = 71 km; UMV = 0.3 × 10^{21} Pa.s; LMV = 30 × 10^{21} Pa.s (Figure 3-4, black curve, χ^2 = 1.27); these two models do not provide equivalent fits at the 95% confidence level. The lowest χ^2 value using ICE-5G (χ^2 = 0.79) is obtained with the following Earth model parameters: LT = 96 km; UMV = 0.5 × 10^{21} Pa.s; LMV = 2 × 10^{21} Pa.s. This value is just above the cut-off value defined for this dataset, meaning that this model and the best of the two aforementioned models based on EUST3 provide an almost equivalent fit.

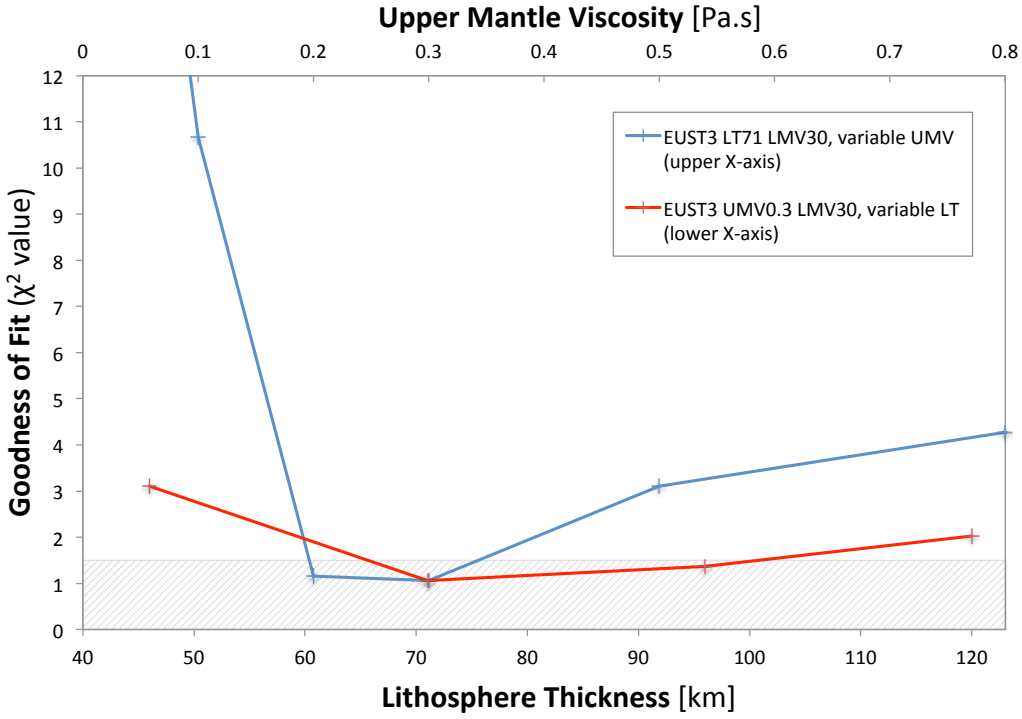

Figure 3-1. **Misfit calculation for combined datasets, French Polynesia and Christmas Island.** χ2 (per degree of freedom) is represented as a function of lithosphere thickness (lower x-axis) and upper mantle viscosity (upper x-axis), using the EUST3 ice model and a lower mantle viscosity of 30 × 10^{21} Pa.s. Points located within the grey-shadowed area represent models that provide equivalent fits at the 95% confidence level; the cut-off value defining the upper limit of this area is equal to 1.52.

The χ^2 pattern is similar for both datasets (Figure 3-2a, top and bottom graphs), suggesting the existence of a spatially-consistent solution. When combining the two datasets, a minimum χ^2 value of 1.06 was achieved using the EUST3 ice model and the following Earth model: LT = 71 km; UMV = 0.3×10^{21} Pa.s; LMV = 30×10^{21} Pa.s (Figure 3-2b). This parameter set is adopted as the "best-fitting model" and will be used in the following calculations, unless stated otherwise. It should be noted that another local minimum exists in the "low" LMV subspace, but its χ^2 value (2.37) is above the cut-off value. Regarding ICE-5G, no model provides an equivalent fit to the best-fitting model at the 95% confidence level.

Examining time series at both sites (Figure 3-3 and Figure 3-4), data-model fit is generally good between 4 and 2 kyr BP, mainly because data density is higher in this time frame. By contrast, fits tend to be poorer between 6 and 5 kyr BP for all models. This is particularly obvious for Christmas Island, where RSL has been fairly stable over the last 6,000 years. Given the overall shape of the modeled curves, no model derived from either EUST3 or ICE-5G can reproduce such a stable signal trend over the whole period.

Finally, we define a subset of nine best-fitting parameter sets using a 95% confidence cut-off value for χ^2. The model mean and its spread are shown in Figure 3-5, giving a GIA rate of -0.33 mm/yr [-0.40 to -0.24 mm/yr] at the present time for Bora Bora.

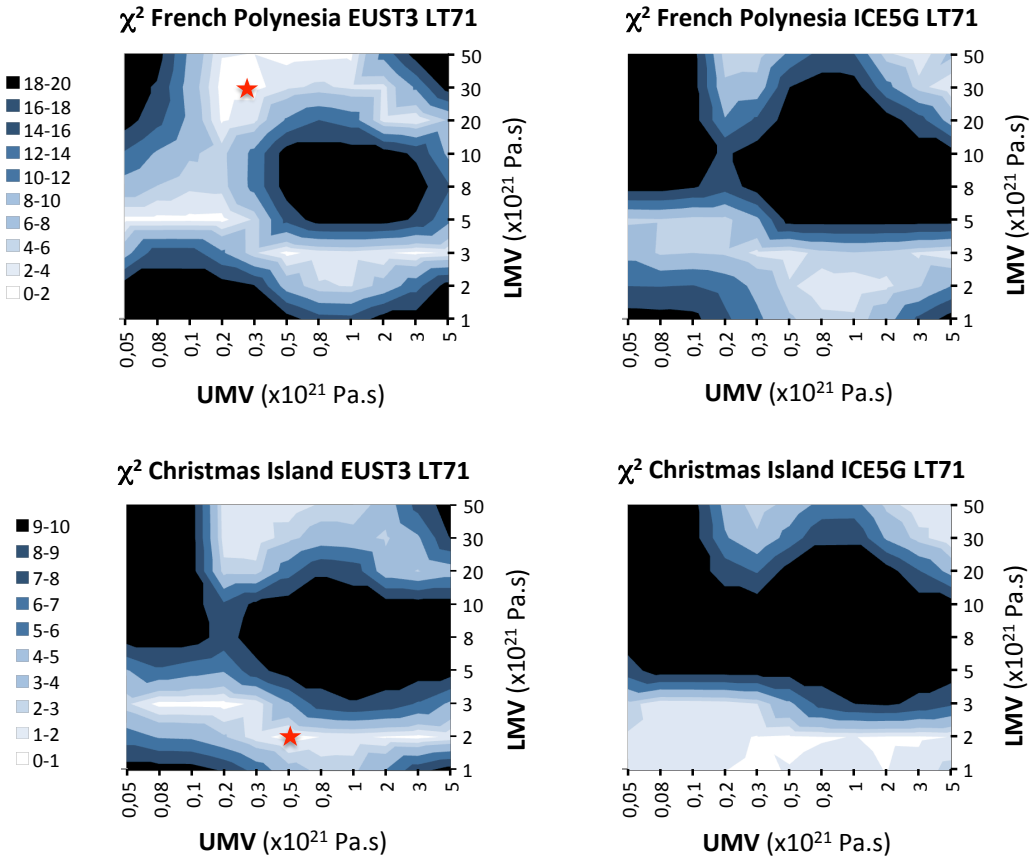

Figure 3-2a. **Misfit calculation for French Polynesia and Christmas Island datasets.** χ2 (per degree of freedom) is represented as a function of upper (x-axis) and lower (y-axis) mantle viscosity, with a lithosphere thickness of 71 km. Top left: for French Polynesia, using the EUST3 ice model. Top right: for French Polynesia, using the ICE-5G ice model. Bottom left: for Christmas Island, using the EUST3 ice model. Bottom right: for Christmas Island, using the ICE-5G ice model. Red stars indicate the best-fitting parameter sets for "low" and "high" lower mantle viscosity, respectively.

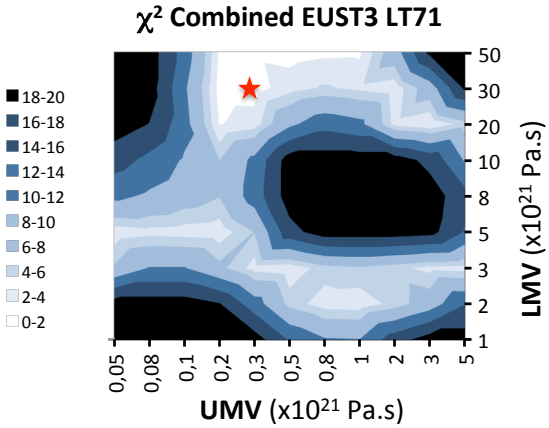

Figure 3-2b. **Misfit calculation for combined datasets, French Polynesia and Christmas Island.** χ2 (per degree of freedom) is represented as a function of upper (x-axis) and lower (y-axis) mantle viscosity, using the EUST3 ice model and with a lithosphere thickness of 71 km. Red star indicates the best-fitting parameter set.

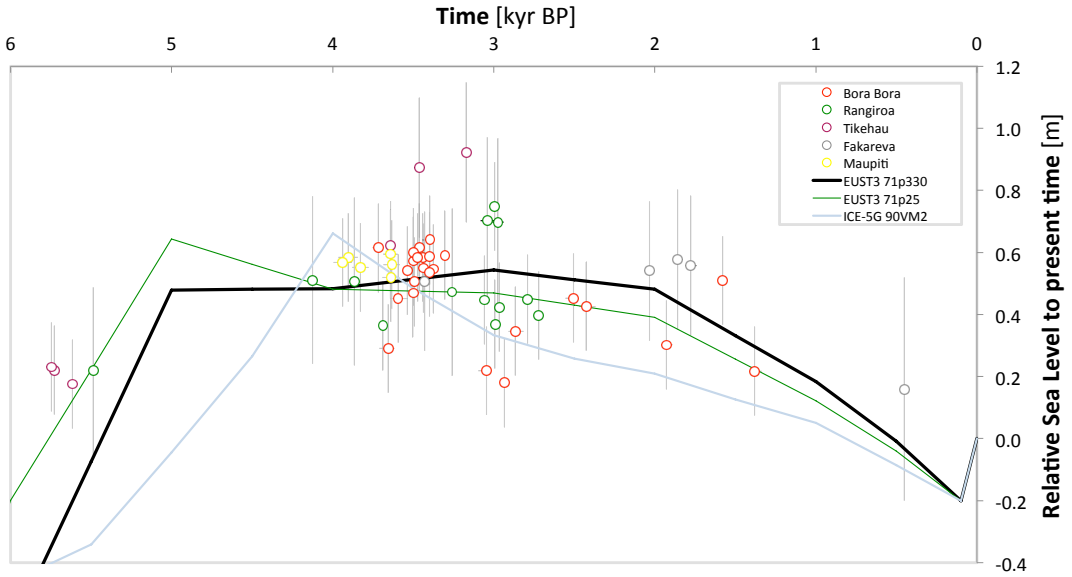

Figure 3-3. **Comparison of observations and predictions of sea-level change for French Polynesia.** Elevations of microatolls from five Polynesian islands (colored plots and grey error bars) compared to three modeled RSL curves (green curve: EUST3; LT = 71 km; UMV = 0.2 × 10^{21} Pa.s; LMV = 5 × 10^{21} Pa.s; black curve: EUST3; LT = 71 km; UMV = 0.3 × 10^{21} Pa.s; LMV = 30 × 10^{21} Pa.s; and light blue curve: ICE-5G; VM2 mantle viscosity profile).

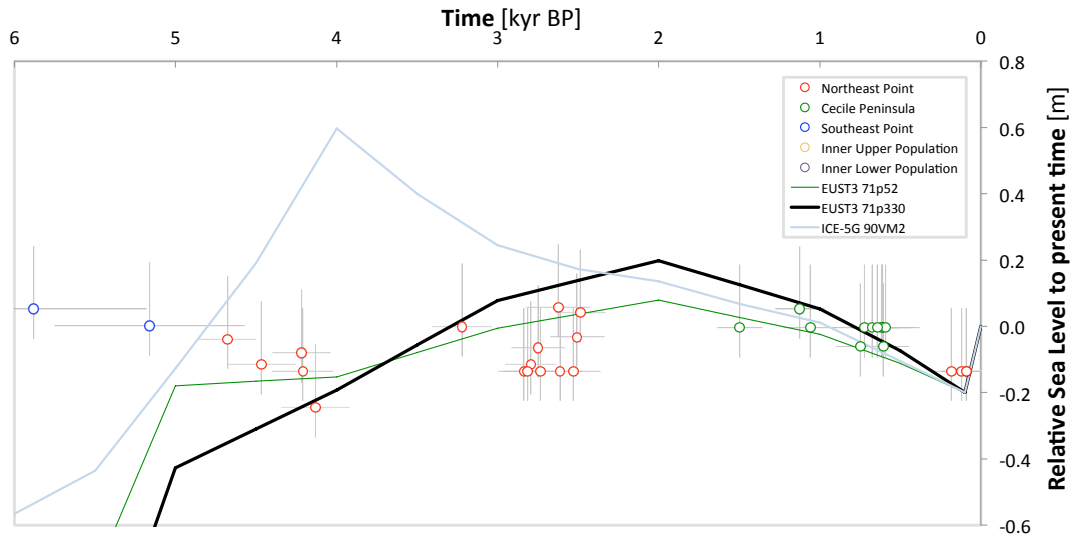

Figure 3-4. **Comparison of observations and predictions of sea-level change for Christmas Island.** Elevations of microatolls from 3 sites of Christmas Island (colored plots and grey error bars) compared to three modeled RSL curves (green curve: EUST3; LT = 71 km; UMV = 0.2 × 10^{21} Pa.s; LMV = 5 × 10^{21} Pa.s; black curve: EUST3; LT = 71 km; UMV = 0.3 × 10^{21} Pa.s; LMV = 30 × 10^{21} Pa.s; and light blue curve: ICE-5G; VM2 mantle viscosity profile).

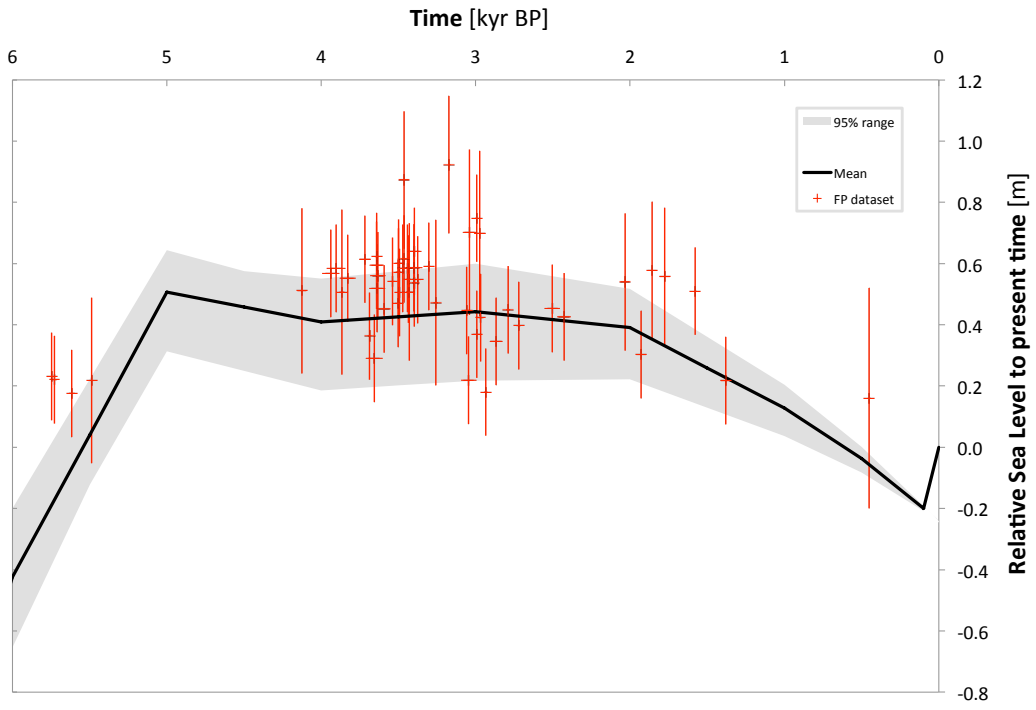

Figure 3-5. **Spread of best-fitting models.** Elevations of microatolls from five Polynesian islands (red plots and error bars) compared to the nine best-fitting models (mean value in black, spread in gray).

3.4 Model applications

3.4.1 Long-term GIA signal

In this section, we apply our best-fitting model to determine the contribution of GIA to sea-level changes. We focus not only on the temporal aspects of the GIA signal but also on its spatial variability across French Polynesia and beyond. Spatial variability of the available dataset is indeed expected to provide additional constraints on the models; on the other hand, model results can be used to identify sites where relevant data could be collected in the future.

3.4.1.1 Temporal aspects

Our best-fitting model was compared to the Polynesian dataset in Figure 3-3 (black curve). Note that data were corrected to the location of Bora Bora for comparison on a single plot, see Section 3.4.1.2 for information on spatial variability of RSL. After a sharp rise driven by the rapid melting of ice sheets until 6-5 kyr BP, the model predicts a sustained highstand from 5 to 2 kyr BP, at 0.5 m above present sea level. It has to be noted our model is relatively well constrained within this time window which includes 80% of the data.

In Figure 3-6, modeled total RSL curves in French Polynesia and Christmas Island are compared to their eustatic and non-eustatic components. For Bora Bora Island, RSL (left graph, black curve) deviates from ESL (blue curve) mainly because of delayed changes in the volume of ocean basins (orange curve), the so-called ocean syphoning effect (described in Section 1.2.2.1). Local changes in RSL (green solid curve) are negligible in comparison with eustatic changes, as the individual components of this signal (i.e. ice-load component, ocean-load component and rotational feedback) are relatively small and tend to cancel each other. After 2 kyr BP, relative sea level is predicted to fall at an almost steady rate of about 0.3 mm/yr. This rate is typical for mid-ocean, far-field regions and is consistent with observations from nearby archipelagos like Cook Islands (Goodwin & Harvey 2008). It reflects a sea-level change almost exclusively dominated by ocean syphoning. For Christmas Island, local changes in RSL (right graph, green solid curve) are significant in comparison to the ocean syphoning effect, generally causing a lower RSL than in French Polynesia. These changes in RSL are clearly dominated by the ice-load component (dotted green curve).

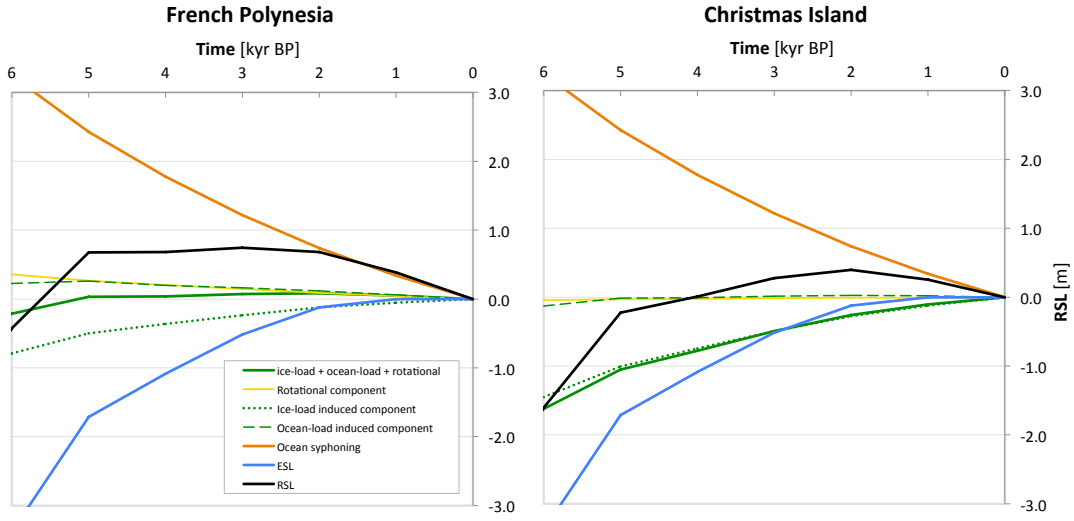

Figure 3-6. **RSL and component signals for French Polynesia (Bora Bora Island) and Christmas Island.** These sea-level curves were generated using the best-fitting model (EUST3; LT = 71 km; UMV = 0.3 × 10^{21} Pa.s; LMV = 30 × 10^{21} Pa.s). RSL (black curve) is decomposed in several signals: ESL (blue curve), ocean syphoning (orange curve) and local changes in RSL (green solid curve) induced by ice-ocean mass redistribution (dashed and dotted green curve) and rotational effects (yellow curve).

3.4.1.2 Spatial aspects

To illustrate the spatial pattern of the GIA signal, predictions of relative sea level in the South Tropical Pacific at 3 kyr BP are shown in Figure 3-7 (top left map). According to the best-

fitting model, the region is dominated by a long-wavelength NNE–SSW gradient in RSL. Three thousand years ago, sea level in Christmas Island (plotted in green) was almost the same as today, while French Polynesia (plotted in blue and light grey) sits on a ridge of positive RSL.

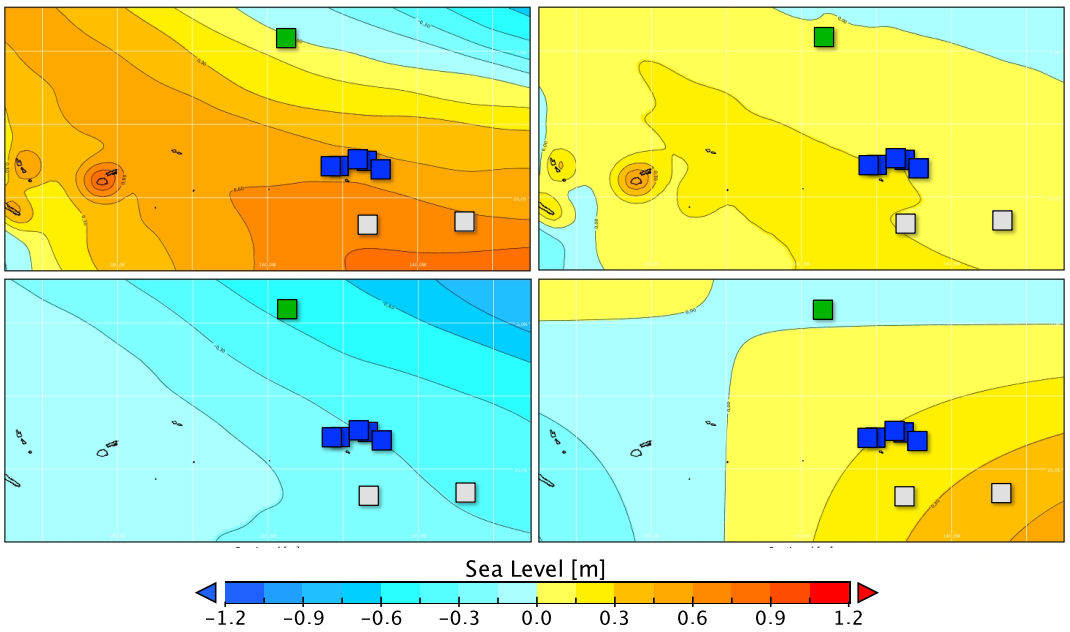

Figure 3-7. **Spatial variability of sea-level change in the South Pacific and decomposition of the GIA signal.** Top left: predicted relative sea level at 3 kyr BP with respect to present time. Included in this plot is a recent global rise of 20 cm and a net eustatic value (meltwater and ocean syphoning) of +0.51 m at 3 kyr BP. Sites plotted: Christmas Island (in green), Bora Bora, Maupiti, Tikehau, Rangiroa, Fakarava (in blue), Gambier and Raivavae (in light grey). Bottom left: ice-load induced component. Top right: ocean-load induced component. Bottom right: rotational component. These maps were generated using the best-fitting model (EUST3; LT = 71 km; UMV = 0.3 × 10^{21} Pa.s; LMV = 30 × 10^{21} Pa.s).

To interpret this result, the signal was decomposed into a eustatic value and three spatial-dependent contributions: the ice-load induced component (Figure 3-7, bottom left map), the ocean-load induced component (Figure 3-7, top right map) and the rotational component (Figure 3-7, bottom right map). On examining these figures, it appears that the ice-load induced signal significantly contributes to the NNE-SSW gradient in RSL observed in the Tropical Pacific, while the rotational feedback produces a NW-SE gradient. The latter is perceptible across French Polynesia (white and blue squares roughly indicate the extent of the area) while the former is partly responsible for the sea-level difference between French Polynesia and Christmas Island (green square). This ice-load pattern features delayed effects resulting from the melting of the Laurentide ice sheet.

3.4.2 Estimating millennial-scale ice volume changes

When the modeled GIA signal is removed from the observations, the residual provides an estimate of non-GIA contributions (plus any error in our GIA estimate). Given that the tectonic signal is negligible and the influence of volcanic loading has been corrected for, the residual most likely reflects sea-level changes due to ice volume (ESL) changes or regional changes in ocean properties leading to a steric sea-level component.

Using elevation records only, it is impossible to dissociate ice and steric contributions. While thermal expansion of the oceans over the last deglaciation was indeed negligible in comparison to the influx of freshwater from melting ice sheets, this is not necessarily the case during the mid-to-late Holocene as the large transient response of the cryosphere initiated 20,000 years ago ended around 6 kyr BP. In addition, dynamic patterns (like sea surface temperatures, atmospheric pressure, surface currents and ocean circulation, wind stress, etc.) can significantly affect regional sea level at both short (decadal) and long (millennial) time scales and may compete with eustatic sea-level changes. This is especially true in the Tropical Pacific, where ENSO is correlated with spatial variability of sea surface temperatures (SST) and sea level (Meyssignac 2012) and has shown fluctuations in intensity and frequency over the Holocene (Woodroffe et al. 2003, Cobb et al. 2013). Such variations of El Niño events could have altered the growing conditions of coral reefs (e.g. wave energy, sea temperature) on the long term and thus have influenced their living depth with respect to sea-level (Rooney et al. 2004). Given the above discussion, and that the ice volume changes inferred in the present section are based on the assumption that steric variations are insignificant over millennial time scales, the inferred volume changes should be treated with caution. It is worth noting, however, that this is a standard procedure followed in numerous past analyses of this type given the lack of additional information from which to estimate the magnitude of the steric signal.

The best-fitting model determined in section 3.3.3 was used to calculate a GIA signal that was then removed from the Polynesian dataset; the result is shown in Figure 3-8. As expected, the residual (red symbols) plots close to the EUST3 eustatic curve (black curve), except for the oldest parts of the dataset between 5.7 and 5.4 kyr BP. These microatolls, located in Tikehau and Rangiroa, are 30 to 70 cm above the model eustatic curve.

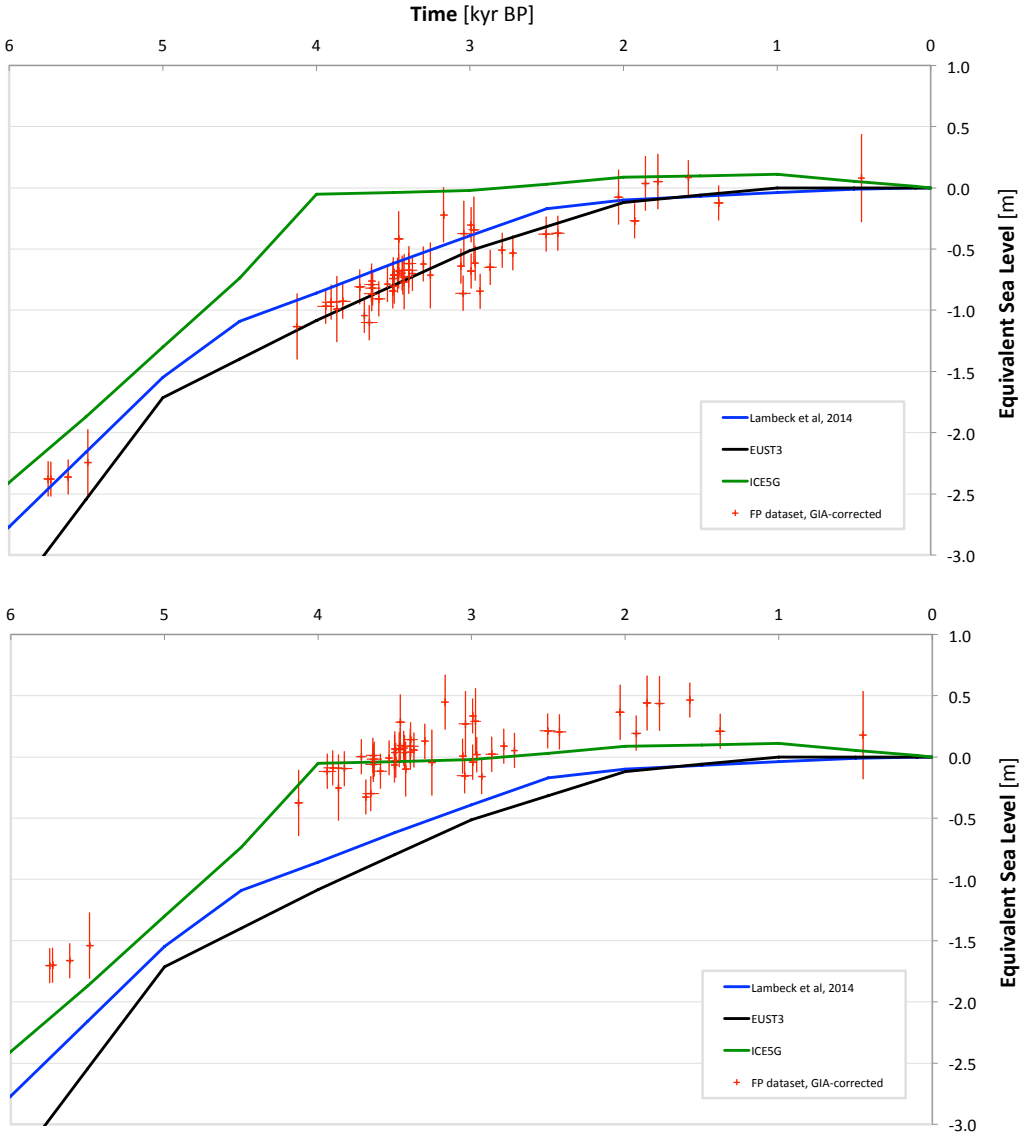

Figure 3-8. **Comparison of observations and predictions of eustatic sea-level change.** Eustatic sea-level changes (changes in ice volume only) as modeled by EUST3 (in black), ICE-5G (in green) and as computed by Lambeck et al. (2014) (in blue). Top: Observations (in red) were corrected from GIA signal based on the best-fitting model (EUST3; LT = 71 km; UMV = 0.3 × 10^{21} Pa.s; LMV = 30 × 10^{21} Pa.s). Bottom: Observations (in red) were corrected for the GIA signal based on the ICE-5G model and its preferred viscosity profile VM2.

Apart from measurement errors, several hypotheses can be made to explain such discrepancy. On one hand, our choice for the Earth model parameters can be discussed. Although displaying a lesser fit with the two combined datasets, the low-LMV model (EUST3; LT = 71 km; UMV = 0.5 × 10^{21} Pa.s; LMV = 3 × 10^{21} Pa.s) mentioned at the end of Section 3.3.3 would catch the oldest points from the Polynesian dataset and so the GIA-corrected data would match the model eustatic curve. It would also catch the oldest plots (5.2 and 5.8 kyrs,

South East Point) from the Christmas Island dataset, which are at least 60 cm above the sea level predicted by our best-fitting model. On the other hand, the accuracy of the EUST3 eustatic component around 5.5 kyr BP can be questioned, as it was in a previous regional study for the Holocene (Milne & Peros 2013). Based on sea-level data from the Caribbean Sea, the results from that study suggested that too much melting occurs after 8 kyr BP in the EUST3 model. To explore this hypothesis further, we compared our GIA-corrected dataset to recent estimates of changes in ice volume (Lambeck et al. 2014) that were obtained by analyzing sea-level records for the past 35 kyr, including nearly 1000 sea-level index points from multiple far-field locations around the world. At around 5.5 kyr BP, their model (blue curve in Figure 3-8) is in better agreement with data than the EUST3 eustatic curve. Slightly revising the EUST3 ice model toward less melt between 6 and 5 kyr BP would improve the fit with the oldest data from both datasets (French Polynesia and Christmas Island), while having a negligible impact on the dominant GIA signal until present time.

These two options illustrate a trade-off between ice and Earth model parameters, highlighting the non-uniqueness issue mentioned in Section 3.2.3. Refining ice models is beyond the scope of this study, but RSL changes between 7 and 4 kyr BP clearly require further attention. Additional observations from high-standing reefs during this period are necessary to test our model further.

3.4.3 Submillennial-scale sea-level variability

When removing the total modeled RSL from the observations, i.e., GIA plus ESL changes, the residual signal is an approximation of ice and steric contributions at sub-millennial timescales.

One aim of this study is to compare present rates and amplitudes of sea-level rise to those during the late Holocene; sub-decimetric accuracy is sought. However, uncertainties associated with the geoidal gradient (Section 2.4) and spatial GIA correction (Section 2.5) between sites are so large that the required accuracy cannot be achieved by considering the dataset as a whole. In an effort to address this issue, we examined the residual signal at each site separately, namely Bora Bora North-East and South-West, Tikehau North and South, Fakarava North and South, Rangiroa North-East and South-West. We also removed samples whose elevations were estimated visually and from isolated microatolls. Thereby, elevations at a given location can be compared to one another using WGS-84 ellipsoid as a common

datum, with the only remaining source of uncertainty being GPS measurement error. Results are presented in Figure 3-9. Unfortunately, height precision has been improved at the expense of time resolution, because the residual signal can only be examined at each individual site. In this respect, the Bora Bora North-East site offers the most comprehensive data subset, spanning 3.7 to 1.6 kyr BP.

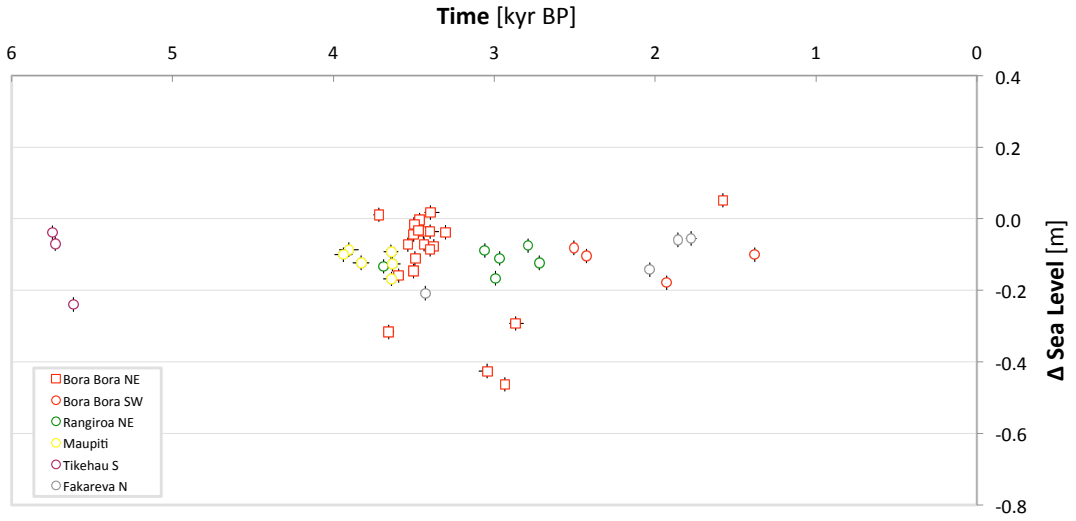

Figure 3-9. **Variability of ice and steric contributions.** Sea-level changes caused by oscillations of ice and steric contributions at submillenial scale at five sites from French Polynesia. Observations were corrected for long-term GIA and meltwater signals based on the best-fitting model. Note that inter-site comparisons and absolute values are not meaningful. Note that error bars (2σ) are indicated by black lines.

Over this period, climate-driven oscillations appear to be limited to a few decimeters in amplitude, in accordance with other observations from French Polynesia and nearby archipelagos (e.g., Pirazzoli & Montaggioni 1986, Yu et al. 2009, Woodroffe et al. 2012). A maximum amplitude is observed in Bora Bora between 2.9 and 1.6 kyr BP, with an ice-steric contribution equivalent to a sea-level rise of 52 cm, and the greatest rate observed at multi-century scales is about 1 mm/yr, due to a sea-level fall from 3.4 to 3 kyr BP. Although our dataset lacks the temporal resolution required for a useful comparison to other physical quantities that may affect sea level, we do make two such comparisons as a preliminary test for possible correlation.

First, we compare our sea-level records with sea-surface temperatures (SST) records for Bora Bora (Rashid et al. 2015) (Figure 3-10). The fall from 3.4 to 3 kyr BP and the rise between 2.9 and 1.6 kyr BP mentioned previously could be respectively linked with the decrease in

SSTs observed around 3.7 kyr BP and the increase around 2.8 kyr BP, but more samples in this period are needed to confirm a possible correlation.

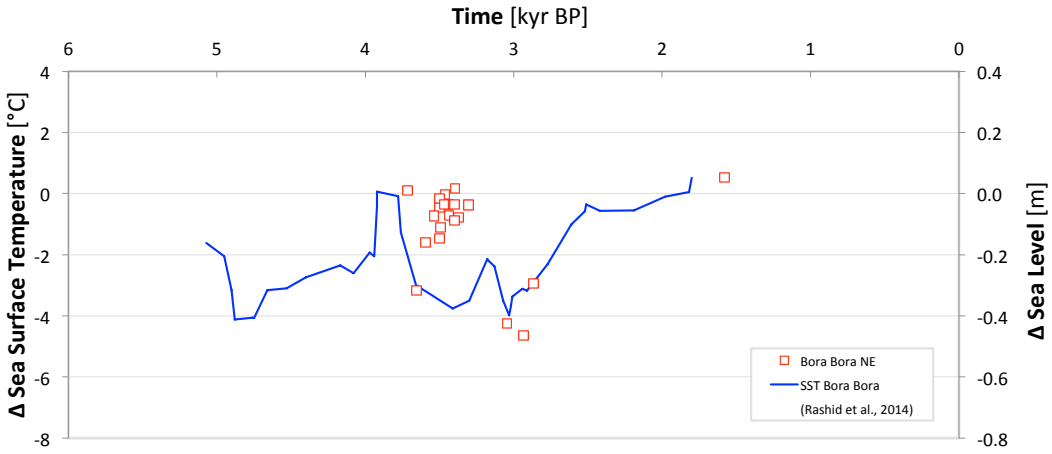

Figure 3-10. **Comparison of sea-surface temperature and sea level.** Sea-surface temperatures (blue curve) in Bora Bora (Rashid et al. 2014) compared to sea-level observations (red squares) from Bora Bora North-East site. These observations were corrected for long-term GIA and meltwater signals based on the best-fitting model.

The potential relationship between sea-level changes and variation of solar irradiance was also investigated through a published dataset of total solar irradiance (TSI); this dataset is based on cosmogenic ^{10}Be measurements in ice cores from Greenland and Antarctica (Steinhilber et al. 2009). Relative elevations from Bora Bora North-East site were compared to short-term and long-term physical quantities related to solar forcing, i.e. calculating a running-mean on the TSI reconstruction using windows of 40 and 500 years, respectively (Figure 3-11). In the absence of other sources of external forcing, the latter is thought to mirror energy intake in the deeper ocean and subsequent global thermal expansion. But, as for SST, more observations are required to establish a robust correlation.

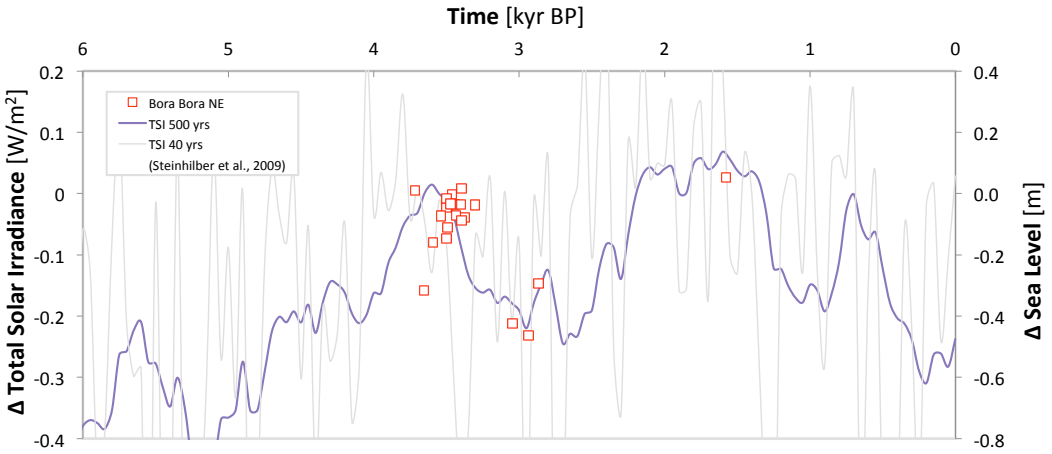

Figure 3-11. **Comparison of total solar irradiance and sea level.** Running-mean of total solar irradiance (Steinhilber et al. 2009) over the previous 40 (grey curve) and 500 (purple curve) years, compared to sea-level observations (red squares) from Bora Bora North-East site. These observations were corrected for long-term GIA and meltwater signals based on the best-fitting model.

Based on the residuals shown in Figure 3-9, it is difficult to estimate rates of change at century scales. Rates up to 2.5 mm/year averaged over 100 years are plausible, but confidence in such values is low for several reasons: (1) upper and lower peaks are defined based on single data points, without any intermediary points to confirm the upward or downward trend of the signal; (2) age errors, even though relatively low, can introduce significant uncertainty in rate calculations over short (< 100 years) periods; (3) some sources of elevation errors like weathering have not been formally taken into account.

3.5 Next steps for data collection and model improvement

Through the course of this interpretation, it appeared that the two major limitations to model parameter determination were the lack of vertical accuracy of the existing dataset, and the lack of resolution of the time series. On the other hand, diversification of spatial information would improve model parameter determination, as achieved here using the Christmas Island dataset. In this section, several suggestions are made upon the results of this analysis.

3.5.1 Reducing vertical uncertainty

As seen in Section 3.4.3, examining individual sites is a more reliable approach to accurately reconstruct sea-level oscillations at submillenial scales. Unfortunately temporal data resolution then becomes an issue because of the existence of large gaps even for the most prolific sites. As an alternative approach, it has been shown in Chapter 2 that the use of

modern microatolls as elevation references for present sea level (the methodology described in Section 2.4.2) would increase the vertical accuracy of the whole dataset. Assuming that the spatial variability of steric variations across the region is limited, systematically applying this method would allow us to combine the time series from all sites, producing a more comprehensive and accurate image of the temporal variability of sea level. Model parameter determination would also greatly benefit from a better-constrained GIA spatial pattern. It is therefore suggested to increase the number of observations of modern microatolls at the Bora Bora North-East site, and to measure a statistically significant number of modern microatolls at the Bora Bora South-West site. It would also be worth measuring the elevation of modern microatolls in localities like Rangiroa (North-East and South-West sites), where the dataset already acquired is quite large but is also affected by a geoidal gradient (see Section 2.4).

3.5.2 Filling temporal gaps

In Section 3.4.3, it has also been shown that the lack of time resolution in our time series restricts our ability to quantify rates and amplitudes of changes in RSL at submillenial scales. Given the number of points already available, the Bora Bora North-East site would be a good candidate for increasing resolution at limited costs and efforts. This could be done either by including more core samples in the existing dataset, or by reconstructing 'time slices' using slabs of fossil microatolls, as achieved by Yu et al. (2009). Time frames of higher interest are defined hereafter; acknowledging the difficulty to target reefs that have formed in a specific time window once in the field, suggestions are accompanied with coarse indications about the areas to be searched.

- *6 to 5 kyr BP*. Given the relatively high meltwater rates during this period, flat-top reefs are less likely to be found, although they would be highly valuable to improve calibration and to constrain ice melting history. Having formed before the highstand, such fossil microatolls may be found on the foreshore or just below present MLWS.

- *3 to 2 kyr BP*. The purpose of focusing on this time frame would be to detect a potential rise in relative sea level associated with the increase in SSTs reported by Rashid et al. (2014). The variation should be discernable in proxy records, as RSL was relatively steady at millennial scales according to the GIA model predictions. No clear indication can be provided with respect to the location of the relevant microatolls, however they should be found on the edge of the Holocene reef flat, between the seashore and the highest-standing fossil reefs.

- *The last millennium*. During this period, sea level has been dominated by GIA-induced processes and the resulting mean rate of change in RSL is quite well constrained by the existing dataset. However, supplementary data is necessary to reconstruct high-frequency sea-level oscillations that have the advantage of being only faintly contaminated by changes in ice sheet volumes. Moreover, a high resolution dataset for this time frame could advantageously be compared with steric sea-surface height from climate model output for the last millennium, namely the experiment 3.6 of the PIMP3/CMIP5 project (Schmidt et al. 2012, Taylor et al. 2011). Finally, such data would overlap the industrial period and could be tuned with recent reconstructions from large living microatolls growing in similar conditions, notably with respect to the ENSO regime. Regarding the area to be searched, such microatolls are most probably recolonized reefs or modern-like fossil microatolls poorly affected by weathering that ought to be found 10 to 20 cm above or below MLWS, next to modern microatolls.

3.5.3 Extending survey area

We conducted a model sensitivity study for the whole Southeast Pacific (results not shown), in which the spatial patterns of several sets of parameters have been examined. This study showed that spatial variability within French Polynesia is significant enough to be detected and used for model calibration purposes, although this exercise can be improved by increasing the vertical precision of the observations. Extending the survey area further to Christmas Island and Tarawa Island, the two ice models considered in the present study (EUST3 and ICE-5G) could be discriminated with a greater level of confidence by using only spatial information regarding the maximum sea level, and the model parameter determination would be improved in any case.

It is therefore suggested to extend the survey area to specific sites remote from Bora Bora. Given the spatial patterns provided by the best-fitting model (Figure 3-7), adding data from Gambier and Raivavae Islands (gray squares on Figure 3-7, top map) would provide improved constraints on model parameters. These two sites have already been surveyed; they both display samples whose elevations are far below the predicted local RSL, suggesting the influence of unidentified processes. However, these observations have to be consolidated. Gambier Island has only provided low-level indicators that don't fulfill the criteria defined in Chapter 2; the Raivavae Island dataset is constituted of only two fossil microatolls without any nearby modern microatolls or any indication on the elevation of present MSL with respect

to the altitude reference. Anyway, consolidated data from these two sites would provide valuable indications about the amplitude of the rotational feedback, which is predicted to be the main contributor to spatial variability within French Polynesia across a NE-SW transect (Figure 3-7, bottom map).

3.6 Conclusions

In this chapter, we identified a best-fitting RSL model that produces optimal fits to two reconstructed sea-level curves from the South Tropical Pacific. Using this model, we analyzed temporal and spatial variability of glacio- and hydro-isostatic adjustments in the region, showing that long-term RSL changes in French Polynesia are mainly correlated to eustatic changes while Christmas Island is partly affected by a local GIA process.

Our analysis shows that global ice melt has progressively decelerated during the mid-to-late Holocene, to become almost negligible after 2 kyr BP. Our best-fitting model and data are in good agreement for the last four millennia, suggesting that global mean sea level at 4 kyr BP was about one meter below present. Before 4 kyr BP, however, both datasets tend to indicate that changes in ice volume are slightly overestimated in the EUST3 and ICE-5G models. Consequently, additional observations from high-standing reefs are required for the mid-Holocene period. Of the two ice models considered, the data indicate that EUST3 is more accurate as it includes melting that ceases less abruptly in the mid-Holocene and extends longer in the late-Holocene (compared to ICE-5G).

Regarding the comparison of past and present rates of sea-level changes, the amplitude of oscillations at sub-millennial time scales appears to be limited to several decimeters. However, no precise baseline can be drawn for French Polynesia based on the existing dataset. In particular, the maximum rate of 2.5 mm/yr estimated from proxy data has to be considered with caution because our dataset lacks the time resolution needed to accurately estimate rates at century scales. Multi-century rates can be inferred with a higher level of confidence, but such rates cannot be compared in a meaningful way with recent instrumental observations like satellite altimetry or tide gauges that span over less than a century but can also capture high frequency oscillations.

In terms of projections, the mean rate of change in RSL for the last two millennia appears to be well constrained by the existing dataset. In French Polynesia, RSL is almost exclusively dominated by ocean syphoning, associated with GIA; this signal is almost linear at the millennial scale and so can be reasonably extrapolated over the coming century. Based on our model calibration, a subset of best-fitting models has been defined, allowing us to estimate a present rate of -0.33 mm/yr [-0.40 to -0.24 mm/yr] in Bora Bora. This subset of models will be used in the next chapter to make similar projections for other nearby Polynesian islands.

CHAP 4: PROJECTING FUTURE SEA-LEVEL CHANGES

4.1 Introduction

In this chapter, we first examine the aspects relative to sea-level rise in the French adaptation strategy, highlighting risks and vulnerabilities specific to French Polynesia (Sections 4.2 & 4.3). By applying recent climate models to two localities, an atoll in French Polynesia and a low-lying area on the French Atlantic coast, we then produce up-to-date, worst-case-scenario projections of sea-level rise by 2100 with the aim of identifying the main causes of spatial variability and their associated sources of uncertainty (Section 4.5). The ultimate goal of this chapter is to assess the ability of the current adaptation strategy to address future risks by comparing our projections with the inputs adopted in regulations and risk studies concerning French Polynesia.

4.2 Sea-level rise in the decision-making process

4.2.1 A challenge for insular communities

4.2.1.1 A latent threat and an aggravating factor

Among various aspects of climate change, sea-level rise poses a major challenge to low-lying coastal areas, and particularly to small islands. French overseas territories include several islands and archipelagos that are presently in the scope of policy-makers for their vulnerability to climate change (Duvat et al. 2012): Martinique and Guadeloupe in the Caribbean Sea, Wallis-and-Futuna and French Polynesia in the Pacific Ocean, Reunion Island and Mayotte in the Indian Ocean (Figure 4-1). In these regions, communities and ecosystems are increasingly exposed to the impacts of sea-level rise, while the lack of space and resources prohibits the “retreat option” as a long-term strategy.

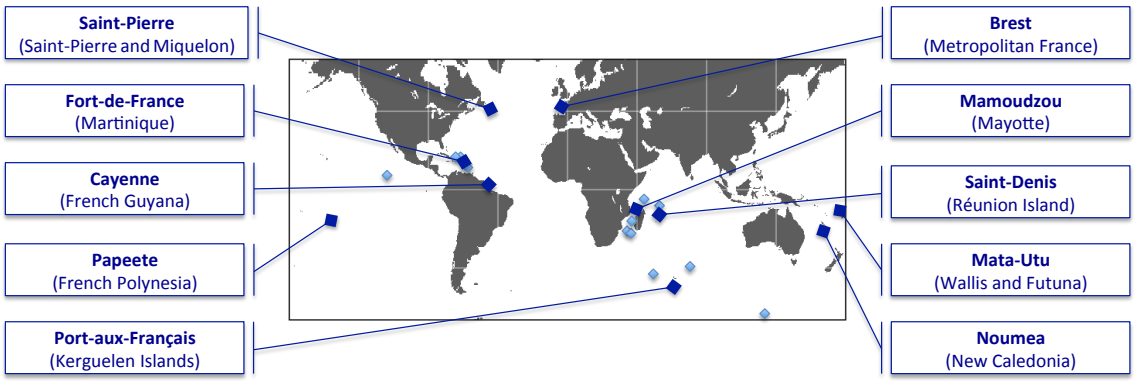

Figure 4-1. **Location of French overseas territories.** Populated French regions, departments and collectivities (in dark blue, named) and other territories and islands under French jurisdiction (in light blue). Brest (metropolitan France) is plotted on this map as a point of comparison.

As the cryosphere and the deep ocean are currently not in balance with current surface temperatures, sea level is committed to rise beyond 2100 (Levermann et al. 2013) even if a world-scale, aggressive mitigation policy is implemented. In this prospective, the most obvious and direct impact of sea-level rise is, ultimately, the complete submergence of low-lying islands and their ecosystems. In the meantime, sea-level rise is also going to have an impact via more frequent and severe flooding events.

Wind stress and low atmospheric pressure accompanying storms and cyclones generate higher sea levels near the coasts, resulting in a so-called storm surge. On the short term, surge amplitude is modulated by the tide height at the moment of the event; thus more severe flooding tends to occur during higher-than-usual spring tides. On the longer term, rising sea level also provides a higher base level for storm surges. When building upon a higher sea surface, waves of similar height and frequency can overflow seawalls, reach higher grounds and run up farther inland, and thus have greater destructive potential.

Located at the limit of the Southern Pacific Convergence Zone, French Polynesia is not spared by tropical storms and cyclones, which may be more frequent in the future (Cai et al. 2012).

4.2.1.2 Impacts in French Polynesia

In the following we list direct and indirect impacts of sea-level rise, with a focus on French Polynesia and its low-lying islands.

Coral reefs and erosion of the shorelines. With elevations not exceeding a few meters above sea level, atolls are particularly exposed to sea-level rise while being protected against wave action only by the surrounding coral reefs. Healthy reefs are able to grow and accommodate a slow and gradual sea-level rise, however this ability is threatened by the ongoing environmental changes: ocean acidification (which tends to inhibit calcification), bleaching caused by ocean warming, and also diseases and invasive species favored by rising temperature and human activities (Avagliano & Petit 2009, Petit & Prudent 2010). Regarding erosion, recent studies show that shorelines have eroded but also accreted in some atolls of French Polynesia (Le Cozannet et al. 2013, Yates et al. 2013). Apart from anthropogenic factors, shoreline dynamics seem to be dominantly controlled by wave action; sea-level rise may have also have an influence but its contribution has not been quantified so far.

Impact on biodiversity. Sea-level rise will have indirect effects on flora and fauna by destroying habitats or submersing land. For instance, it is expected to erode beaches where green sea turtles (*Chelonia mydas*) are nesting (Seminoff 2004). Endemic plant and animal species are also threatened, being unable to migrate landward; according to Bellard et al. (2013), species on French low-lying islands critically endangered at the present time will also be the most exposed species as a result of sea-level rise.

Availability of freshwater. Low-lying islands and atolls have very limited freshwater resources. Apart from direct collection of rainwater, inhabitants can only rely on fresh groundwater stored within the island substrate, floating above seawater (Underwood et al. 1992). Vegetation and crops are also dependent on these water stocks. Being unconfined, this "water lens" is fragile and can easily be contaminated by surrounding salty water as a consequence of a storm surge, drought or overexploitation (Terry & Falkland 2009, van der Velde et al. 2006, White et al. 2007), but also on the long term by sea-level rise. In an attempt to model freshwater lenses on atoll islands, Terry and Chui (2012) have shown that a sea-level rise of only 40 cm would have a major impact on freshwater availability, while, in contrast, storm surges have limited consequences over time.

Food security and cash crop. Several island communities are unable to sustain themselves by local agriculture and fisheries, therefore food and goods have to be imported from remote locations. In this unfavourable context, subsistence crops may be threatened by a diminution of the surface of arable land, leading to greater food insecurity. For instance, some sea-tolerant cultivated species like coconut tree (*Cocos nucifera*) or pandan (*Pandanus*) living along the shoreline may be damaged by storms or by shore erosion (Prasad 2013), while inland species like breadfruit (*Artocarpus altilis*) are going to be affected by the progressive salinization of land and groundwater. Another example is the taro (*Colocasia esculenta*), a traditional crop across the South Pacific; grown in swamp pits, its cultivation seems to be already affected by sea-level rise in the nearby archipelago of Tuvalu (Webb 2007). Raw resources or processed agricultural products like copra (coconut oil) are also a significant source of income for small insular communities who rely on trade and food importation to subsist. Like most of the insular communities throughout the Pacific, French Polynesia is also dependent on fisheries and aquaculture (Institut d'émission d'Outre-mer 2014), including coral reef fisheries and coastal aquaculture that are expected to be adversely affected by climate change (Bell et al. 2013).

Infrastructure and housing. Sea-level rise may progressively submerge low-lying areas, but it is also expected to enhance the destructive power of storm surges and swells. On atolls, strict zoning regulation, housing requirements and building codes are not yet implemented; critical infrastructure like energy, transportation and communication cannot be totally secured even though they are essential for disaster resilience; and tourism infrastructure, mostly based along the seashore, is intrinsically exposed to the adverse effects of sea-level rise and extreme events (Nurse et al. 2014). Apart from damage to buildings, beaches can be narrowed or washed away; this would have a negative impact on the tourism industry, which is another major source of income and resilience for Polynesian communities.

4.2.2 The need for updated and regionalized projections

4.2.2.1 Recent advances in climate-related sciences

In an effort to tackle climate change issues, French policy-makers have been building a national adaptation strategy over the last decade. Regarding sea-level rise, the national observatory for impacts of climate change (*Observatoire National sur les Effets du Réchauffement Climatique, ONERC*) made recommendations (ONERC 2010) based on the

upper bound of the "worst-case scenario"; this scenario has been defined as the highest-emission scenario (SRES A1FI) used in the IPCC's Fourth Assessment Report (Meehl et al. 2007). Considering that spatial variability of sea-level change is too complex to be taken into account, a uniform sea-level rise of 60 cm in 2100 (hereafter referred to as the "working hypothesis") was specified for further institutional work related to adaptation. These recommendations are now broadly used, both at a national level in ministerial guidelines relative to coastal flooding (Ministère de l'Ecologie 2011) and at a local level in risk prevention policies, cost-benefit analysis, land use planning or civil engineering projects.

This evaluation has not been revised so far even though our understanding of physical processes has evolved. Notably the scientific community is now able to model the atmosphere and ocean with a better spatial resolution and has included various aspects of the carbon cycle into climate models. Acknowledging these improvements, one of the goals of this chapter is to produce sea-level projections for French Polynesia using recent climate model outputs. As the worst-case scenario is more commonly used in risk assessment and decision making, our projections are based on the highest-emission scenario (RCP 8.5) defined in the IPCC's Fifth Assessment Report (Church et al. 2013).

These projections are compared to the working hypothesis specified in 2010, with the purpose of assessing the ability of current national regulations to mitigate future risks. Even though sea-level and climate projections are subject to uncertainties, such a critical analysis cannot be avoided in a strategic approach: ultimately, scientific inputs are going to be translated into long-term infrastructure investments, costly adaptation measures and mandatory land use policies.

4.2.2.2 Considering spatial variability

Spatial variability of sea-level rise is expected to be perceptible and even significant at a national scale (see Figure 4-2), with a rise of up to 20 % above the global mean in French overseas territories. It is therefore important to explore this issue, as adaptation measures relative to coastal flooding should be differentiated not only to reflect uneven vulnerabilities and capacities but also to take regional levels of risk exposure into account. To this end, two sites have been selected for a comparative study given their higher sensitivity to coastal flooding: Rangiroa, an atoll in the Polynesian archipelagos of Tuamotu (Section 4.3.1) and Ile de Sein, a low-lying island off West Brittany, on the Atlantic coast side of France (Section

4.3.2). Additionally, we decompose the total sea-level rise between 2010 and 2100 in various contributions, which allows us to identify the main causes of the projected rise in each region.

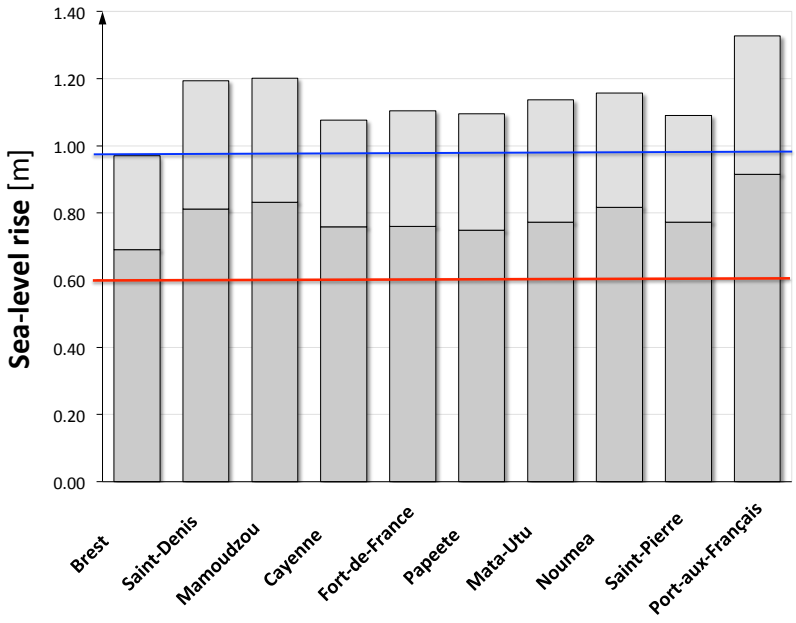

Figure 4-2. **Projected spatial variability of sea-level rise for French coasts.** Mean value (dark grey) and upper limit of likely range (light grey) of sea-level rise (in meters) for 2100 relative to 1986-2005 at several sites. In blue: global mean sea-level change (98 cm). In red: the working hypothesis adopted in French regulations (60 cm). Projections are based on gridded data compiled by the IPCC (Church et al. 2013) for the worst-case scenario (RCP8.5).

4.2.2.3 Dealing with uncertainty

As stated in Section 4.2.2.1, the question of sea-level rise reveals time lapses between scientific advances, their incorporation into adaptation strategies at the national level, and the actual implementation of relevant policies at the local level. More generally, this is one of the challenges that governments have to meet when tackling climate change: on the one hand, scientific assessment is associated with uncertainties that require further observation and research to be reduced; on the other hand, policy-makers need robust information and clear messages to overcome indecisiveness and initiate a process which is usually long-running and costly. Dealing with uncertainty and improving reactivity in science-policy interactions requires, among other things, building a flexible and integrated framework. However, such a task is well beyond the scope of this study. At this stage, we try to point out what are the major sources of uncertainties and how they may influence the spatial variability of sea-level rise along the French coasts.

4.3 Description of studied localities

4.3.1 Rangiroa

4.3.1.1 Generalities and geographic specificities

Rangiroa is located in the Tuamotu Archipelago, 360 km away from Tahiti. With 75 km in length and 30 km in width, it is the largest atoll of French Polynesia and one of the largest lagoons in the world (Figure 4-3). The atoll is composed of more than 200 islets, or *motu*, separated by *channels*, or *hoa*, that connect the lagoon to the sea (Hirsh & Hurley 2011). Housing and infrastructure are mostly located on the windward, northern end of the atoll. As of 2012, the population of the atoll was 2,567 inhabitants, mostly concentrated in the two villages of Avatoru and Tiputa.

Figure 4-3. **The southern side of the atoll of Rangiroa**. The islets on this side of the atoll are uninhabited. Picture adapted from "Rangiroa from the sky" by tensaibuta (https://www.flickr.com/photos/97657657@N00/3124177574/), licensed under CC BY 2.0 (http://creativecommons.org/licenses/by/2.0/), reframed from original.

With a mean altitude of 3 meters, and a rim of less than 600 meters wide in the inhabited areas, Rangiroa is especially sensitive to variations in sea level. Located in the vicinity of an amphidromic point, a microtidal regime prevails on Rangiroa, and tide range does not exceed 60 cm during spring tides (see Section 2.4.1). As a consequence, the foreshore is narrow; buildings are close to the shoreline (as in Figure 4-4) and are more exposed to storm surge and wave run-up, albeit the relative protection granted by the surrounding reefs. In addition,

varying tide height is only a minor component of the storm surge, leading to a nearly constant level of exposure throughout the whole duration of an extreme event.

4.3.1.2 Specific impacts and vulnerabilities

In this section we seek to highlight the main vulnerabilities of Rangiroa by reviewing the list of potential impacts presented in Section 4.2.1.

Coral reefs on Rangiroa are not permanently monitored, consequently the protection they offer in the face of sea-level rise or extreme events cannot be assessed. Nevertheless a few facts are remarkable, and among them the coral bleaching event of summer 1998 – one of the most severe events of this type ever recorded. Attributed to a strong El Niño event and SSTs higher than usual for a long period of time, it caused the loss of more than 15 % of the world's coral reefs. Rangiroa was not spared by this massive disruption in coral productivity: mortality rates of 25% to 99% were observed in the lagoon, depending on the species (Mumby et al. 2001). Although reefs have regenerated faster than expected (Roff et al. 2014), coral growth has been stunned for a few years. In the context of a warming climate associated with ocean acidification, an increase in mean SST, and a possible – but controversial – enhancement of ENSO (Collins et al. 2010), the ability of corals reefs to keep up with an accelerating sea-level rise can be questioned. Coastal erosion of the island may be another matter of concern but is also poorly documented. While a possible retreat of shorelines on the sea side is suspected by the inhabitants of Rangiroa, erosion of beaches has been clearly observed on the lagoon side (Worliczek 2013).

As for most of the atolls in the Pacific, freshwater is scarce on Rangiroa. Rainwater is the major source of fresh water and is collected in tanks; a few wells providing brackish water are available and a freshwater production and distribution program is currently developed under the supervision of the government of French Polynesia (Rios Wilks 2013), but no public or scientific information is available on the quality of groundwater and its recent evolution.

Regarding food security, situation has evolved over the last decades. Rangiroa used to be a net exporter, providing fish to Tahiti, but a decline in the fish population of the lagoon has been observed since the 90s, allegedly attributed to changes in fishing practice (Feldman & Andrews 2011). Besides the fragile balance of the ecosystem and the other negative consequences of climate change, progressive sea-level rise is not expected to impact this

sector, whereas extreme events may have a strong but temporary impact on lagoon fisheries by destroying fish traps. Another important source of income for the island is pearl farming that have been through a crisis over the last decade but still helps to maintain population in the Tuoamotus (Institut d'émission d'Outre-mer 2014). This economic sector is not directly threatened by sea-level rise or even by tropical cyclones, as the adult oysters are kept in cage; more indirectly, the spats (young oyster) nurtured in the smaller lagoons of nearby islands could be washed away by a cyclone, temporarily disrupting the supply chain (Rios Wilks 2013).

Figure 4-4. **A beach on Rangiroa, French Polynesia**. This narrow beach is located on the lagoon side, near bungalows that were upgraded in 2010; the root system of the cononut trees (visible in the foreground) helps to stabilize the shoreline. Picture adapted from "Kia Ora Resort" by dany13 (https://www.flickr.com/photos/dany13/8271446339), licensed under CC BY 2.0 (http://creativecommons.org/licenses/by/2.0/), reframed from original.

However, damage to the infrastructure hosting the aforementioned activities, or damage to other economic assets like tourism infrastructure, is recognized as a latent threat. Tuaomotus are susceptible to hurricanes especially between December and February, but with a lower occurrence than in the other archipelagos of French Polynesia. Using a retrospective analysis, Larrue and Chiron (2011) showed that Rangiroa and the surrounding islands are out of the conical-shaped cyclone track followed by most of the storms and cyclones that were observed in French Polynesia between 1970 and 2009. Although the atoll has not been directly hit by a cyclone during this period, it experienced significant surges during the cyclone season of

1982–1983. A reanalysis of the Orama-Nisha cyclone (1983) using 2-D hydrodynamic models indicates that the maximum significant wave height in front of the village of Avatoru was 5.8 m (Damlamian & Kruger 2013). Would Rangiroa be directly hit by a similar cyclone, waves of 12 m are expected, as recorded on the nearby atoll of Aana which was devastated in 1983 (Lecacheux et al. 2013). Located along the seashore, tourism infrastructure in Rangiroa has been identified for its high level of exposure to flooding risk. One of the main hotels of the atoll was closed during a year in the aftermath of Cyclone Oli in February 2010. Rios Wilks (2013) explains that about one third of its bungalows were upgraded to cyclone-proof standards and were elevated 60 cm above ground level, but the other buildings of the hotel could be entirely destroyed in case of a cyclone, according to the author.

4.3.1.3 Current inputs relative to sea-level rise at the local level

Being in the scope of national regulations about flooding risk, Rangiroa has the obligation to issue a risk prevention plan (*Plan de Prevention des Risques,* PPR), like 45 other communes of French Polynesia. Prescribed since 2005[2], this PPR has not yet been issued as of February 2014. Given the complexity of the assessment to be conducted, two public research offices – the French Geological Survey (*Bureau des Recherches Géologiques et Minières*, BRGM) and the Applied Geoscience and Technology Division of the Secretariat of the Pacific Community (SPC Division) – have provided support in the form of a suite of technical reports.

The first report (Lecacheux et al. 2013), issued under the ARAI project, is a probabilistic evaluation of swell and storm surge in French Polynesia. Focused on Tahiti and Moorea, this study should be extended in the future to other communes like Rangiroa, pursuant to an agreement[3] signed in 2002 between the government of French Polynesia and the BRGM. The noticeable point is that a sea-level rise of 50 cm by 2100 has been taken into account in this study, based on regional projections made by Slangen et al. (2011).

The next two studies (Damlamian et al. 2013, Damlamian & Kruger 2013) are surge and flood projections based on 2-D hydrodynamic models and wave inundation models. Focused on Rangiroa, the outcomes of these studies are applicable to land planning and have been

[2] "Arrêté n°645 CM ordonnant l'établissement du plan de prévention des risques naturels prévisibles de la commune de Rangiroa" (2005)

[3] "Convention BRGM / Territoire de la Polynésie Française n°2.2513 relative à la prévention des risques naturels" (2002)

integrated by the urbanism department of French Polynesia[4]. However the models have been developed for the present time and no sea-level rise has been taken into account, meaning that any future projection of flooding events solely based on these studies would underestimate the risk.

The last report (Rios Wilks 2013) is a cost-benefit analysis (CBA) exploring various options in terms of adaptation to storm surge in Rangiroa. Although the study period is 50 years, sea-level rise occurring during this period is not considered. It appears that a single type of extreme event is considered in this preliminary analysis, i.e., a surge with a significant wave height of 12 m and a return period of 50 years. In this case, the contribution of sea-level rise would be negligible.

The municipality of Avatoru has recently defined a setback zone in which building or maintenance is prohibited. Even though this area is one of the most populated places of the island, Rios Wilks (2013) notes that owners are not going to be compensated for the loss of value of their land. At the present time, compliance to this regulation is problematic; according to a public official, "the mere thought of moving to a different plot of land is unacceptable for many people inhabiting the red [setback] zone […] and the people feel a strong connection to their land." (Rios Wilks 2013: 16). To improve compliance, the author suggests informing the population more clearly about the potential damage.

4.3.2 Ile de Sein

A succinct description of Ile de Sein is proposed here as a point of comparison with the focus of our case study, Rangiroa.

Located less than 10 kilometers west of the continent, Ile de Sein is a prime example of the threat posed by sea-level rise on the French Atlantic coast (de la Baume 2012). With a mean altitude of 1.5 meters, this flat and treeless island is constantly exposed to winds and waves (Figure 4-5) and does not benefit of any natural protection, like a coral barrier. But in contrast to Rangiroa, the maximal tide range in Ile de Sein exceeds 6 meters. In this prevalent macro-tidal, semi-diurnal regime, storms can only trigger a severe flooding at high tide, during the

[4] These studies are available on the website of the urbanism department, in the section of the ongoing projects related to coastal flooding. URL: http://www.urbanisme.gov.pf/spip.php?rubrique244

spring tide period, and the actual duration of the flooding event is limited in time, a few hours at most.

Figure 4-5. **Ile de Sein**. "Ile de Sein depuis la pointe du Raz." by philippematon (https://www.flickr.com/photos/philippeos/10036553666). Licensed under CC BY 2.0 (http://creativecommons.org/licenses/by/2.0/). Reframed from original.

More than 1,200 people used to live on the island before 1940, but a shift in lifestyle and the decline of fish stocks hampered, among others, the development of the island, leading to an urban migration (Commissariat général au développement durable 2009). Today, its sole economic resource is tourism: a hundred people live on the island all year round, but in summer, the population is increased tenfold. In any case, Ile de Sein can hardly be self-sufficient and its adaptation capacities are dependent on public subsidies, for instance when it comes to reinforcing dikes (Conseil général du Finistère 2013).

Since 1989, a state of natural disaster has been declared four times for the commune of Ile-de-Sein. In particular, costly work has been undertaken in the aftermath of Cyclone Emma in 2008 (Demey 2013). It includes the repair and the reinforcement of seawalls, the creation of a disaster response headquarter, and the hardening of vital equipment like the desalination plant and the power generators – the island is isolated from the electricity grid.

As for Rangiroa, risk prevention policies face a strong public opposition on the island, and no PPR has been issued or even prescribed[5]. In a comprehensive study about risk perception in Ile-de-Sein, Oiry (Oiry 2011) highlights the objections of the inhabitants to the implementation of setback zones, and among them the perception that top-down approaches and nation-wide policies are irrelevant in the face of local issues. In that respect, proposing regionalized sea-level projections would be a first step to address this argument.

[5] The commune does not appear on the official list available at: http://www.finistere.gouv.fr

4.4 Methodology for sea-level projections

In this study the following contributions to sea-level change were considered: ocean warming and the associated steric and dynamic changes (Section 4.4.1), changes in ocean mass caused by melting land ice and land water storage (Section 4.4.2), and glacial isostatic adjustment (Section 4.4.3). Methods to estimate each of these contributions are similar to those used by the IPCC (see Supplementary Material in Church et al. 2013), but using slightly different datasets, sea-level fingerprints and climate model outputs. Based on the above processes, the total predicted change in RSL is formalized as follows:

$$\Delta SL(\varphi, t) = SL(t) - SL(t_0) = \Delta SLs(\varphi, t) + \Delta SLm(\varphi, t) + \Delta SLi(\varphi, t) \quad (4\text{-}1)$$

where $\Delta SL(\varphi,t)$ is the sea-level change at location φ between t_0 and t, and ΔSLs, ΔSLm, ΔSLi are respectively the steric, mass and isostatic contributions to this sea-level change. The baseline year t_0 for the time series is 2006; for projections of sea-level rise between 2010 and 2100, meaning calculations were performed in order to smooth sub-decadal oscillations: at the beginning of the period, the mean sea level over 2006-2015 was adopted for the 2010 value, and at the end of the period, the mean sea level and the mean rate over 2091-2100 were used to determine a value for 2100.

4.4.1 Steric contribution

Steric contribution to sea-level change at a given location can be described as the sum of two components: the global average thermal expansion, which mirrors global heat uptake by the oceans; and the local change in sea surface height, which are caused by energy transfer within the coupled atmosphere-ocean system.

These two physical variables are modeled in the Coupled Model Inter-comparison Project phase 5 (CMIP5) (Taylor et al. 2011), in which they are referred to as '*zostoga*' (steric sea level change, global average variable) and '*zos*' (sea surface height above geoid, gridded variable). For this study, the most recent model experiment outputs of 15 CMIP5 Atmosphere-Ocean General Circulation Models and Earth System Models (Table 4-1) were used. For a given model *m* forced with a given emissions scenario (RCP8.5 in the present case), change in sea level is equal to:

$$\Delta SLs_m(\varphi, t) = \Delta zga_m(t) + \Delta z_m(\varphi, t) - (t - t_O) \cdot \delta_m(\varphi) \quad (4\text{-}2)$$

where *Δzga* is the change in global average (*zostoga*), *Δz* is the change in local sea level (*zos*), and δ is the model drift correction, as explained below.

Table 4-1. **Climate models used for calculating the steric contribution and global mean steric sea-level change.** These atmosphere-ocean general circulation models or Earth system models were developed under the fifth phase of the Coupled Model Intercomparison Project. Sea level changes are calculated for scenario RCP8.5.

Model	Global steric sea-level rise (m e.s.l.)
ACCESS1-0	0.333
bcc-csm1-1	0.249
bcc-csm1-1-m	0.247
CCSM4	0.261
CSIRO-Mk3-6-0	0.310
CCCma-CanESM2	0.272
GFDL-ESM2M	0.307
HadGEM2-CC	0.269
HadGEM2-ES	0.268
inmcm4	0.215
MIROC-ESM	0.457
MIROC-ESM-CHEM	0.473
MRI-CGCM3	0.225
NorESM1-M	0.298
NorESM1-ME	0.290

During the initialization phase, CMIP models are usually run without forcing for five hundred years, which is not enough for some long-term processes to reach an equilibrium state. The transient climate simulation is then undertaken while such adjustment processes are still ongoing, causing an unwanted "drift" that is independent of internal variability or external forcing. Model drift particularly affects depth-integrated outputs like steric sea level, as heat fluxes to the deeper ocean lag over thousands of years. Although model drift is a relatively small contribution in an experiment with a strong anthropogenic forcing and is expected to cancel when considering multi-model means, we decided to remove the drift detected in the pre-industrial control ("piControl") run for each model considered. Among the three correction methods suggested in Sen Gupta et al. (2013), the "full linear drift" method was applied: yearly averaging the piControl time series, calculating the linear trend of the resulting time series and subtracting this trend from the RCP-experiment time series.

4.4.2 Mass contribution

4.4.2.1 Glaciers and ice caps

Mass changes of glacier and ice caps (GIC) were projected using numerical data made available by Marzeion et al. (2012, see tables in Supplement). In their study, glaciers of the world were arranged into 19 regional groups following the Randolph Glacier Inventory (RGI) (Arendt et al. 2012) and mass changes for each glacier group were computed using a combination of surface mass balance (SMB) modeling and scaling techniques. SMB models were forced with temperatures and precipitations from 15 CMIP5 model outputs. Cumulative mass changes between 2010 and 2100 for RCP8.5 scenario are reported in Table 4-2.

Table 4-2. **Projections of GIC mass losses.** Cumulative mass loss between 2010 and 2100 for 19 groups of GICs (in millimeters of equivalent sea level). The standard error for each group is equal to one standard deviation of the multi-model mean.

Name of GIC group	**Cumulative mass loss** (mm e.s.l.)
Alaska	27 [20 to 33]
Western Canada and US	2
Arctic Canada (North)	30 [19 to 41]
Arctic Canada (South)	10 [7 to 13]
Greenland	18 [15 to 21]
Iceland	5 [3 to 8]
Svalbard	14 [12 to 16]
Scandinavia	0
Russian Arctic	36 [23 to 48]
North Asia	0
Central Europe	0
Caucasus and Middle East	0
Central Asia (North)	10 [9 to 11]
Central Asia (West)	4 [4 to 5]
Central Asia (South)	2 [2 to 3]
Low latitudes	1
Southern Andes	7 [6 to 8]
New Zealand	0
Antarctic and Subantarctic	36 [28 to 44]
Total GIC	**202 [158 to 247]**

Each projected mass change was then used to scale the normalized fingerprint of its corresponding group in order to compute the global pattern of sea-level change. Fingerprints describe the spatial redistribution of water caused by elastic Earth deformation, gravitational and rotational effects following a change in ice mass at a given location. The fingerprints used in this study (Figure 4-6) were produced by Love (2014) using a sea level calculation code

based on Mitrovica et al. (2001); volumes of glaciers were calculated using area-to-thickness coefficients (Huss & Farinotti 2012) and glacier outlines were obtained from the RGI. Fingerprints are provided as gridded files of change in relative sea level, normalized by the global mean of sea-level change. Grids were summed in order to obtain the total sea-level distribution over the globe, for each model. Finally a multi-model mean of the projected GIC contribution to sea-level change was calculated, associated with a standard error equal to one standard deviation of the mean. It can be formalized as follows:

$$\Delta SL_{GIC}(\varphi, t) = \frac{1}{m}\sum_{m}\sum_{n}\Delta M_{n,m}(t)\times Fp_{n}(\varphi) \tag{4-3}$$

where ΔSL_{GIC} is the contribution of GIC mass changes to sea-level change at location φ between t_0 and t, $\Delta M_{n,m}$ is the cumulative mass change of glacier group n derived from model m, and $Fp_n(\varphi)$ is the normalized fingerprint associated with glacier group n.

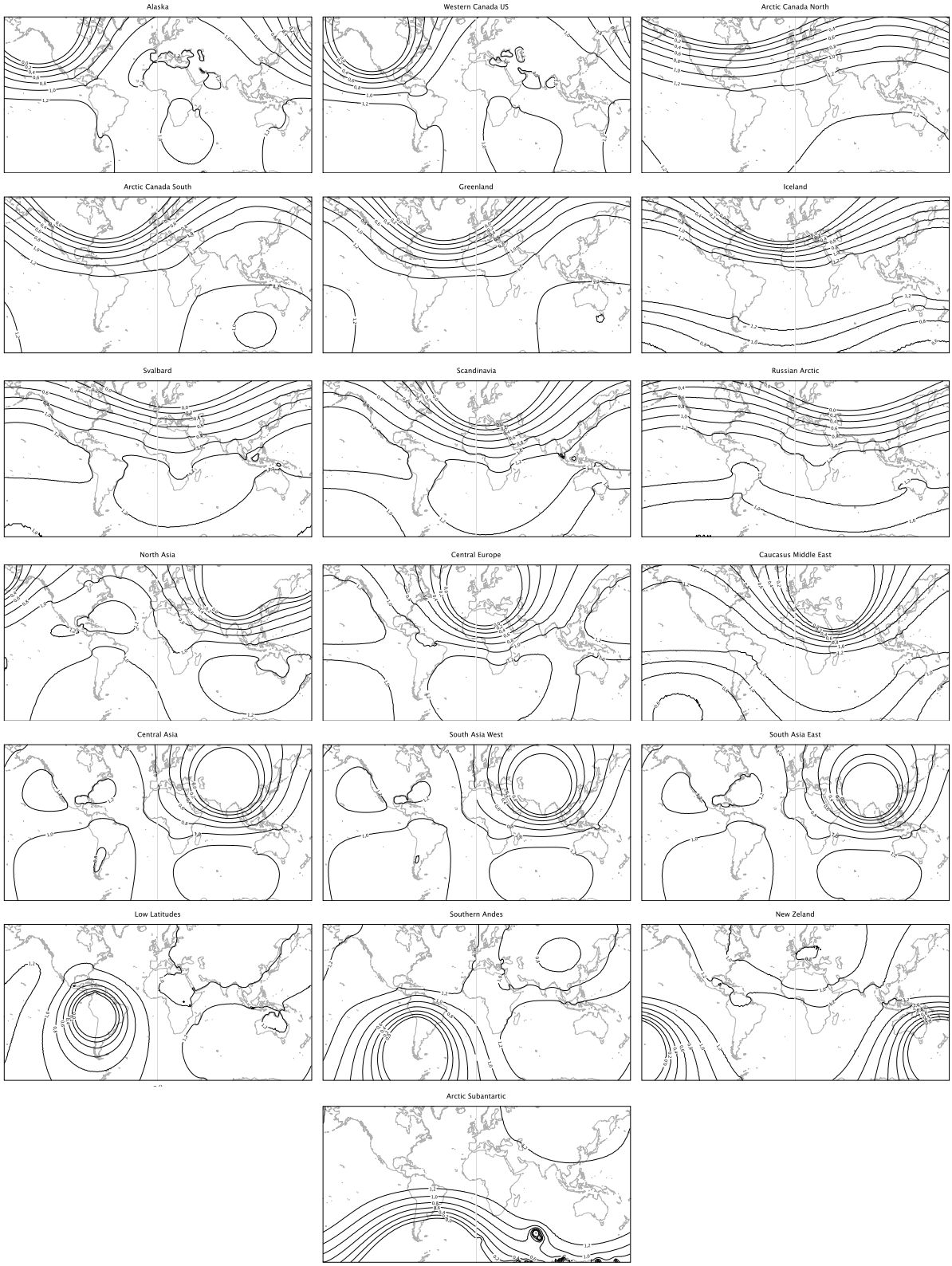

Figure 4-6. **Fingerprints of GIC groups.** Fingerprints are provided for each of the 19 groups of glaciers defined in the RGI. Contours indicate change in relative sea level, normalized by the global mean sea-level change. Only positive sea-level change contours are drawn for clarity. Maps based on data courtesy of Love (2014).

4.4.2.2 Greenland and Antarctic ice sheets

A similar method was applied to compute spatial patterns of sea-level change associated with the Greenland Ice Sheet (GIS) and the Antarctic Ice Sheet (AIS). Regarding ice sheets, both surface mass balance and ice sheet dynamics can contribute significantly to sea-level changes and have to be taken into account. Mass changes and associated uncertainties were derived from IPCC AR5, Chapter 13 (Church et al. 2013).

Table 4-3. **Projections of GIS and AIS mass changes.** Cumulative mass loss between 2010 and 2100, in meters equivalent to sea level, derived from Church et al. (2013). Interval is given for 90% confidence.

Ice sheet and decay process	**Cumulative mass loss** (mm e.s.l)
GIS surface mass balance	0.09 [0.03 to 0.20]
GIS dynamics	0.05 [0.02 to 0.08]
AIS surface mass balance	-0.04 [-0.08 to 0.02]
AIS dynamics	0.08 [-0.02 to 0.17]

Fingerprints for GIS and AIS (Love 2014) were produced using the sea level calculation code mentioned previously, but unlike the case for GICs, ice sheet changes were derived from gridded data provided by the Gravity Recovery and Climate Experiment (GRACE). Therefore sea-level change induced by changes in ice sheets can be written:

$$\Delta SL_{AIS}(\varphi, t) = \Delta M_{AIS}(t) \times Fp_{AIS}(\varphi) \tag{4-4}$$

and:

$$\Delta SL_{GIS}(\varphi, t) = \Delta M_{GIS}(t) \times Fp_{GIS}(\varphi) \tag{4-5}$$

where ΔSL_{AIS} and ΔSL_{GIS} are the contribution of AIS and GIS to sea-level change at location φ between t_0 and t, ΔM_{AIS} and ΔM_{GIS} are the cumulative mass changes of AIS and GIS, and $Fp_{AIS}(\varphi)$ and $Fp_{GIS}(\varphi)$ are the fingerprints of AIS and GIS.

4.4.2.3 Changes in land water storage

Changes in land water storage were directly derived from gridded sea-level data compiled by the IPCC (Church et al. 2013). The contributions to local sea-level changes between 2010 and 2100 are 0.03 m [-0.01 to 0.08 m] for Ile de Sein, and 0.05 [-0.02 to 0.11 m] for Rangiroa. The uncertainty intervals are relatively large, as the projections are dependent on climate-driven parameters as well as socio-economic scenarios.

4.4.3 Isostatic contribution and vertical land motion

4.4.3.1 French Polynesia and Rangiroa

Given that isostatic adjustments are long-term, secular processes, variations at millennial scales are almost linear. As a consequence, GIA rates observed or modeled over the last thousand years can be reasonably extrapolated over the coming century in order to calculate the isostatic contribution. A subset of nine GIA models that fit well observational data from French Polynesia has been presented in Section 3.3.3. The rate of RSL change was estimated to -0.33 mm/yr [-0.40 to -0.24 mm/yr] for Bora Bora; using the same subset of models, the rate of change in Rangiroa has been estimated to -0.34 mm/yr [-0.40 to -0.25 mm/yr]. Given the geological structure of Rangiroa and the age of the lithosphere surrounding the atoll, other plausible causes of vertical land motion (i.e., volcanic loading and thermal subsidence) have been neglected.

4.4.3.2 West Britanny and Ile de Sein

Regarding West Britanny, observational data from surrounding salt-marshes (Stéphan et al. 2015) were compared to the results of a set of GIA models calibrated for the nearby British Isles (Bradley et al. 2011). These models and the data from Brittany display a good fit, as shown in Figure 4-7; applying these models gives a present rate of RSL change of +0.65 mm/yr [+0.59 to +0.71 mm/yr] for the Ile de Sein. It should be emphasized that RSL changes in the region are influenced by a number of regional GIA factors including continental levering coupled with ocean loading in the Bay of Biscay, and collapse of the forebulges of the British-Irish and Fennoscandian ice sheets (Figure 4-8). As a consequence, modeled GIA rates are more sensitive to parameter choice than those for French Polynesia. In producing sea-level projections for this region, we assume that local tectonic processes or other sources of land vertical motion do not contribute significantly on century time scales. We refer to the work of Lenôtre et al. (1999) for a discussion of this assumption.

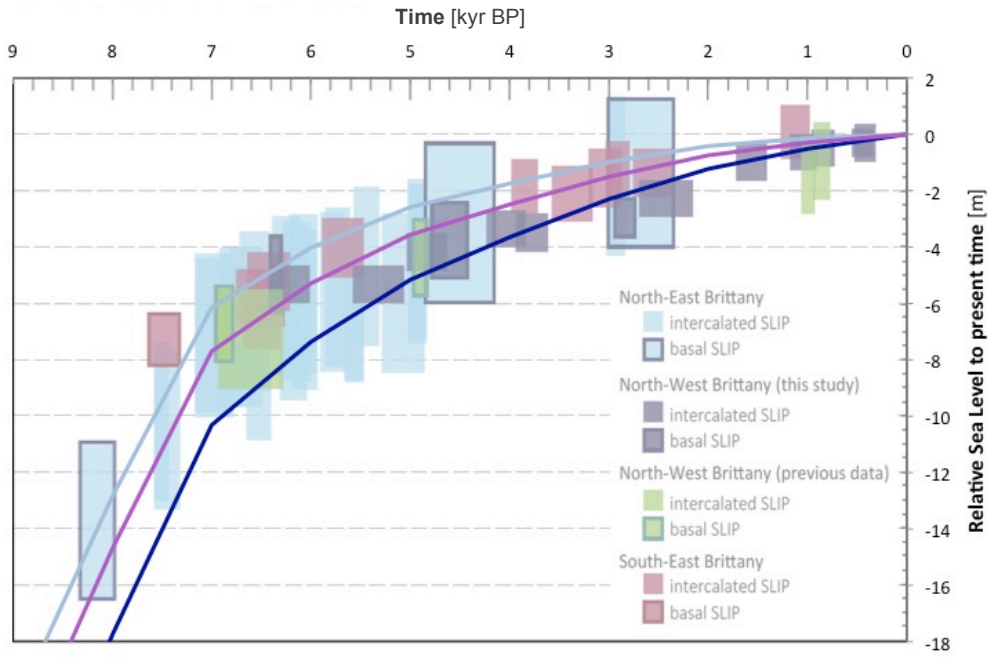

Figure 4-7. **Data-model fit of relative sea-level change near Brest during the Holocene.** In the background: sea-level index points from Britanny salt marshes. Figure courtesy of Stéphan et al. (2015), reproduced with the consent of the authors. Superimposed: modeled RSL curves for North-West (dark blue), North-East (light blue) and South-East Britanny (purple), using the following set of parameters: EUST3, LT 71 km, UMV $0.5x10^{21}$ Pa.s, LMV $50x10^{21}$ Pa.s.

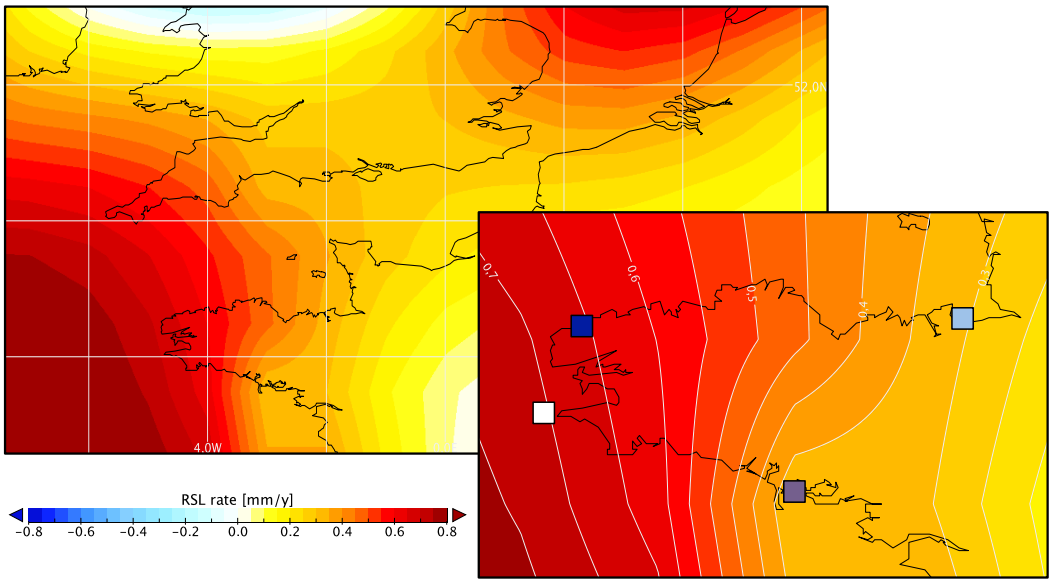

Figure 4-8. **Present-time GIA rates in West Britanny.** Left map: general map showing present-time GIA rates for the Atlantic/English Channel/North Sea area. Right inserted map: RSL rates in the Britanny region. GIA rates were computed using the following set of parameters: EUST3, LT 71 km, UMV $0.5x10^{21}$ Pa.s, LMV $50x10^{21}$ Pa.s. Localities of interest are indicated as follow: Ile de Sein (white square), and salt marshes from North-West (dark blue square), North-East (light blue square) and South-East Britanny (purple square).

4.4.4 Combination of contributions and uncertainties

Gridded data of the aforementioned contributions were projected on a 1°x1° rectangular grid and were added together to produce global maps of projected sea-level changes between 2010 and 2100 (Figure 4-9). Local projections for Rangiroa and Ile de Sein were then extracted (Table 4-4), but no interpolation was used – the value of the nearest node was considered. As the steric contribution is usually undetermined along the continental coastlines, due to limited model resolution, missing values were filled with the mean of the 4-nearest neighbor values. In addition, a specific treatment was applied to marginal seas, where models giving values well outside the range of other models were not taken into account to generate the local mean.

Gridded values of uncertainties were also combined, but following a more complex process. In this study, uncertainties are expressed at 90% confidence, corresponding to a "very likely" outcome on the likelihood scale defined by the IPCC (Cubasch et al. 2013). This means that sea-level change has at least a 9 out of 10 chance of remaining within the projected interval.

For steric contribution, the spread of the climate models is treated as a normal distribution. Therefore the standard error for the ensemble mean is equal to one standard deviation (66% confidence) of the spread, for both global and local projections. The 90% confidence interval limits were then obtained by multiplying the standard deviation by 1.645.

Regarding mass contributions (ice sheets, glaciers and land water storage), the global uncertainties are provided at 90% confidence, as for the last IPCC report. The local uncertainties were then calculated by combining the global uncertainty of the considered source with its fingerprints, following the same process used to compute the local mean (see Section 4.4.2)

GIA is not included in global projections published by the IPCC. However the value of the standard deviation (66% confidence) of the isostatic contribution can be calculated using the two models presented in the Supplementary Material of the report (Church et al. 2013); the difference between the two models was then multiplied by 1.645 to obtain the 90% confidence interval. Regarding local projections of isostatic contributions, GIA models were calibrated at 95% confidence level on local sea-level index points, and so we multiplied the uncertainties by 0.822 to calculate the 90% confidence interval limits.

The methodology described by Church et al. (2013) was followed to combine these uncertainties: uncertainties of contributions that correlate with global air temperature (i.e., steric sea level, GIS SMB and AIS SMB) were added linearly. The resulting uncertainty was then combined in quadrature with the other uncertainties.

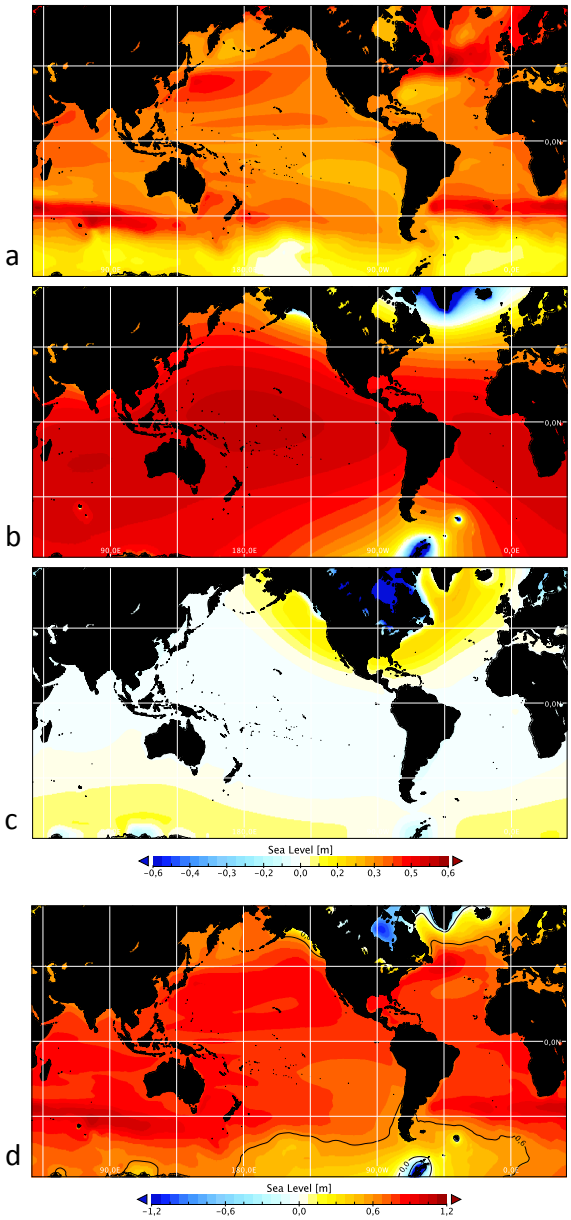

Figure 4-9. **Mean regional contributions to sea-level change between 2010 and 2100.** (a) steric contribution, as derived from 15 CMIP5 models for scenario RCP8.5; (b) mass contribution, including GIC, GIS, AIS and groundwater; (c) isostatic contribution; (d) total sea-level change.

4.5 Projections of sea-level changes

4.5.1 Amplitude and rate of sea-level changes

Sea-level projections are presented in Table 4-4. By the end of this century, a sea-level rise of 76 cm (median estimate) is expected in Rangiroa, while Ile de Sein would experience a rise of 67 cm, identical to the estimated global mean sea-level rise. The upper estimates (90% confidence interval) are 105 cm and 95 cm for Rangiroa and Ile de Sein, respectively. These two values are far above the working hypothesis of 60 cm mentioned in Section 4.2.2.1.

Table 4-4. **Contributions to sea-level changes between 2010 and 2100 in Rangiroa and Ile de Sein.** Contributions are in meters. Uncertainty interval for 90% confidence is given.

Contribution	Global mean	Ile de Sein	Rangiroa
Glaciers and ice caps	0.20 [0.13 to 0.28]	0.14 [0.09 to 0.19]	0.26 [0.15 to 0.36]
Greenland ice sheet surface mass balance	0.09 [0.03 to 0.20]	0.03 [0.01 to 0.06]	0.11 [0.05 to 0.26]
Antarctic ice sheet surface mass balance	-0.04 [-0.08 to -0.02]	-0.05 [-0.09 to -0.018]	-0.05 [-0.10 to -0.02]
Greenland ice sheet ice dynamics	0.05 [0.02 to 0.08]	0.01 [0 to 0.02]	0.06 [0.02 to 0.10]
Antarctic ice sheet ice dynamics	0.08 [-0.02 to 0.17]	0.09 [-0.03 to 0.20]	0.09 [-0.03 to 0.22]
Land water storage	0.04 [-0.01 to 0.09]	0.03 [-0.01 to 0.08]	0.05 [-0.02 to 0.11]
Mass contribution	0.40 [0.24 to 0.60]	0.25 [0.10 to 0.40]	0.52 [0.31 to 0.77]
Steric contribution	0.30 [0.17 to 0.42]	0.36 [0.13 to 0.59]	0.28 [0.14 to 0.41]
Isostatic contribution	-0.03 [-0.05 to 0]	0.06 [0.05 to 0.06]	-0.03 [-0.04 to -0.02]
Total sea level change	0.67 [0.47 to 0.91]	0.67 [0.40 to 0.95]	0.76 [0.52 to 1.05]

Regarding temporal aspects, models predict an acceleration of sea-level rise in Rangiroa, with a mean rate of 11 mm/yr [8 to 16 mm/yr] over the last decade of the century in the worst-case scenario (Figure 4-10). As a matter of comparison, this rate is far greater than the rates inferred from past observations of sea level in the region (see Section 3.4.3), and is roughly equivalent to the growth rate of healthy massive-shaped coral reefs developing in normal

conditions. Regarding the working hypothesis, uncertainty increases systematically with time, but the value of 60 cm would be hit before 2075 based on our upper estimates.

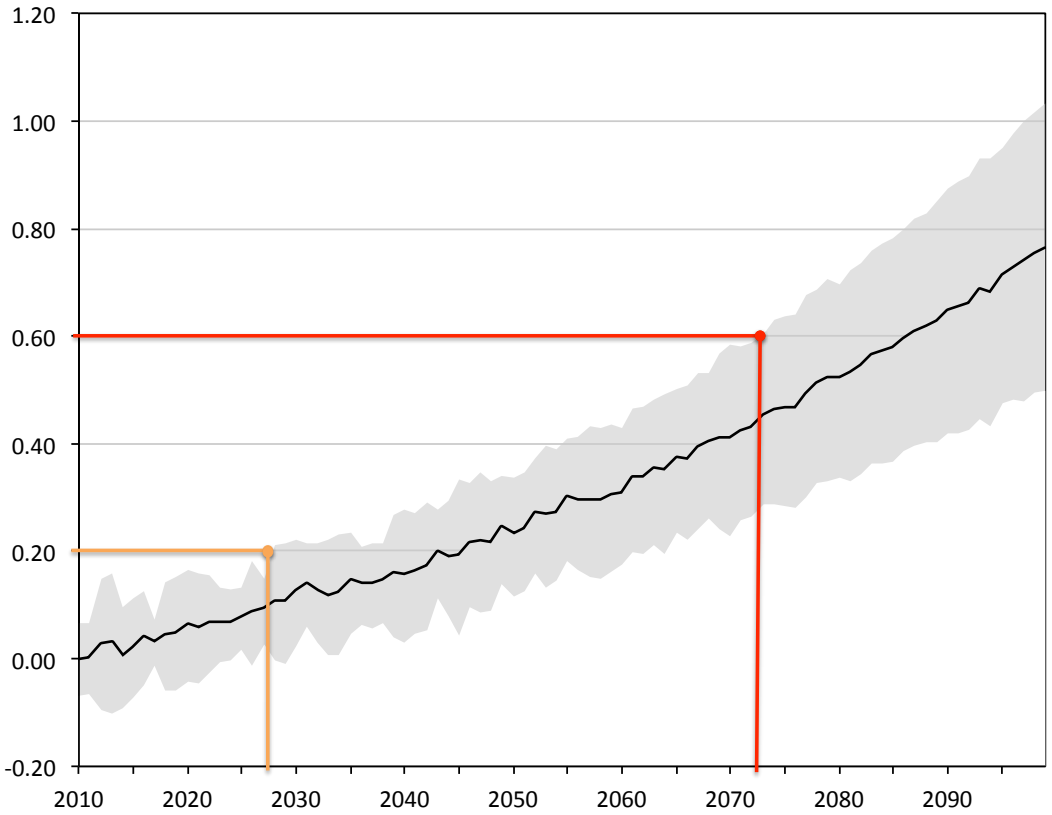

Figure 4-10. **Projection of sea level in Rangiroa between 2010 and 2100.** In black: median curve of sea level (in meters) in the worst-case scenario (RCP8.5), including all contributions (mass, steric and isostatic). Grey area delimits the 90% confidence interval. Orange and red lines indicate the years when sea level (upper estimate) would hit 20 and 60 cm of rise above the 2010 level.

Observed sea levels display significant decadal-scale variability in French Polynesia, as they do for the rest of the South Pacific. This is driven by the Southern Oscillation and the succession of El Niño and La Niña events; variations of up to 40 cm in amplitude can occur every 4 to 7 years. These abrupt changes have been recorded by instrumentation like the tide gauge located on Tahiti (Figure 1-1), and their amplitude and frequency are quite well captured by many AOGCMs (Figure 4-11, red curve). Sea level changes along the coast of Brittany are also subject to fluctuations (but of lesser amplitude compared to those in the South Pacific) that are mainly caused by the North Atlantic Oscillation (Figure 4-11, blue curve), but this phenomena is less well simulated by climate models at the moment (Flato et al. 2013). Sea-level projections based on multi-model means tend to smooth these

oscillations; this is an issue for flood risk studies (e.g., Lecacheux et al. 2013), where it would be necessary to consider annual peaks via stochastic approaches.

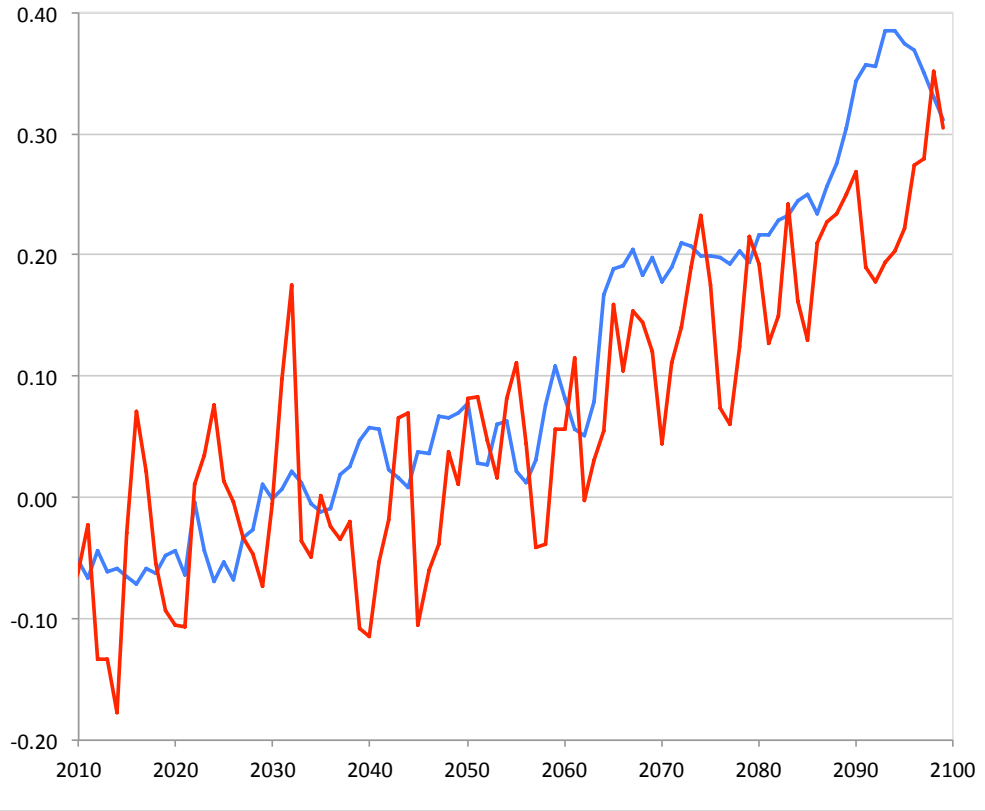

Figure 4-11. **Projections of steric sea level in Rangiroa and Ile de Sein between 2010 and 2100.** Sea level in Rangiroa (red curve) and Ile de Sein (blue curve) using CSIRO-Mk3.6.0 model.for scenario RCP8.5.

4.5.2 Causes of spatial variability

Taking a closer look at the global maps (Figure 4-9), it can be noted that our localities of interest are situated in two regions which differ in the relative weight of the contributions to sea-level changes: mass contribution appears to be a primary driving factor in the Tropical Pacific, while sea level is more affected by steric effects in the North Atlantic.

In Rangiroa, the mass contribution is projected to exceed 50 cm, almost 30% more than the global average (Figure 4-12, gray bars). This reflects the influence of gravitational and rotational effects: at low latitudes, contributions of the AIS and GIS are both near their global maximum value and are cumulating. Located far from any glacier or ice cap, French Polynesia is also unaffected by the fall of RSL that occurs in the vicinity of these smaller ice masses. In contrast, mass contribution on the coasts of Europe is dampened by the gravitational influence of surrounding sources of melt water, i.e., Greenland, Canada,

Svalbard and the Russian Arctic. As a result, the contributions of the GIS and GIC to RSL changes in Ile de Sein are expected to be lower than their global average by 70% and 30%, respectively.

On the contrary, the steric contribution in the inter-tropical zone is almost equal to its global average, while it estimated to be higher by 20-30% in some areas of the North Atlantic, including the coast of Britanny (Figure 4-12, blue bars). Dynamic patterns of compensating changes between halosteric and thermosteric contributions, in combination with the weakening of the Atlantic meridional oceanic circulation, could be responsible for the higher-than-average sea-level changes predicted in this region (Pardaens et al. 2010).

The isostatic contribution is relatively small in comparison with climate-driven contributions in a high-emission scenario. However, it should be emphasized that the isostatic contribution in Rangiroa is negative and driven by eustatic changes (i.e., ocean syphoning, see Section 3.4.1), while isostatic adjustment in Brittany is positive and mainly caused by regional processes (see Section 4.4.3.2). This leads to a difference of 9 cm in amplitude between the two sites (Figure 4-12, orange bars).

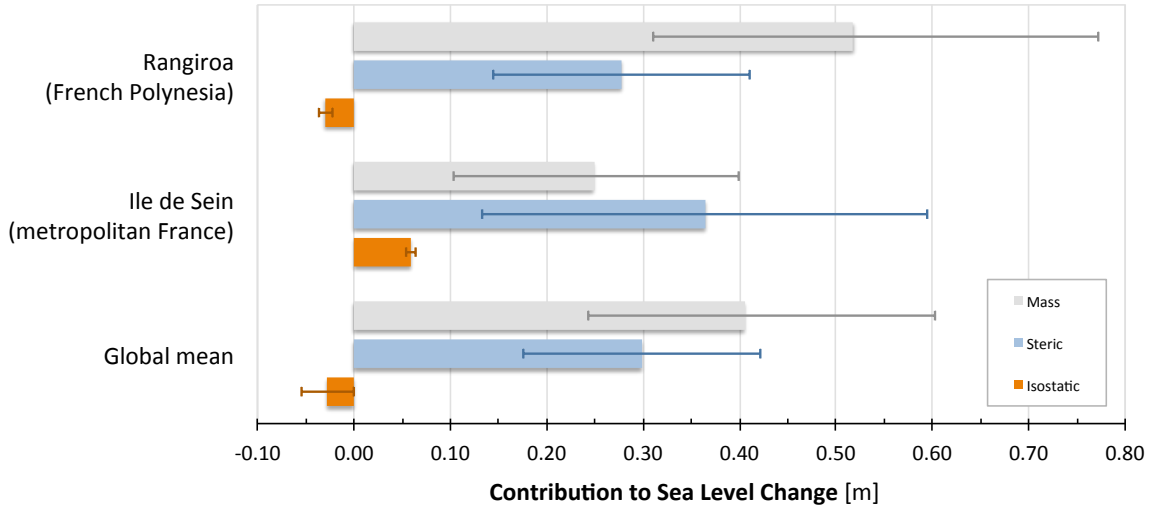

Figure 4-12. **Contributions to sea-level changes at Rangiroa and Ile de Sein.** Contributions are calculated between 2010 and 2100. In grey: mass contribution, including changes in glaciers and ice caps, Greenland and Antarctic ice sheets, and land water storage. In blue: steric contribution, as derived from 15 CMIP5 models for scenario RCP8.5. In orange: isostatic contribution. Error bars indicate the 90% confidence limits.

4.5.3 Sensitivity of projections to uncertainties

Beyond the uncertainties associated with anthropogenic forcing described by the spectrum of GHG emissions scenarios, uncertainties arise from methods and models used for predicting sea level at global and regional scales.

First, the dynamic response of peripheral glaciers and ice shelves of Antarctica, especially in its western sector, is a matter of concern and a major source of uncertainty in sea-level projections. Their instability could lead to a global sea-level rise beyond the upper estimates; however, this additional contribution should not exceed a few tens of centimeters by 2100 (IPCC 2013). The above sensitivity analysis shows that the French coasts would be more affected than the global average by this phenomenon, but in a relatively uniform manner. As an illustration, a loss of 10 cm e.s.l caused by rapid ice dynamics would result in an increase of approximately 12 cm for both Rangiroa and Ile de Sein.

By contrast, a greater melting of the GIS would increase the difference between metropolitan France and overseas territories. In the most pessimistic projections, Greenland could contribute 28 cm to global mean sea-level rise by 2100, which scales to a contribution of only 8 cm at Ile de Sein, but of 36 cm at Rangiroa. These upper estimates could be revised in the future, as recent observations suggest that other processes need to be further understood and modeled. This includes the basal lubrication of the ice sheet by the drainage of supraglacial lakes or the ocean thermal forcing below glaciers outlets, where the bedrock is still poorly mapped (Leeson et al. 2015, Morlighem et al. 2014).

As for the steric contribution, a wider use of ESMs and an increase in spatial resolution should help refine projections, but some physical processes are not yet fully captured by models. For example, global climate models and ice sheet models are not coupled (Church et al. 2013). Therefore, the impact of melt water on local steric changes is poorly described. In addition, this input of freshwater could alter the thermohaline circulation, which would in turn modify the heat fluxes at mid-latitudes (IPCC 2013). Ultimately it would affect the spatial variability of sea level to an unknown extent.

Finally the isostatic contribution is the only contribution for which the uncertainty range does not exceed the value of the mean estimate. Decoupled from the rapid changes in the climate

forcing, long-term GIA processes can be well constrained as long as observations are available in the regions of interest, which is the case for Rangiroa and Ile de Sein.

4.6 Conclusion

In this chapter, we first reviewed the sea-level risks for low-lying islands. Among other impacts, French Polynesia is increasingly exposed to the risk of coastal flooding because sea-level rise will increase the severity of flooding events caused by storms and cyclones, while its adaptation options and its resilience capacities are restricted. We reviewed several studies that were conducted in Rangiroa in the recent years, noting that sea-level rise was not systematically considered as a contributing factor of coastal flooding, and when it was, analysis was conducted using global and outdated projections.

To re-evaluate the contribution of sea-level rise to this risk, we combined recent outputs of global climate models and estimates of ice volume changes to produce regional projections of sea-level change between 2010 and 2100 in a worst-case scenario. We conclude that sea level in the atoll of Rangiroa is projected to rise by 1.05 m (upper bound of the 90% confidence interval) over this period of time, resulting in a greater level of exposure than the rest of the world or on the French Atlantic coast. While sea-level rise in metropolitan localities is mainly driven by changes in steric sea level and ocean dynamics, French Polynesia will be relatively more impacted by the melting of ice sheets and glaciers. Additionally, spatial variability of sea level along the French coasts is highly sensitive to changes affecting the Greenland ice sheet, while the potential instability of the Antarctic ice sheet is a significant source of uncertainty but is not going to generate any disparities between these two regions.

Finally, we compared our projections to the working hypothesis adopted by policy-makers. In the worst-case scenario, a sea-level rise of 0.60 m by 2100 has been assumed in the national adaptation strategy and the associated regulations. Based on this comparison, we conclude that the contribution of sea-level rise to the overall risk of coastal flooding is considerably underestimated. In addition, the spatial variability of sea-level rise at the national level appears to be significant enough to be considered in future sea-level risk analyses.

CHAP 5: CONCLUSION

Having quantified the GIA signal in French Polynesia and provided estimates of global ice volume changes for the mid-to-late Holocene, we have partly achieved our primary research goal, which was to set a baseline for sea-level changes in this region. However, additional data are needed to compare our reconstructed sea-level curve with present sea-level changes. Regarding our secondary goal, we have delivered regional projections of a "worst-case" sea-level rise that could be used in an adaptation strategy for this region. Various knowledge gaps and limitations have been identified in the course of our study; they are reviewed in the second section of this chapter along with potential avenues for future work. To begin we provide a summary of the key findings.

5.1 Summary of key results

In Chapter 2, we presented a reconstruction of past sea level changes for the mid-to-late Holocene. In regions that experienced a sea level highstand like French Polynesia, fossil microatolls are among the most accurate sea-level proxies for the studied period; using state-of-the-art positioning and dating techniques, microatolls allowed us to reconstruct sea level at the decimeter scale. However, several sources of uncertainty, mainly relating to estimating the height of fossil corals relative to present mean sea level, emerged in the course of this work; measuring modern microatolls is the suggested alternate method to improve the overall accuracy of this aspect of the dataset.

We then compared our dataset and the outputs of a sea-level model to examine temporal and spatial variability of GIA. One of the main conclusions of this analysis is that long-term RSL changes in French Polynesia are mainly correlated to eustatic changes. Ice melt has progressively decelerated to become almost negligible after 2 kyr BP and ocean syphoning is the dominant signal in the region since then. In addition, we emphasize that the mean GIA rate for the last two millennia is sufficiently constrained by the existing dataset to make projections of the isostatic contribution to future sea-level changes. However, no precise baseline can be drawn regarding the ice and steric contributions due to temporal gaps in the data. While the amplitude of oscillations at the sub-millennial time scales appears to be limited to a few decimeters, our dataset lacks the time resolution needed to accurately

estimate rates at century time scales, precluding any meaningful comparison between past and present sea level observations.

In the previous chapter, we focused on the impacts of sea-level rise in French Polynesia. Acknowledging that sea-level risks in the region are being evaluated using global-averaged and outdated projections, we provided regional projections based on recent outputs of climate models and estimates of ice volume changes. In a worst-case scenario, we estimated that sea level would rise by 1.05 m between 2010 and 2100 in the atoll of Rangiroa, with the largest contribution from the melting of ice sheets and glaciers. This rise exceeds by a considerable amount the value adopted in national regulations; the future exposure to coastal flooding is therefore underestimated. This is an important result given that the vulnerability of these isolated, low-lying islands is assessed to be high. Having compared the Polynesian atoll with another island located off the French Atlantic coast, we also conclude that the spatial variability of sea-level rise at the national level is significant enough to be considered in future sea-level risk analyses.

5.2 Future work

At the time of writing, the research project that has produced the dataset from French Polynesia is still in progress and additional fieldwork is planned in the near future. As mentioned previously, reducing vertical uncertainties would be an improvement at every step of the interpretation: not only would it help to better constrain the GIA signal, but it would also allow to compile data from various sites in order to examine higher-frequency variations. For this reason, modern microatolls will be systematically measured along with their fossil counterparts during the next field trip.

Some of the gaps identified in the dataset have been also taken into account; in particular, several time frames (see Section 3.5.2) will be more closely investigated thanks to additional sampling. These data would help to narrow the parameter space associated with the Earth model or to modify the ice model, in spite of the non-uniqueness issue highlighted in Chapter 4.

Another problem lies in the lack of time resolution of the existing dataset, which limits our ability to attribute the observed sea-level changes to specific processes. Longer and more temporally dense records are needed to seek a correlation between sea-level changes and

other signals, for instance variations in solar irradiance or ocean temperatures. Data resolution (in time and height) is also critical to infer rates of changes at the century time scales and thus to be able to compare past and present rates of change. Unfortunately, increasing the number of points is useful only until the temporal density of the dataset reaches the observational precision, which can hardly be reduced further. Conversely, collecting and analyzing slabs of well-preserved fossil microatolls would produce the relevant data. This sampling technique has already been tested in the field and applied to modern microatolls in an effort to reconstruct recent climate variations in French Polynesia, and will be a component of the upcoming field trip.

Finally, examining the spatial variability of past sea level changes would help to improve model parameter determination and to detect possible discrepancies in models. This is going to be achieved by surveying other sites across the Tropical Pacific and beyond.

In terms of future sea-level changes, our regionalized projections are more elaborate than the values currently adopted in the French national strategy, and could be used advantageously in decision-making at the local level. In addition, our results could be extended to all of the French overseas territories, either by following the methodology presented in Chapter 4 or by extracting regionalized projections (Botella 2015) from the IPCC's most recent assessment (Church et al. 2013).

However, we emphasize that a significant amount of work is required to provide more robust projections and to reduce the uncertainties to acceptable levels. As shown in Chapter 3, the isostatic contribution in French Polynesia can be predicted relatively accurately, but it would be dwarfed in the near future by other contributions, especially in the worst-case scenario. The issue is that the two largest contributions, i.e., mass and steric, are associated with large uncertainty ranges that often exceed the value of the contributions themselves. As sea-level rise in the region is primarily sensitive to changes that affect GIC and ice sheets, this field of research should receive more attention. The transfer function (fingerprint) is well known and is not time-dependent at the century time scales, however the source term is less well modeled, particularly the mass loss that would result from ice dynamics. Regarding the steric contribution, the ability of AOGCMs to reproduce past sea level changes is yet to be demonstrated, and the spread in projections is large, thus questioning the maturity of these models for such an application. In both cases, projections rely on complex models; refining

these models is already the main focus of many advanced research projects involving multidisciplinary teams. A way to improve our projections without additional development lies in the calibration of AOGCM: instead of using a multi-model mean, it is suggested to select a small subset of models that best reproduce recent sea-level changes at the regional or basin scale, provided that the steric contribution can be isolated from observations.

Expanding upon the broader implications of this study in terms of environmental durability, we underline that the issue of sea-level rise in French Polynesia poses a dilemma at the science-policy interface. On the one hand, there is an urgent need for projections, driven by the necessity to implement as soon as possible an adaptation strategy that intrinsically relies on large investments and long-term commitments. To this end, developing an integrated framework at the research level is a small yet necessary step to reduce the time needed to produce a comprehensive scientific assessment. On the other hand, proceeding immediately to the next level and taking action based on current knowledge would mean incorporating large uncertainties into the decision-making process. Such uncertainties are not easily communicated to the public; combined with the perception that adaptation requires costly efforts, uncertainties tend to hamper social acceptance of the risk, offering an excuse for delaying action or even to discard the scientific evidence. To put it another way, dealing with uncertainty is not only a challenge for the scientist, but also for the policy-maker.

References

Andersen OB, Knudsen P, Berry PAM. 2010. The DNSC08GRA global marine gravity field from double retracked satellite altimetry. *Journal of Geodesy*. 84(3):191–99

Arendt AA, Bolch T, Cogley JG, Gardner A, Hagen J-O, et al. 2012. Randolph Glacier Inventory [v3.2]: A Dataset of Global Glacier Outlines.

Avagliano E, Petit J. 2009. Etat des lieux sur les enjeux du changement climatique en Polynésie française. Ministère de l'Environement de la Polynésie française, Direction de l'Environnement de la Polynésie française, Station Gump, UC Berkeley

Bard E, Hamelin B, Arnold M, Montaggioni L, Cabioch G, et al. 1996. Deglacial sea-level record from Tahiti corals and the timing of global meltwater discharge. *Nature*. 382(6588):241–44

Bassett SE, Milne GA, Mitrovica JX, Clark PU. 2005. Ice sheet and solid Earth influences on far-field sea-level histories. *Science*. 309(5736):925–28

Bellard C, Leclerc C, Courchamp F. 2013. Potential impact of sea level rise on French islands worldwide. *Nature Conservation*. 5:75–86

Bell JD, Ganachaud A, Gehrke PC, Griffiths SP, Hobday AJ, et al. 2013. Mixed responses of tropical Pacific fisheries and aquaculture to climate change. *Nature Climate Change*. 3(6):591–99

Botella A. 2015. Projections régionalisées de la hausse du niveau marin dans les territoires français d'outremer. *Submitted for publication*

Bradley SL, Milne GA, Shennan I, Edwards R. 2011. An improved glacial isostatic adjustment model for the British Isles. *Journal of Quaternary Science*. 26(5):541–52

Cai W, Lengaigne M, Borlace S, Collins M, Cowan T, et al. 2012. More extreme swings of the South Pacific convergence zone due to greenhouse warming. *Nature*. 488(7411):365–69

Cazenave A, Lago B, Dominh K, Lambeck K. 1980. On the response of the ocean lithosphere to sea-mount loads from Geos 3 satellite radar altimeter observations. *Geophysical Journal International*. 63(1):233–52

Church JA, Clark PU, Cazenave A, Gregory JM, Jevrejeva S, et al. 2013. Sea Level Change. In *Climate Change 2013: The Physical Science Basis. Contribution of Working Group I to the Fifth Assessment Report of the Intergovernmental Panel on Climate Change*, eds. TF Stocker, D Qin, G-K Plattner, M Tignor, SK Allen, et al., pp. 1137–1216. Cambridge, United Kingdom and New York, NY, USA: Cambridge University Press

Church JA, White NJ. 2011. Sea-level rise from the late 19th to the early 21st century. *Surveys in Geophysics*. 32(4-5):585–602

Clark JA, Farrell WE, Peltier WR. 1978. Global changes in postglacial sea level: A numerical calculation. *Quaternary Research*. 9(3):265–87

Cobb KM, Westphal N, Sayani HR, Watson JT, Lorenzo ED, et al. 2013. Highly variable El Niño–Southern Oscillation throughout the Holocene. *Science*. 339(6115):67–70

Collins M, An S-I, Cai W, Ganachaud A, Guilyardi E, et al. 2010. The impact of global warming on the tropical Pacific Ocean and El Niño. *Nature Geoscience*. 3(6):391–97

Commissariat général au développement durable. 2009. Atlas des îles de l'Atlantique

Conseil général du Finistère. 2013. *Inaugurations des ouvrages maritimes et de la déchèterie de l'île de Sein*. http://www.finistere.fr/Le-Conseil-departemental-et-vous/Territoires/Toutes-les-actualites/Archive-2013-Inaugurations-des-ouvrages-maritimes-et-de-la-decheterie-de-l-ile-de-Sein

Cubasch U, Wuebbles D, Chen D, Facchini MC, Frame D, et al. 2013. Introduction. In *Climate Change 2013: The Physical Science Basis. Contribution of Working Group I to the Fifth Assessment Report of the Intergovernmental Panel on Climate Change*, eds. TF Stocker, D Qin, G-K Plattner, M Tignor, SK Allen, et al., pp. 119–58. Cambridge, United Kingdom and New York, NY, USA: Cambridge University Press

Damlamian H, Kruger J. 2013. Modèle bidimensionnel couplé de Rangiroa (modèle hydrodynamique et modèle spectral de vague) - Cyclone tropical Orama-Nisha (1983). Secretariat of the Pacific Community - Applied Geoscience and Technology Division, Suva, Fidji

Damlamian H, Kruger J, Turagabeci M, Kumar S. 2013. Cyclone wave inundation models for Apataki, Arutua, Kauehi, Manihi and Rangiroa atolls, French Polynesia. *PR176*, Secretariat of the Pacific Community - Applied Geoscience and Technology Division, Suva, Fiji

De la Baume M. 2012. Having Defied the Nazis, Islanders Take On the Sea. *The New York Times*, July 23, . http://www.nytimes.com/2012/07/24/world/europe/french-islanders-face-rising-sea-levels.html

Demey J. 2013. Montée des eaux : l'île de Sein flotte encore. *Le Journal du Dimanche*, Nov. 9, . http://www.lejdd.fr/Societe/Montee-des-eaux-l-ile-de-Sein-flotte-encore-637923

Dutton A. 2015. Uranium-thorium dating. In *Handbook of Sea-Level Research*, eds. I Shennan, AJ Long, BP Horton, pp. 386–403. John Wiley & Sons, Ltd

Duvat V, Magnan A, Mossot G, Galliot M, Mondon S, Reysset B. 2012. Les outre-mer face au défi du changement climatique. La documentation française

Dziewonski AM, Anderson DL. 1981. Preliminary reference Earth model. *Physics of the Earth and Planetary Interiors*. 25(4):297–356

Egbert GD, Erofeeva SY. 2002. Efficient inverse modeling of barotropic ocean tides. *Journal of Atmospheric and Oceanic Technology*. 19(2):183–204

Farrell WE, Clark JA. 1976. On postglacial sea level. *Geophysical Journal of the Royal Astronomical Society*. 46(3):647–67

Feldman T, Andrews A. 2011. *Rangiroa: Maritime Culture*. Sustainability in Polynesian Island Cultures and Ecosystems. http://www.sea.edu/spice_atlas/rangiroa_atlas/maritime_culture_of_rangiroa

Fietzke J, Liebetrau V, Eisenhauer A, Dullo C. 2005. Determination of uranium isotope ratios by multi-static MIC-ICP-MS: method and implementation for precise U- and Th-series isotope measurements. *Journal of Analytical Atomic Spectrometry*. 20(5):395–401

Flato G, Marotzke J, Abiodun B, Braconnot P, Chou SC, et al. 2013. Evaluation of climate models. In *Climate Change 2013: The Physical Science Basis. Contribution of Working Group I to the Fifth Assessment Report of the Intergovernmental Panel on Climate Change*, eds. TF Stocker, D Qin, G-K Plattner, M Tignor, SK Allen, et al., pp. 741–866. Cambridge, United Kingdom and New York, NY, USA: Cambridge University Press

Goodwin ID, Harvey N. 2008. Subtropical sea-level history from coral microatolls in the Southern Cook Islands, since 300 AD. *Marine Geology*. 253(1-2):14–25

Griffiths SD, Hill DF. 2015. Tidal modeling. In *Handbook of Sea-Level Research*, eds. I Shennan, AJ Long, BP Horton, pp. 438–51. John Wiley & Sons, Ltd

Hallmann N, Camoin G, Eisenhauer A, Samankassou E, Vella C, et al. 2014. A 6,700 years sea-level record based on French Polynesian coral reefs. *In preparation*

Hill DF, Griffiths SD, Peltier WR, Horton BP, Törnqvist TE. 2011. High-resolution numerical modeling of tides in the western Atlantic, Gulf of Mexico, and Caribbean Sea during the Holocene. *Journal of Geophysical Research: Oceans*. 116(C10):C10014

Hirsh H, Hurley J. 2011. *Rangiroa: The physical environment*. Sustainability in Polynesian Island Cultures and Ecosystems.
http://www.sea.edu/spice_atlas/rangiroa_atlas/the_physical_environment_of_rangiroa

Holgate SJ, Matthews A, Woodworth PL, Rickards LJ, Tamisiea ME, et al. 2012. New data systems and products at the permanent service for mean sea level. *Journal of Coastal Research*. 493–504

Huss M, Farinotti D. 2012. Distributed ice thickness and volume of all glaciers around the globe. *Journal of Geophysical Research: Earth Surface*. 117(F4):F04010

IGN. 2013. *Logiciel Circé*

Institut d'émission d'Outre-mer. 2014. Polynésie française, rapport annuel 2013. Institut d'émission d'Outre-mer, Paris

IPCC. 2013. Summary for Policymakers. In *Climate Change 2013: The Physical Science Basis. Contribution of Working Group I to the Fifth Assessment Report of the Intergovernmental Panel on Climate Change*, eds. TF Stocker, D Qin, G-K Plattner, M Tignor, SK Allen, et al., pp. 1–30. Cambridge, United Kingdom and New York, NY, USA: Cambridge University Press

Jouzel J, Planton S, Le Cozannet G, Cazenave A, Costa S, et al. 2015. Le climat de la France au XXIe siècle. Volume 5 : Changement climatique et niveau de la mer : de la planète aux côtes françaises. Ministère de l'Écologie, du Développement durable et de l'Énergie

Kendall RA, Mitrovica JX, Milne GA. 2005. On post-glacial sea level – II. Numerical formulation and comparative results on spherically symmetric models. *Geophysical Journal International*. 161(3):679–706

Lambeck K, Rouby H, Purcell A, Sun Y, Sambridge M. 2014. Sea level and global ice volumes from the Last Glacial Maximum to the Holocene. *Proceedings of the National Academy of Sciences*. 111(43):15296–303

Larrue S, Chiron T. 2011. Les îles de Polynésie française face à l'aléa cyclonique. *VertigO - la revue électronique en sciences de l'environnement*. (Volume 10 Numéro 3):

Lecacheux S, Bulteau T, Pedreros R, Delvallée E, Paris F. 2013. Projet ARAI 3 : Evaluation probabiliste des houles et des surcotes cycloniques en Polynésie Française. *BRGM/RP - 61888 - FR*, Bureau de recherches géologiques et minières

Le Cozannet G, Garcin M, Petitjean L, Cazenave A, Becker M, et al. 2013. Exploring the relation between sea level rise and shoreline erosion using sea level reconstructions: an example in French Polynesia. *Journal of Coastal Research*. 65 (Special Issue):pp. 2137–42

Leeson AA, Shepherd A, Briggs K, Howat I, Fettweis X, et al. 2015. Supraglacial lakes on the Greenland ice sheet advance inland under warming climate. *Nature Climate Change*. 5(1):51–55

Lemoine FG, Smith DE, Kunz L, Smith R, Pavlis EC, et al. 1997. The development of the NASA GSFC and NIMA joint geopotential model. In *Gravity, Geoid and Marine Geodesy*, eds. PDJ Segawa, PDH Fujimoto, PDS Okubo, pp. 461–69. Springer Berlin Heidelberg

Lenôtre N, Thierry P, Blanchin R, Brochard G. 1999. Current vertical movement demonstrated by comparative levelling in Brittany (northwestern France). *Tectonophysics*. 301(3–4):333–44

Lenton TM, Held H, Kriegler E, Hall JW, Lucht W, et al. 2008. Tipping elements in the Earth's climate system. *Proceedings of the National Academy of Sciences*. 105(6):1786–93

Levermann A, Clark PU, Marzeion B, Milne GA, Pollard D, et al. 2013. The multimillennial sea-level commitment of global warming. *Proceedings of the National Academy of Sciences*. 110(34):13745–50

Levermann A, Griesel A, Hofmann M, Montoya M, Rahmstorf S. 2005. Dynamic sea level changes following changes in the thermohaline circulation. *Climate Dynamics*. 24(4):347–54

Love R. 2014. *Projections of sea level along the East Coast of North America*. MSc thesis. University of Ottawa

Lowe JA, Gregory JM. 2006. Understanding projections of sea level rise in a Hadley Centre coupled climate model. *Journal of Geophysical Research: Oceans*. 111(C11):C11014

Marzeion B, Jarosch AH, Hofer M. 2012. Past and future sea-level change from the surface mass balance of glaciers. *The Cryosphere*. 6(6):1295–1322

Meehl GA, Stocker TF, Collins WD, Friedlingstein P, Gaye AT, et al. 2007. Global climate projections. In *Climate Change 2007: The Physical Science Basis. Contribution of Working Group I to the Fourth Assessment Report of the Intergovernmental Panel on Climate Change*, eds. S Solomon, D Qin, M Manning, Z Chen, M Marquis, et al. Cambridge, United Kingdom and New York, NY, USA. Cambridge University Press ed.

Meltzner AJ, Woodroffe CD. 2015. Coral microatolls. In *Handbook of Sea-Level Research*, eds. I Shennan, AJ Long, BP Horton, pp. 125–45. John Wiley & Sons, Ltd

Meyssignac B. 2012. *La variabilité régionale du niveau de la mer*. PhD thesis. Université Paul Sabatier Toulouse III

Meyssignac B, Salas y Melia D, Becker M, Llovel W, Cazenave A. 2012. Tropical Pacific spatial trend patterns in observed sea level: internal variability and/or anthropogenic signature? *Climate of the Past*. 8(2):787–802

Milanković M. 1941. *Kanon Der Erdbestrahlung Und Seine Anwendung Auf Das Eiszeitenproblem [Canon of Insolation and the Ice-Age Problem]*. Belgrade: Israel Program for Scientific Translations [available from U.S. Dept. of Commerce, Clearinghouse for Federal Scientific and Technical Information, Springfield, Va.]

Milne G A, Mitrovica J X. 1998. Postglacial sea-level change on a rotating Earth. *Geophysical Journal International*. 133(1):1–19

Milne GA, Peros M. 2013. Data–model comparison of Holocene sea-level change in the circum-Caribbean region. *Global and Planetary Change*. 107:119–31

Ministère de l'Ecologie. 2011. *Circulaire du 27 juillet 2011 relative à la prise en compte du risque de submersion marine dans les plans de prévention des risques naturels littoraux*

Mitrovica JX, Forte AM, Simons M. 2000. A reappraisal of postglacial decay times from Richmond Gulf and James Bay, Canada. *Geophysical Journal International*. 142:783–800

Mitrovica JX, Milne GA. 2002. On the origin of late Holocene sea-level highstands within equatorial ocean basins. *Quaternary Science Reviews*. 21(20–22):2179–90

Mitrovica JX, Milne GA. 2003. On post-glacial sea level: I. General theory. *Geophysical Journal International*. 154(2):253–67

Mitrovica JX, Peltier WR. 1991. On postglacial geoid subsidence over the equatorial oceans. *Journal of Geophysical Research*. 96(B12):20053

Mitrovica JX, Tamisiea ME, Davis JL, Milne GA. 2001. Recent mass balance of polar ice sheets inferred from patterns of global sea-level change. *Nature*. 409(6823):1026–29

Mitrovica JX, Wahr J, Matsuyama I, Paulson A. 2005. The rotational stability of an ice-age Earth. *Geophysical Journal International*. 161(2):491–506

Morlighem M, Rignot E, Mouginot J, Seroussi H, Larour E. 2014. Deeply incised submarine glacial valleys beneath the Greenland ice sheet. *Nature Geoscience*. 7(6):418–22

Mumby P, Chisholm J, Edwards A, Clark C, Roark E, et al. 2001. Unprecedented bleaching-induced mortality in Porites spp. at Rangiroa Atoll, French Polynesia. *Marine Biology*. 139(1):183–89

Nicholls R, Hanson S, Herweijer C, Patmore N, Hallegatte S, et al. 2008. Ranking port cities with high exposure and vulnerability to climate extremes. *OECD Environment Working Papers*

Nunn PD. 2007. *Climate, Environment, and Society in the Pacific during the Last Millennium*. Elsevier

Nurse LA, McLean RF, Agard J, Briguglio LP, Duvat-Magnan V, et al. 2014. Small islands. In *Climate Change 2014: Impacts, Adaptation, and Vulnerability. Part B: Regional Aspects. Contribution of Working Group II to the Fifth Assessment Report of the Intergovernmental Panel of Climate Change*, eds. VR Barros, CB Field, DJ Dokken, MD Mastrandrea, KJ Mach, et al., pp. 1613–54. Cambridge, United Kingdom and New York, NY, USA: Cambridge University Press

Oiry A. 2011. *La fabrication de l'île comme territoire de risques*. Master 2 thesis. Université Paris 1 - Panthéon-Sorbonne

ONERC. 2010. Prise en compte de l'élévation du niveau de la mer en vue de l'estimation des impacts du changement climatique et des mesures d'adaptation possibles. Observatoire National sur les Effets du Réchauffement Climatique

PALSEA. 2010. The sea-level conundrum: case studies from palaeo-archives. *Journal of Quaternary Science*. 25(1):19–25

Pardaens AK, Gregory JM, Lowe JA. 2010. A model study of factors influencing projected changes in regional sea level over the twenty-first century. *Climate Dynamics*. 36(9-10):2015–33

Pavlis NK, Holmes SA, Kenyon SC, Factor JK. 2012. The development and evaluation of the Earth Gravitational Model 2008 (EGM2008). *Journal of Geophysical Research: Solid Earth*. 117(B4):B04406

Peltier WR. 1974. The impulse response of a Maxwell Earth. *Reviews of Geophysics*. 12(4):649–69

Peltier WR. 1998. Postglacial variations in the level of the sea: Implications for climate dynamics and solid-Earth geophysics. *Reviews of Geophysics*. 36(4):603–89

Peltier WR. 2004. Global glacial isostasy and the surface of the ice-age Earth: the ICE-5G (VM2) model and GRACE. *Annual Review of Earth and Planetary Sciences*. 20(32):111–49

Petit J, Prudent G. 2010. *Climate Change and Biodiversity in the European Union Overseas Entities*. International Union for Conservation of Nature

Pirazzoli PA, Montaggioni LF. 1985. Lithospheric deformation in French Polynesia (Pacific Ocean) as deduced from Quaternary shorelines. In *Proceedings of the Fifth International Coral Reef Congress: Symposia and Seminars*, p. 583. Moorea, French Polynesia. Antenne Museum - EPHE ed.

Pirazzoli PA, Montaggioni LF. 1986. Late Holocene sea-level changes in the northwest Tuamotu islands, French Polynesia. *Quaternary Research*. 25(3):350–68

Prasad SS. 2013. *The value of local knowledge for climate change adaptation planning : case studies from Fiji and Vanuatu*. MSc thesis. University of the South Pacific

PSMSL. 2015. *Tide Gauge Data*. http://www.psmsl.org/data/obtaining/

Rashid R, Eisenhauer A, Liebetrau V, Fietzke J, Böhm F, et al. 2015. Early Diagenetic imprint on temperature proxies in Holocene Corals: A case study from French Polynesia. *In preparation*

Rashid R, Eisenhauer A, Stocchi P, Liebetrau V, Fietzke J, et al. 2014. Constraining mid to late Holocene relative sea level change in the southern equatorial Pacific Ocean relative to the Society Islands, French Polynesia. *Geochemistry, Geophysics, Geosystems*. 15(6):2601–15

Rios Wilks A. 2013. Preliminary benefit cost analysis of storm surge hazard mitigation in the Tuamotu Islands, French Polynesia. *PR171*, Secretariat of the Pacific Community - Applied Geoscience and Technology Division

Roff G, Bejarano S, Bozec Y-M, Nugues M, Steneck RS, Mumby PJ. 2014. Porites and the Phoenix effect: unprecedented recovery after a mass coral bleaching event at Rangiroa Atoll, French Polynesia. *Marine Biology*. 161(6):1385–93

Rooney J, Fletcher C, Grossman E, Engles M, Field M. 2004. El Nino Influence on Holocene Reef Accretion in Hawai'i. *Pacific Science*. 58(2):305–24

Schmidt GA, Jungclaus JH, Ammann CM, Bard E, Braconnot P, et al. 2012. Climate forcing reconstructions for use in PMIP simulations of the Last Millennium (v1.1). *Geoscientific Model Development*. 5(1):185–91

Seminoff JA. 2004. *Chelonia mydas. The IUCN Red List of Threatened Species. Version 2014.3*. http://www.iucnredlist.org/details/4615/0

Sen Gupta A, Jourdain N, Brown J, Monselesan D. 2013. Climate drift in the CMIP5 models. *Journal of Climate*. 26(21):8597–8615

SHOM. 2014. *Références Altimétriques Maritimes*. Brest: Service Hydrographique et Océanographique de la Marine

Slangen ABA. 2012. *Modelling regional sea-level changes in recent past and future*. PhD thesis. Universiteit Utrecht

Slangen ABA, Katsman CA, van de Wal RSW, Vermeersen LLA, Riva REM. 2011. Towards regional projections of twenty-first century sea-level change based on IPCC SRES scenarios. *Climate Dynamics*. 38(5-6):1191–1209

Smithers SG, Woodroffe CD. 2001. Coral microatolls and 20th century sea level in the eastern Indian Ocean. *Earth and Planetary Science Letters*. 191(1–2):173–84

Stattegger K, Tjallingii R, Saito Y, Michelli M, Trung Thanh N, Wetzel A. 2013. Mid to late Holocene sea-level reconstruction of Southeast Vietnam using beachrock and beach-ridge deposits. *Global and Planetary Change*. 110, Part B:214–22

Steinhilber F, Beer J, Fröhlich C. 2009. Total solar irradiance during the Holocene. *Geophysical Research Letters*. 36(19):L19704

Stéphan P, Goslin J, Pailler Y, Manceau R, Suanez S, et al. 2015. Holocene salt-marsh sedimentary infilling and relative sea-level changes in West Brittany (France) using foraminifera-based transfer functions. *Boreas*. 44(1):153–77

Stoddart DR, Scoffin TP. 1979. Microatolls: review of form, origin and terminology. *Atoll Research Bulletin*. 224:1–17

Tamisiea ME, Mitrovica JX, Davis JL, Milne GA. 2003. II: Solid Earth physics: long wavelength sea level and solid surface perturbations driven by polar ice mass variations: fingerprinting Greenland and Antarctic ice sheet flux. *Space Science Reviews*. 108(1-2):81–93

Taylor KE, Stouffer RJ, Meehl GA. 2011. An overview of CMIP5 and the experiment design. *Bulletin of the American Meteorological Society*. 93(4):485–98

Terry JP, Chui TFM. 2012. Evaluating the fate of freshwater lenses on atoll islands after eustatic sea-level rise and cyclone-driven inundation: A modelling approach. *Global and Planetary Change*. 88–89:76–84

Terry JP, Falkland AC. 2009. Responses of atoll freshwater lenses to storm-surge overwash in the Northern Cook Islands. *Hydrogeology Journal*. 18(3):749–59

Tushingham AM, Peltier WR. 1991. ICE-3G: A new global model of Late Pleistocene deglaciation based upon geophysical predictions of post-glacial relative sea level change. *Journal of Geophysical Research*. 96(B3):4497

Uehara K, Scourse JD, Horsburgh KJ, Lambeck K, Purcell AP. 2006. Tidal evolution of the northwest European shelf seas from the Last Glacial Maximum to the present. *Journal of Geophysical Research: Oceans*. 111(C9):C09025

Underwood MR, Peterson FL, Voss CI. 1992. Groundwater lens dynamics of atoll islands. *Water Resour. Res.* 28(11):2889–2902

Uto K, Yamamoto Y, Sudo M, Uchiumi S, Ishizuka O, et al. 2007. New K-Ar ages of the Society Islands, French Polynesia, and implications for the Society hotspot feature. *Earth Planet Sp*. 59(7):879–85

Van der Velde M, Javaux M, Vanclooster M, Clothier BE. 2006. El Niño-Southern Oscillation determines the salinity of the freshwater lens under a coral atoll in the Pacific Ocean. *Geophysical Research Letters*. 33(21):L21403

Van Vuuren DP, Edmonds J, Kainuma M, Riahi K, Thomson A, et al. 2011. The representative concentration pathways: an overview. *Climatic Change*. 109(1-2):5–31

Webb A. 2007. Assessment of salinity of groundwater in swamp taro (cyrtosperma chamissonis) “pulaka” pits in Tuvalu. Pacific Island Applied Geoscience Commission

White I, Falkland T, Perez P, Dray A, Metutera T, et al. 2007. Challenges in freshwater management in low coral atolls. *Journal of Cleaner Production*. 15(16):1522–28

Woodroffe CD. 2013. Sea level studies: coral records of relative sea-level changes. In *Encyclopedia of Quaternary Science (Second Edition)*, ed. SA Elias, pp. 409–18. Amsterdam: Elsevier

Woodroffe CD, Beech MR, Gagan MK. 2003. Mid-late Holocene El Niño variability in the equatorial Pacific from coral microatolls. *Geophysical Research Letters*. 30(7):1358

Woodroffe CD, McGregor HV, Lambeck K, Smithers SG, Fink D. 2012. Mid-Pacific microatolls record sea-level stability over the past 5000 yr. *Geology*. 40(10):951–54

Woodroffe SA, Barlow NLM. 2015. Reference water level and tidal datum. In *Handbook of Sea-Level Research*, eds. I Shennan, AJ Long, BP Horton, pp. 171–80. John Wiley & Sons, Ltd

Woodward RS. 1888. On the form and position of mean sea level. *United States Geological Survey Bulletin*. 48:87–170

Worliczek E. 2013. *La vision de l'espace littoral sur l'île Wallis et l'atoll Rangiroa dans le contexte du changement climatique*. PhD thesis. Universität Wien

Yates ML, Le Cozannet G, Garcin M, Salaï E, Walker P. 2013. Multidecadal Atoll Shoreline Change on Manihi and Manuae, French Polynesia. *Journal of Coastal Research*. 870–82

Yu K-F, Zhao J-X, Done T, Chen T-G. 2009. Microatoll record for large century-scale sea-level fluctuations in the mid-Holocene. *Quaternary Research*. 71(3):354–60